

NATIONAL ADVISORY COMMITTEE FOR AERONAUTICS

TECHNICAL MEMORANDUM

No. 1181

INVESTIGATIONS ON REDUCTIONS OF FRICTION ON WINGS, IN
PARTICULAR BY MEANS OF BOUNDARY LAYER SUCTION

By Werner Pfenninger

Translation

“Untersuchungen über Reibungsverminderungen an Tragflügeln,
insbesondere mit Hilfe von Grenzschichtabsaugung”
Mitteilungen aus dem Institut für Aerodynamik an der Eid-
genössischen Technischen Hochschule in Zurich. Heraus-
gegeben von Prof. Dr. J. Ackeret, Nr. 13.



Washington

August 1947

UNIVERSITY OF FLORIDA
DOCUMENTS DEPARTMENT
120 MARSTON SCIENCE LIBRARY
P.O. BOX 117011
GAINESVILLE, FL 32611-7011 USA

TABLE OF CONTENTS

	Page
Preface	
Chapter 1: Introduction, Abstract	1
1. General remarks	1
2. Earlier reports published on the reduction of frictional and profile drags and on related fields	1
3. Influence of the transition-point position on the profile drag for larger Reynolds numbers; statement of the purpose	4
Chapter 2: Causes of Transition	6
1. Influence of the external pressure gradient on the transition	6
2. Influence of the external turbulence on the transition; turbulence of the atmosphere	10
Chapter 3: Laminar Profiles with the Transition Taking Place Far Toward the Rear (without Boundary-Layer Suction)	16
1. General considerations	16
2. Preliminary tests on laminar profiles for smooth entrance	16
3. Laminar profiles for propellers	18
4. Laminar profiles for wings	21
Chapter 4: Laminar Boundary-Layer Suction, General Remarks .	26
1. Aims for further development	26
2. Effect of suction of laminar boundary layer on the flow characteristics	26
3. Statement of the problem	27
4. History of development of the laminar boundary-layer suction	28
Chapter 5: Investigation of the Laminar Pressure Increase with Boundary-Layer Suction for Smaller and Medium Reynolds Numbers	36
1. Laminar suction tests with three suction slots arranged one after the other	36
2. Tests with laminar boundary-layer suction with a single suction slot	38

	Page
Chapter 6: Investigation of the Slot Flow for Laminar	
Boundary-Layer Suction with Single Slots	45
1. Laminar suction tests with straight suction slot	45
2. Investigation of the slot flow for laminar boundary- layer suction with suction slot (i) curved forward (definitions, see beginning of chapter 5)	47
3. Investigation of the slot flow for laminar boundary- layer suction with the rearward curved suction slot (h)	48
Chapter 7: Tests about Keeping a Boundary Layer for High Reynolds	
Numbers Laminar with the Aid of Boundary-Layer Suction	50
1. Purpose of the tests	50
2. Test apparatus	50
3. Measurements	51
4. Symbols and evaluation of the section tests	52
5. Test results	59
6. Extension of Schlichting's theory on the laminar boundary-layer development with area suction in the case of the acceleration of the sucked air to the undisturbed free-stream velocity U_0	62
Chapter 8: Investigation of a Slightly Cambered Laminar	
Suction Profile of 10.5-Percent Thickness	65
1. Purpose of the investigation	65
2. Profile, test arrangement	65
3. Measurements with laminar boundary-layer suction	66
4. Test results	69
5. Conclusions from the tests of chapters 7 and 8 for the design of laminar suction profiles with the lowest possible drag for high Reynolds numbers	72
6. Prospects for application of laminar boundary-layer suction in flight for high Reynolds numbers	73
Appendix	75
References	77

P R E F A C E

The present report deals with the reduction of frictional drag by maintaining a more extended laminar boundary layer, particularly with the aid of boundary-layer suction. The first chapters treat publications in this field, the causes of the boundary-layer transition and a few laminar profiles without boundary-layer suction. Next, tests with laminar suction profiles are described. The behavior of the suction slots for laminar boundary-layer suction was separately examined.

The present report was begun in 1940 and financially supported by the Committee for Study of Aviation. I feel obliged and am glad to express here my sincere gratitude to this committee and particularly to its president, Prof. W. J. Ackeret for energetic support of my work.

Digitized by the Internet Archive
in 2011 with funding from
University of Florida, George A. Smathers Libraries with support from LYRASIS and the Sloan Foundation

NATIONAL ADVISORY COMMITTEE FOR AERONAUTICS

TECHNICAL MEMORANDUM NO. 1181

INVESTIGATIONS ON REDUCTIONS OF FRICTION ON WINGS,
IN PARTICULAR BY MEANS OF BOUNDARY-LAYER SUCTION*

By Werner Pfenninger

CHAPTER 1

INTRODUCTION, ABSTRACT

1. General Remarks

The drag of an airplane consists of the induced drag, the frictional and form drag of wing, fuselage, tail unit, and, occasionally, radiator drag. Investigations have shown the frictional drag to be the main portion of the drag. Thus the reduction of surface friction has gained considerable importance during the last years.

Since the laminar friction is, in general, considerably lower than the turbulent friction, the frictional drag could be reduced by a laminar boundary layer as long as possible. The aim of the tests described here was to keep the boundary layer completely laminar up to the trailing edge of the wing.

2. Earlier Reports Published on the Reduction of
Frictional and Profile Drags and on Related Fields

(a) The possibility of reducing friction by maintaining a laminar boundary layer for a longer time has been mentioned by B. M. Jones (reference 1). B. M. Jones proved later (reference 2) that on finished wing profiles in flight there might appear laminar boundary layers of much greater extent and with the

"Untersuchungen über Reibungsverminderungen an Tragflügeln, insbesondere mit Hilfe von Grenzschichtabsaugung" Mitteilungen aus dem Institut für Aerodynamik an der Eidgenössischen Technischen Hochschule in Zürich Herausgegeben von Prof. Dr. J. Ackeret Nr. 13.

transition point lying farther to the rear than was expected so far (compare Serby, Morgan, and Cooper (reference 3)). B. M. Jones (reference 2), Squire-Young (reference 4), Pretsch (reference 5), and Serby, Morgan, and Cooper (reference 3) investigated to what degree the transition-point position affects the frictional and profile drag.

According to these investigations a farther rearward position of the transition point should make low profile drags possible even for thicker profiles at higher Reynolds numbers, Re . In fact, tests on "laminar profiles" of this type resulted in considerably smaller profile drags, particularly for weak external turbulence and larger Re (references 6, 7, and 8). During the second world war these laminar profiles were thoroughly investigated in various countries.

(b) The position of the transition point depends mainly on the external pressure distribution, the external turbulence, and the nature and curvature of the surface. The influence of the external pressure distribution on the transition-point position was investigated by B. M. Jones (reference 2), Serby, Morgan, and Cooper (reference 3), Hall and Hislop (reference 10), G. I. Taylor (reference 11), Faye and Preston (reference 12), Schubauer (reference 13), Faye (reference 14), etc. Flight tests by Jones (reference 2), Serby, Morgan, and Cooper (reference 3), and the NACA (references 9 and 15) showed that for "clean" surfaces transition in flight generally takes place in the region of the point of separation, even for higher Reynolds numbers. Wind-tunnel tests at moderate Re showed that the transition after a slight pressure increase, in general, takes place shortly after the separation point of the laminar layer as long as the external turbulence does not affect the transition (for instance, Hall and Hislop (reference 10)). A similar behavior in transition was found on bodies of revolution (reference 16).

(c) Under the influence of an external turbulence the transition for higher Re occurs sometimes at a considerable distance before the point of laminar separation. The dependence of the transition on an external turbulence was studied by G. I. Taylor (references 11, 17, and 18), von Karman (references 19 and 20), Dryden (references 21 to 24), L. Prandtl (for instance (reference 25)), Schlichting (references 26 and 27), Tollmien (references 28 and 29), Schubauer (reference 13), Faye and Preston (reference 12), Faye (reference 30), etc. For weaker external turbulence, in general, higher critical Reynolds numbers are obtained at the point of transition; compare, for instance, B. M. Jones (reference 2), Hall and Hislop (reference 10), Tani (reference 7), Lewis (reference 6), and also (reference 15).

For accelerated flow, too, there result higher critical Re , compare Dryden (reference 21) and Peters (reference 31).

(d) For application of laminar profiles in flight for higher Re , knowledge of atmospheric turbulence and its influence on the transition is important. The atmospheric turbulence was investigated in flight with hot wires, among others by Stephens and Hall (reference 32). These two authors reached the conclusion that in their tests the influence of the atmospheric turbulence on the transition was negligible.

American flight tests on a laminar profile of 15.9-percent thickness at $Re = 17 \times 10^6$ confirmed this result (reference 15). The influence of the wall curvature on the transition was investigated experimentally, for instance, by M. and F. Clauser (reference 33) and theoretically by H. Görtler (reference 34). The measurements by Clauser showed at the transition for convex (or concave) wall curvature higher (or lower) Re than for a straight wall (compare also L. Prandtl (reference 35) and Rayleigh (reference 86)).

(e) The influence of surface disturbances on the transition (roughnesses, turbulence wires, trip wires, rivets, unevennesses in the sheet-metal skin, surface leaks, waves, etc.) was investigated, for instance, by Young (reference 36), Hood (reference 37), Tani (reference 38), and Faye and Preston (reference 12). Tests of the author showed that laminar profiles at higher Re are sensitive to waviness of the surface and that surface leaks must be avoided in order to prevent the air from being sucked from the wing interior and the boundary layer thus from becoming turbulent.

(f) The pressure distribution of suitable profile shapes may be calculated with the aid of conformal mapping, for instance, according to Theodorsen (reference 39) (compare also references 40, 41, and 42). The singularity methods which replace the profile by vortices, sources and sinks, take less time for the detailed numerical calculation, but are less accurate. From the pressure distribution one may calculate the development of the boundary layer in the laminar and turbulent part of the profile.

(g) The laminar boundary-layer development may be determined, for instance, according to Pohlhausen (reference 43), Falkner and Skan (reference 44), Falkner (references 45 and 46), and Howarth (reference 48). For moderately accelerated and slightly retarded flow the approximation method of Pohlhausen is well applicable as demonstrated by a comparison with Falkner's method (references 45 and 46) for an external velocity distribution $U = kx^m$. According to Pohlhausen, the laminar-plate friction (pressure-gradient zero)

is overestimated by 3.3 percent. (Comparison with Blasius (reference 47).) According to Howarth (reference 48), the laminar separation starts in the case of the external velocity distribution $U = U_0 - bx$ at $\lambda = \frac{\delta^2}{\gamma} u' \approx -7.5$ instead of $\lambda = -12$ according to Pohlhausen. For the case $U = kx^{-0.0904}$ the method of Falkner (references 45 and 46) results in boundary-layer profiles with vertical tangent already at $\lambda \approx -5$.

Howarth (reference 51) gave a compilation of various methods for calculation of the laminar boundary-layer development. L. Prandtl (reference 49) and H. Görtler (reference 50) investigated the laminar boundary-layer development by exact calculation and compared the different known solutions with each other.

Tomotika (reference 52) developed a method corresponding to that of Pohlhausen for the three-dimensional case.

(h) The turbulent boundary-layer development may be calculated according to A. Buri (reference 53), Gruschwitz (reference 54), Kehl (reference 55), Squire-Young (reference 4), and Young (reference 56). In most cases, the turbulent shear stress at the wall is the same as that for the flat plate with turbulent flow without pressure gradient for equal Re_θ . The ratio $\frac{\delta^*}{\theta} = H$ was frequently assumed constant ($H = 1.4$ for not too large pressure increase). Otherwise, H could be determined from turbulent boundary-layer measurements as a function of the pressure increase (compare, for instance, Gruschwitz (reference 54)). The turbulent boundary-layer development along the flat plate without pressure gradient was investigated by Th. von Karman (references 57 and 58) and L. Prandtl (reference 59).

The boundary-layer development of the wake may be calculated, for instance, according to Squire-Young (reference 4).

3. Influence of the Transition-Point Position on the

Profile Drag for Larger Reynolds Numbers;

Statement of the Purpose

For slightly cambered profiles of various thickness ratio d/t at $Re = 15 \times 10^6$ the profile drag was calculated according to Squire-Young (reference 4) for various positions of the transition point x/t (compare fig. 1). Furthermore, the profile drag was

calculated for a profile of 16-percent thickness for various Re and different positions of the transition point. (See fig. 2.)

For a rearward movement of the transition point at larger Re , C_{w0} would drop to low values. In the ideal case (boundary layer kept completely laminar up to the trailing edge), even thicker profiles would give very low drags for larger Re 's. Thicker profiles are structurally more favorable and permit larger spans, thereby reducing the induced drag which would regain significance due to the decrease of the frictional drag. Moreover, thicker profiles permit a more favorable installation in the wing of fuel tanks, power plants, other loads, and finally, suction ducts. Furthermore, thicker profiles possess higher maximum lift with suitable high-lift devices. For faster airplanes the maximum profile thickness is probably dependent on the stipulation of sufficiently small superstream velocities in order to reach high Mach numbers without compression shocks.

According to these considerations, the following aim was set: Development of thicker profiles with small superstream velocities where the boundary layer remains, in flight, at high Reynolds numbers, laminar as far toward the rear as possible, if possible as far as the trailing edge. The maximum lift for take-off and landing is to be as high as possible.

The possibilities of keeping the boundary layer laminar for a long time are, for instance:

(a) Use of profile forms where, by special design of the contour, the transition is shifted rearward (flat pressure distribution with small superstream velocities and delayed pressure increase).

(b) Preventing the boundary layer from becoming turbulent by means of boundary-layer suction, possibly in combination with profile forms with flat pressure distribution.

In order to study the methods for keeping the boundary layer laminar for a longer time, one must know the presumable causes of transition.

CHAPTER 2

CAUSES OF TRANSITION

1. Influence of the External Pressure Gradient
on the Transition

Transition tests showed that, in general, the transition takes place after a slight pressure increase in the neighborhood of the point of laminar separation, as long as an external turbulence does not affect the transition (references 2, 3, 10, 12, 13, 15, 16, and 60). These observations were confirmed by tests of the author, for instance, on an NACA 0010 profile (fig. 3), on laminar profiles of 10-percent and 14-percent thickness (figs. 4 and 5), on a body of revolution (fig. 6) and, later, by laminar suction tests. With increasing Re the transition point moves forward more slowly for laminar profiles than for so far conventional ones.

These tests, as well as those of chapter 3 and the later suction tests of chapter 4, 4C, chapter 6, 3, chapters 7 and 8, were performed in the large wind tunnel of the Institute described in reference 61a. The wind-tunnel turbulence was

$$\frac{u'}{U_0} = \frac{\sqrt{u_T^2}}{U_0} = 0.0040 \text{ to } 0.0045$$

The pressure gradient in the adjustable test section is very small.

In figure 3 the pressure distribution $\frac{p}{q_0}$ is plotted on an NACA-0010 profile (so far conventional profile form) for $c_a = 0$ and various $Re = \frac{U_0 t}{\nu}$ along the chord (U_0 free-stream velocity, $t = \text{chord} = 0.60 \text{ m}$). The static pressure p was measured through 0.5 millimeter ϕ bore holes compared to the static pressure p_0 in the test section without wing. The free-stream stagnation

pressure was $q_0 = g_0 - p_0$ (g_0 = undisturbed total pressure¹). The positions of the transition point (arrows) were ascertained from the break in the pressure-distribution curves at the transition (compare transition tests on NACA 0010-profile with soot coating and stethoscope (reference 6lc)). For larger Re the determination of the position of the transition point from the break in the pressure distributions became unreliable. With increasing Re the transition point shifts rapidly forward.

In figures 4 and 5 the pressure distribution p/q_0 of two laminar profiles (fig. 12) is plotted versus the chord with $d/t = 10$ percent, $t = 0.74$ m; $d/t = 14$ percent, $t = 0.70$ m. The static pressure p was measured with a static-pressure tube of $d = 2.0$ -millimeter diameter, which was put tangentially to the test point in the flow direction versus p_0 (static pressure in the test section for "tunnel-empty" condition). The four 0.4 millimeter ϕ connecting static-pressure holes of the static-pressure tube were located 10 millimeters behind the semicircular head and 100 millimeters ahead of the sting of 3.0 millimeters ϕ . A comparison of pressure-distribution measurements on a laminar profile of 14.7 -percent thickness and 2.4 -percent camber of the profile mean line showed that p/q_0 on the upper and lower side, respectively, was measured with the static-pressure tube on the average by 0.007 and 0.004 , respectively, too high, as compared with the measurement by means of connecting static-pressure holes.

The transition (arrow) was determined by means of the stethoscope (reference 6lc) and from the break in the pressure-distribution curves (reference 14).

¹By means of an annular equalizer opening at the end of the closed test section one succeeds in establishing there atmospheric pressure (for model present and tunnel empty condition). The undisturbed static pressure for "model present" very far in front of the model is approximately equal to the static pressure p_0 in the test section at the location of the model if the tunnel is empty (neglecting of the wake behind model and suspension).

It is self-evident that thereby the profile properties are given in such a manner as if the profile were working in a closed tunnel, not in the unlimited air stream. Since the models investigated here were small relative to the tunnel cross section (2.1×3 m, octagonal), the respective jet correction was omitted (about a corresponding correction of q_0 , U_0 , p_0 for larger model dimensions for two-dimensional flow. (See chapter 8.)

The pressure distribution $\frac{p}{p_0}$ is plotted on figure 6 for a body of revolution of $\frac{D}{L} = 0.212$ at $0.47 \times L$ from the front for symmetrical flow at various $Re_L = \frac{UL}{\nu}$, (D = maximum diameter of the body of revolution, L = length of the body of revolution = 0.85 m).

The body of revolution was held from behind by a cylindrical sting, suspension wires on the body were avoided. p was measured versus p_0 (static pressure in the empty tunnel) by means of a 2.0-millimeter ϕ static-pressure tube.

The position of the transition point (arrow) was ascertained with the stethoscope and from the break in the pressure-distribution curve. The slight superstream velocities result in a pressure increase and transition far to the rear.

Drag measurements: At the end of the body of revolution at the juncture to the sting the boundary-layer profiles were measured for symmetrical flow at various Re_L . The total pressure g in the boundary layer was determined by means of a flat total head tube of 0.2-millimeter \times 2.5-millimeter inner cross section and 0.5-millimeter external height. The static pressure in the boundary layer was measured by means of a 2.0-millimeter static pressure tube. From the boundary-layer measurement at the end of the body the momentum-loss area X_∞ far to the rear was calculated for the undisturbed static pressure p_0 according to Young (reference 56).

$$X_\infty = 2\pi \int_{\text{wake}} \frac{u}{U} \left(1 - \frac{u}{U}\right) r \, dr \text{ far toward rear}$$

The drag coefficient c_{w0} and c_{wH} , referred to the body surface area $O = 0.369 \text{ m}^2$ and the maximum cross-section area $\frac{\pi}{4} \times D^2 = 0.0254 \text{ m}^2$, respectively, then becomes:

$$c_{w0} = \frac{2X_\infty}{O}, \quad c_{wH} = \frac{2X_\infty}{\frac{\pi}{4} D^2}, \quad c_{wV^{2/3}} = \frac{2X_\infty}{\frac{V^{2/3}}{2/3}}, \quad \frac{V^{2/3}}{2/3} = 0.0570 \text{ m}^2 \quad (V = \text{Volume})$$

$c_{w0} (Re_L)$ is plotted on figure 6. c_{w0} decreases with Re_L at first similarly to the friction of the laminar flat plate

$c_{wR} = \frac{1.328}{\sqrt{Re}}$ see Blasius (reference 47) and increases again for higher Re_L , due to more pronounced shifting forward of the transition point (observations by stethoscope), caused by the tunnel turbulence. The minimum drag coefficient referred to the maximum cross section resulted as $c_{wH} = 0.0196$. For smaller Re , stethoscope observations showed that the boundary layer at the end of the body undergoes laminar separation and does not readhere with the properties of a turbulent boundary layer, thereby greatly increasing pressure and total drag.

The position of the transition point can be determined in different ways:

- (a) From hot-wire observations (compare, for instance, Dryden (reference 21))
- (b) By measurement of the total surface pressure along the chord with a fine total head tube (references 2 and 10)
- (c) By boundary-layer measurements (compare, for instance, (reference 16))
- (d) From the break in the pressure-distribution curve at the transition, caused by the sudden decrease of the displacement thickness δ^* at the transition (compare A. Fage (reference 14) and the pressure-distribution curves of figures 3, 4, 5, 6, 39, 40, 77-80, etc., compare also calculations by A. Betz (reference 77) for discontinuous change of the curvature)
- (e) Acoustically by stethoscope observations (reference 61c)
- (f) By soot coating (reference 61c)
- (g) By measurement of the total head of the boundary layer along the chord at a greater distance from the wall (reference 2)

As long as the transition is caused by an external pressure increase and not by an external turbulence, it takes place in a narrow comparatively well-defined zone. The methods indicated then yield, in general, the transition-point position reliably.

Presumable cause for transition: According to Rayleigh (reference 62), Tietjens (reference 63b), and Tollmien (reference 29)

laminar boundary-layer profiles with inflection point, as they originate with rising pressure, are unstable. Transition tests showed that the transition occurs when laminar boundary-layer profiles having a slight rearward flow in the neighborhood of the wall exist (compare, for instance (references 10, 13, and 78), this was confirmed by transition observations of the author with soot coating for medium Re . The originating of sufficiently strong vortices in the immediate neighborhood of the wall (as they form, for instance, for larger laminar pressure increase, for discontinuities in the surface, by an external turbulence, or for tube flows with sharp-edge inlet) seems to be required for the transition (compare L. Prandtl (reference 63a), J. Patry (reference 64), and L. Schiller (reference 79)).

The Reynolds number $Re_1 = \frac{U \times l}{\nu}$ referred to the distance l between the laminar separation point and the start of transition resulted as $Re_1 = 40,000$ to $70,000$ as long as the external turbulence does not affect the transition (compare references 9 and 10, confirmation by measurements of the author). U = mean velocity at the edge of the boundary layer between laminar separation point and start of transition.

For very weak external turbulence and larger Re the transition for laminar profiles is probably to be expected in the region of the laminar separation point.

2. Influence of an External Turbulence on the Transition; Turbulence of the Atmosphere

(a) Various drag measurements and transition measurements on flat plates, profiles, and bodies of revolution had shown that for larger Reynolds numbers the transition, under the influence of the external turbulence, takes place considerably farther in front and that the drag increases again. The same observation was made in tests of the author on laminar profiles without boundary-layer suction (see, for instance, $c_{w\infty}(Re)$ of a profile of 3.35-percent thickness (chapter 7: fig. 88, curve a, and corresponding position of the transition point, fig. 89, also figs. 7, 8, and 10) and on a body of revolution with flat pressure distribution and transition lying far back (fig. 6, chapter 2, 1). For larger Reynolds numbers, individual turbulent bursts were determined in the boundary layer with a stethoscope which occur more and more frequently downstream with increasing boundary-layer thickness until the boundary layer becomes fully turbulent. The transition takes place in a more or

less wide transition region; its position is less readily ascertained according to the methods indicated in chapter 2, 1 than in the case of transition due to external pressure increase. A renewed increase of the profile drag due to the external turbulence was also observed for laminar profiles with boundary-layer suction, for larger

$$Re = \frac{U_0 t}{\nu} \quad (\text{figs. 18, 88, 95 or chapter 4, 4c, chapters 7 and 8}).$$

(b) Causes of transition for transition due to an external turbulence: By the external turbulent velocity fluctuations considerable velocity fluctuations in flow direction originate in a boundary layer (see Tollmien (reference 28b), G. J. Taylor (references 11 and 18) and Dryden (reference 21)), thus causing temporarily unstable boundary-layer profiles with inflection point and finally reverse flow in the neighborhood of the wall. The transition then occurs, as in the case of larger laminar pressure increase, due to the formation of vortices at the surface. There originate isolated turbulent discontinuities which become more and more frequent downstream with increasing boundary-layer thickness until the boundary layer is fully turbulent.

G. I. Taylor (reference 18), Hall and Hislop (reference 10), Fage and Preston (reference 12), and Fage (reference 30) attempted to find a criterion for the transition due to an external turbulence. They assumed that the transition starts when there originate, under the influence of the external turbulent pressure fluctuations, momentarily boundary-layer profiles with vertical tangent, that is, λ Pohlhausen = -12, or, respectively, its mean square value

$$\lambda' = - \frac{\delta^2}{\nu} \frac{1}{U} \left(\frac{dp}{dx} \right)' = \lambda'_{\text{critical}}$$

According to G. I. Taylor (references 11 and 18) turbulent pressure fluctuations originate in the case of an external turbulence, their mean square value is, for isotrope turbulence,

$$\sqrt{\left(\frac{dp}{dx} \right)^2} = \left(\frac{dp}{dx} \right)' = \sqrt{2} \rho \frac{u'^2}{\lambda_\eta}$$

with

$$u'^2 = u_p'^2$$

λ_η is a parameter connected with the diffusion in a turbulent flow (λ_η = length of the diffusion).

(λ_η and Λ (mean magnitude of the smallest vortices significant for the dissipation) were, for instance, experimentally determined by Hall and Hislop (reference 10) from temperature distribution measurements behind a heated wire and from measurements of correlation behind grids.)

Taylor deduces by insertion of $\left(\frac{dp}{dx}\right)'$ for isotrope turbulence behind a grid (mesh width M) that the critical Reynolds number $Re_{x_{critical}} = \left(\frac{U_x}{\nu}\right)_{critical}$ is a function of

$$\left(\frac{x}{M}\right)^{0.2} \left(\frac{u'}{U}\right) \text{ is: } (\lambda'_{critical})^2 = \left(\frac{U_x}{\nu}\right)_{critical} \left(\frac{x}{M}\right) \left(\frac{u'}{U}\right)^5 \left(\frac{34 \sqrt{2}}{A} \frac{\Lambda}{\lambda_\eta}\right)^2$$

wherein A = constant,

$$\frac{\Lambda}{M} = A \sqrt{\frac{\nu}{Mu}}$$

according to Taylor. This relation was experimentally tested by Hall and Hislop (reference 10). According to it, $Re_{x_{critical}}$ increases with diminishing values $\left(\frac{x}{M}\right)^{0.2} \left(\frac{u'}{U}\right)$ somewhat more slowly than according to the theory, that is, $\lambda'_{critical}$ decreases with increasing $Re_{x_{critical}}$. This circumstance may perhaps be explained from the fact that a sufficiently strong reverse flow at the wall ($\lambda < -12$) and not only $\lambda = -12$ (vertical tangent to the velocity profile) is decisive for the transition. For small Re_x larger negative λ -values are necessary for the transition if one assumes the reverse flow required for transition to be of equal strength (with equal circulation).

Turbulence criterion of Fage (reference 30): Under the assumption that the transition starts when momentarily a critical negative λ -value is reached due to the turbulent-pressure fluctuations, Fage finds that the value

$$\xi_L = 3.35 (Re_{\theta_{critical}})^{0.6} \left(\frac{u'}{U}\right) \left(\frac{\theta}{L}\right)^{0.2}$$

ought to be constant, with

$$L \quad \text{turbulence scale} \left(\int R_y \, dy \right)$$

R_y correlation for velocity fluctuations in 2 points at distance y perpendicular to flow

$$Re_{\theta \text{ critical}} = \left(\frac{U\theta}{\nu} \right)_{\text{critical}} \quad \text{at the transition}$$

Page finds that ξ_L decreases with increasing $Re_{\theta \text{ critical}}$

For accelerated or for retarded flow the transition occurs, due to external turbulence, at higher or at considerably lower $Re_{\theta \text{ critical}}$ -values, respectively, compare, for instance, figures 3 and 4. Influence of the atmospheric turbulence on the transition:

The turbulence measurements in flight by Stephens and Hall (reference 32) had given the result that, in their tests, the influence of the atmospheric turbulence on the transition was negligible. In most cases, the turbulence-degree of the atmosphere

was very small: $\frac{u'}{U} \approx 0.0003$ for $U \approx 46$ m/sec in calm air,

U = velocity outside the boundary layer. Considerably larger turbulent fluctuations were found for unstable stratification of the air ($u'/U \approx 0.003$ for $U = 46$ m/sec), however; due to the turbulence scale which was so much larger than in the wind tunnel, their effect on the transition was, according to Stephens and Hall, of secondary importance. (Magnitude of the smallest vortices ~ 0.3 m). Stephens and Hall found the fluctuations in the boundary layer to be considerably smaller in flight than in wind-tunnel tests (reference 21). The same observation was made in tests of laminar boundary layers in tunnels of low turbulence (reference 6) and in tests of the author with a tube flow at low turbulence. American measurements in flight on a laminar profile of 15.9-percent thickness seem to confirm that the atmospheric turbulence affects the transition only

slightly, even for larger Re (reference 15): For $Re = \frac{U_0 t}{\nu} = 19 \times 1.06$ and a Mach number $M = 0.52$ the measured value was $c_{wco} = 0.0030$,

which from the viewpoint of calculation would correspond to a mean position of the transition point (mean of upper and lower side) of about $0.68t$ from the front in the region of the point of laminar separation. From boundary-layer calculations, shortly before the transition give a Reynolds number $Re_{\theta} = \frac{U\theta}{\nu} = 2600$, referred to the

momentum loss thickness θ and the velocity U at the edge of the boundary layer, that is, essentially more than was observed in conventional wind tunnels.

$$\theta = \text{momentum loss thickness} = \int_0^{\delta} \frac{u}{U} \left(1 - \frac{u}{U}\right) dy$$

$$\delta^* = \text{displacement thickness} = \int_0^{\delta} \left(1 - \frac{u}{U}\right) dy$$

with

δ total boundary-layer thickness

u velocity in the boundary layer at the distance from the wall y

U_0 flight velocity

Tests of the author with a laminar-tube flow in the starting region showed that considerably higher Re can be reached for a free stream free of turbulence.

Tests with a laminar-tube flow in the starting region.- The purpose of these tests was to obtain high laminar Reynolds numbers by means of a laminar-tube flow in the starting region.

Test arrangement.- A conical inlet funnel of 0.9 meter length (maximum diameter at the entrance 0.18 m) was fixed to one end of a cylindrical anticorrosion tube of 6 meter length and 0.025-meter inner diameter. The transition to the tube was smooth. At the entrance of the inlet funnel was a rectifier consisting of circular tubules of 3 millimeters ϕ , about 0.1-millimeter wall thickness and 0.2 meter length in stacks. A Laval nozzle was attached to the other end of the tube which was connected with the evacuated supersonic tunnel of the Institute (reference 61a). The air was sucked from the space. The air motion at the entrance of the inlet funnel was kept as small as possible.

Measurements.- The static pressure along the tube was measured with 0.8 millimeter ϕ connecting static-pressure holes with the atmosphere as reference level. Further, the state of the boundary layer along the tube was tested with the stethoscope (reference 61c) which was attached to the static-pressure holes. Constant air velocity was obtained through the Laval nozzle at the rear end of

the tube and disturbances from upstream affecting the boundary layer of the tube were avoided. With this test arrangement the tube flow could be kept laminar up to considerable Reynolds numbers, it is true, accelerated flow existed. The maximum stagnation pressure at the end of the tube, in its center, with laminar boundary layer up to the end of the tube, amounted to 180 kilograms per meter², corresponding to a velocity of 56.5 meters per second in the center of the tube. The numerical evaluation, according to L. Schiller (reference 83), resulted in a total boundary-layer thickness $\delta = 6.2$ millimeters at the tube end and the following Reynolds numbers:

$$Re_{\theta_1} = 2400 \quad Re_{\delta_1}^* = 6450$$

and

$$N_1 = \frac{1}{3} (Re_{\delta_1}^*)^2 = 13.9 \times 10^6$$

with

$$Re_{\theta_1} = \frac{U\theta_1}{\nu}, \quad \theta_1 = \int_0^{\delta} \frac{u}{U} \left(1 - \frac{u}{U}\right) \frac{r}{R} d(R - r)$$

U velocity at the edge of the boundary layer

$$Re_{\delta_1}^* = \frac{U\delta_1^*}{\nu}, \quad \delta_1^* = \int_0^{\delta} \left(1 - \frac{u}{U}\right) \frac{r}{R} d(R - r)$$

u velocity in boundary layer

r variable radius

R tube radius (0.0125 m)

So far, sphere or hot-wire measurements were performed frequently for determination of the turbulence. The sphere test, in particular, becomes unreliable when the external turbulence is very weak. For many purposes, for instance, the application of wind-tunnel tests on laminar profiles to flight conditions, the Re_{θ} -values, which can be obtained with a laminar boundary layer and a flat pressure distribution, are the main object of interest. The manner in which these values are reached is often of little importance.

CHAPTER 3

LAMINAR PROFILES WITH THE TRANSITION TAKING PLACE FAR
TOWARD THE REAR (WITHOUT BOUNDARY-LAYER SUCTION)

1. General Considerations

Since the transition occurs mostly after a slight pressure increase, probably those profile forms will be favorable for keeping the boundary-layer laminar for a longer time in which the pressure distribution is flat and the pressure increase lies far toward the rear. The flat pressure distribution results in smaller superstream velocities and thus higher Mach numbers without compression shocks; of course, separations in the region of the pressure rise must be avoided.

Profiles with such pressure distributions have the maximum thickness at $(0.4 \text{ to } 0.5)t$ from the front.

2. Preliminary Tests on Laminar Profiles

for Smooth Entrance²

A few slightly cambered laminar profiles of various thicknesses were designed according to these considerations (fig. 9).

The profile drag was determined for smooth entrance for various $Re = \frac{U_0 t}{\nu}$ by means of the momentum method. (See, for instance, reference 61c) (fig. 10).)

The laminar profiles investigated here are, for larger Re , superior with respect to drag to profiles of equal thickness used so far. (Compare with the NACA profile 23012.) With increasing Re , c_{w_∞} decreases more rapidly than for conventional profiles. The drag increase for larger Re (caused by the faster forward travel of the transition point due to the external turbulence) starts at higher Reynolds numbers than it did for profiles used so far.

²Smooth entrance: No flow around the profile mean line at the nose of the wing.

For smaller Re the laminar profiles become more unfavorable with respect to drag since the boundary layer remains laminar for too long, therefore undergoes laminar separation in the rear part of the profile and does not readhere again in a purely turbulent manner. (Observations by stethoscope.) The pressure drag is thereby strongly increased. By artificially creating a turbulent boundary layer in the region of the point of laminar separation it is possible, in many cases, to prevent a more extensive laminar separation and to obtain a turbulent readhering of the boundary layer connected with a corresponding drag decrease. Thus, the drag of the thin laminar profile number 7 for smaller Re could be essentially reduced by blowing-off of air from fine blowing holes which rendered the boundary layer in the region of the point of laminar separation turbulent.

The blowing holes of 0.8-millimeter ϕ and 5-millimeter length were placed vertically to the wing surface, they were on the upper side 133 millimeters, on the lower side 91 millimeters ahead of the trailing edge. The wing chord was $t = 0.60$ meter. The spacing of the holes was 26 millimeters. The total energy of the air at the entrance of the blowing holes was practically equal to the undisturbed total head in the tunnel. Turbulent wedges originated behind the blowing holes (observations by stethoscope and with soot coating) which rapidly fused, thus causing the boundary layer to become turbulent over the entire span.

The mean profile drag $c_{w\infty}$ over the series of spaced holes was measured by the momentum method at various $Re = \frac{U_0 t}{\nu}$. The following drags resulted:

$$Re = 1.65 \times 10^6, 1.13 \times 10^6, 0.76 \times 10^6, 0.52 \times 10^6$$

$$c_{w\infty} = 0.0033, 0.00365, 0.00425, 0.0053$$

$c_{w\infty}$ was reduced mainly in the region $Re = (0.6 \text{ to } 1.7) \times 10^6$

A further slight drag reduction for smaller Re (0.3×10^6 to 0.6×10^6) was obtained by placing the 0.8 millimeter ϕ blowing holes farther to the front of the wing (on the upper surface 155 millimeters, on the lower surface 110 millimeters ahead of the trailing edge) for equal spacing of the holes. Test results:

$$Re = 0.33 \times 10^6, 0.50 \times 10^6, 0.68 \times 10^6, 1.10 \times 10^6$$

$$c_{w\infty} = 0.0063, 0.0051, 0.0045, 0.00395$$

For larger Re , $c_{w\infty}$ is larger than for the case of the blowing holes lying farther toward the rear.

The dashed $c_{w\infty}$ -curve of figure 10 of profile number 7 gives the optimum $c_{w\infty}$ -values for the most favorable position of the blowing holes in the direction of the chord.

Further tests showed that the spacing of the holes, the hole-diameter, and the total head at the entrance of the blowing holes may be widely varied in order to make the boundary layer for smaller Re artificially turbulent. For smaller Re , boundary-layer measurements at the trailing edge of the wing, with and without blowing holes, resulted in considerably thinner and fuller boundary layers (larger δ^*/θ values) when air was blown into the boundary layer.

Similar tests showed that a laminar boundary layer can be made turbulent in a desired place by other measures, too (steps in the surface, considerable roughnesses, etc.), compare, for instance, the tests with the profile number 32 of 6-percent thickness with disturbances. (See the appendix.) An increase of the angle of attack beyond the angle of smooth inflow has the same effect in obtaining for smaller Re a turbulent readhering on the upper side and, hence, a smaller profile drag. (See profile-drag polars of the propeller profile number 11 for smaller Re (fig. 11).)

3. Laminar Profiles for Propellers

On the basis of the preliminary tests described above, propeller profiles with highest possible lift-drag ratios were developed at moderate c_a and with small superstream velocities. A few test results on a propeller profile of 9-percent thickness (number 11) are shown as an example. (See fig. 11.)

The corresponding profile coordinates may be seen from the table of coordinates.

The investigated wing was a rectangular wing of $b = 1.50$ meters span, $t = 0.252$ meter chord and $F = 0.376$ meter² area of projection (= area of reference). The wing ends, seen from the front, were rounded semicircularly. (See, for instance, reference 61c $b^2/F = 5.98$.)

Measurements.- (a) Determination of:

$$c_a = \frac{A}{q_0 F}, \quad c_w = \frac{W}{q_0 F}, \quad c_{m_t}/4 = \frac{M_t/4}{q_0 F t}$$

for various angles of attack by means of three-component measurements

(b) Momentum-measurements (total pressure and static pressure) 0.146 meter behind the wing in a wing section 0.22 meter laterally from the wing plane of symmetry outside of the suspension fittings for various $Re = \frac{U_0 t}{\nu}$ and c_a

(c) Transition measurements with the stethoscope 0.22 meter laterally from the wing plane of symmetry for various Re and c_a (start of transition and beginning of the fully developed turbulent boundary layer)

The chord of the camber line was chosen as line of reference for α . The point of reference for $c_{m_t}/4$ ($c_{m_t}/4 > 0, \alpha$ -increasing) lies at a distance of $t/4$ from the front on this line.

The jet corrections for the downwash and the induced drag for the closed tunnel were calculated according to de Haller (reference 84).

The momentum measurements were evaluated in the customary manner. The local lift coefficient c_a at the momentum measuring station was put equal to $1.10c_a$.

A few test results can be seen from figure 11: variation of c_a with c_{w_0} at various Re (momentum measurements), and the beginning of the developed turbulent boundary layer on upper and surfaces for various c_a and Re ,

$$\left. \begin{array}{l} c_a(\alpha) \\ c_{m_t}/4(\alpha) \end{array} \right\} \text{ for } Re = 0.76 \times 10^6$$

In an optimum c_a -range, decreasing with increasing Re , the transition on both wing surfaces occurs far toward the rear which results in low profile drags. When this range is exceeded the drag increases and the transition point on upper and lower sides travels rapidly forward, the reason is the appearance of a suction peak at the wing nose due to the angle of attack. For larger c_a a slight local turbulent separation occurs on the upper side (tufts and stethoscope observations). $c_{w\infty opt}$ decreases with increasing Re somewhat more slowly than the laminar friction of the flat plate. For larger Re at moderate c_a -values, more favorable profile drag-lift ratios result. For smaller Re and smooth inflow $c_{w\infty}$ deteriorates since the boundary layer of the upper wing surface undergoes laminar separation and does not readhere with the properties of a turbulent boundary layer (observation by stethoscope). Only for larger c_a the laminar boundary layer is disturbed so strongly by the incipient suction peak at the wing nose that the transition occurs in time to bring about a turbulent readhering of the boundary layer for smaller Re (observation by stethoscope). $c_{w\infty}$ then decreases with increasing c_a , and $c_{w\infty opt}$ lies at considerably larger c_a than would correspond to the smooth inflow. A similar reduction of $c_{w\infty}$ with increasing c_a had resulted also in earlier measurements on ordinary profiles for smaller Re (Göttinger Lieferungen I to IV (reference 80), F. Schmitz (reference 81), NACA measurements (reference 82) etc.)

The lift and pitching-moment distribution $c_{m_t/4}$ shows standard behavior in the optimum c_a -region. For larger angles of attack, discontinuities appear in $c_a(\alpha)$ the variations of c_a with α and $c_{m_t/4}(\alpha)$, due to the change of the effective profile camber by the thickening of the boundary layer on the upper wing surface which is caused by the forward shifting of the transition point after exceeding the optimum c_a -region.

The use of laminar profiles for propellers reduces their friction losses. Due to the smaller superstream velocities, compression shocks start at higher Mach numbers than for conventional profiles. The use of laminar profiles for propellers will probably rather lead to wider blades of smaller thickness ratio with relatively low c_a -values under standard flight conditions. Hence, there results again higher admissible Mach numbers and a larger starting thrust.

4. Laminar Profiles for Wings

A basic requirement for good wing profiles is a large range $\frac{c_{a_{max}}}{c_{w_{min}}}$, that is, low drag under standard flight conditions and highest possible maximum lift with extended landing aids. Further desired characteristics are small superstream velocities in order to attain high Mach numbers without compression shocks, low-diving moments c_{mo} , steady pitching-moment behavior, favorable static conditions for bending and torsion of the wing, and favorable conditions of installation for landing flaps. These latter are to improve not only the landing but also the take-off considerably and should, if possible, extend over the entire span.

Based on these stipulations, a few laminar profiles were developed which are probably appropriate for wings. The profile shapes of laminar profiles of 10-percent and of 14-percent thickness can be seen from figure 12 and the table of coordinates.

Profile data:

Thickness ratio	$d/t = 0.10$ in $0.49 t$ from the front
	curvature ratio of the mean line of the profile,
	$f/t = 0.006$ in $0.5 t$ from the front
	$R_0 t = 0.009$ (R_0 = nose curvature radius)
Chord	$t = 0.74$ meter
	$d/t = 0.14$ in $0.44 t$ from the front
	$f/t = 0.0245$ in $0.41 t$ from the front
	$R_0 t = 0.019$
	$t = 0.70$ meter

The rear part of the profile gradually converges into a pointed trailing edge. Hence, the pitching-moment behavior was improved as compared with laminar profiles with blunt trailing edge, as tests of the author on laminar profiles with various trailing-edge angles had demonstrated. The profile of 14-percent thickness shows an S-shape camber line far toward the rear which made it possible to keep c_{mo} low, without considerable forward shifting of the transition point on the upper surface.

$c_{w_{min}}$ was determined for various Re by means of the momentum method. (See fig. 7.) The pressure distributions p/q_0 along the chord and the position of the transition point can be seen from figures 4 and 5.

The pressure distributions of both profiles are flat. Pressure increase and transition occur far toward the rear, thus causing low $c_{w_{\infty \min}}$. For larger $Re (> 2 \times 10^6)$ the drag is increased by the influence of the tunnel turbulence which is caused by the more rapid forward moving of the transition point due to an external turbulence (fig. 8). Verifying calculations of the profile drag for $Re = 2 \times 10^6$ on laminar profiles of various thicknesses for the positions of the transition point, which had been experimentally determined, gave the following result: The drag increase with the profile thickness is primarily due to earlier transition for a larger profile thickness, only secondarily to higher form drag and increased skin friction because of the higher superstream velocities for thicker profiles.

In order to test suitable landing aids and ailerons for laminar profiles, three-component measurements were performed for a laminar profile of 14-percent thickness (fig. 12) on a rectangular wing of $b = 1.50$ meters span and $t = 0.250$ meter chord. (The wing ends seen from the front were rounded off semicircularly.) Figure 13 shows the landing aids investigated in retracted condition. A Fowler flap C of a chord of $0.348 t$ which extended over the entire span was used as landing aid. It extends somewhat beyond the main wing toward the rear and hence makes possible the attachment of a trailing-edge aileron D of $0.125 t$ chord which also extends over the entire span. For standard flight conditions, this aileron serves as twist with resulting small flap control moments whereas for low-speed flight the extended Fowler flaps could assume the lateral control, perhaps in combination with the trailing-edge aileron. In this manner the Fowler flap may be constructed so as to extend over the entire span.

A further $c_{a_{\max}}$ -increase for extended Fowler flaps could be obtained by additional use of the trailing-edge aileron D, by extending of slats B and A at the Fowler flap C and at the main profile. The retracted front slat A would cause, under standard flight conditions, an early turbulence of the boundary layer on the upper wing surface, in order to avoid this, the slat A was built partly into the upper surface of the main wing and thus a smooth surface obtained.

Momentum measurements showed that the profile drag was not measurably increased by the installation of landing aids at $Re = 1.07 \times 10^6$ when the slot between Fowler flap and trailing-edge aileron was sealed. In the full-scale model, probably the grooves between main wing and the two slats also ought to be sealed.

The receding corner on the upper wing surface between main wing and trailing-edge aileron also does not measurably increase the drag in high-speed flight (according to momentum measurements).

COMPILATION OF THE HIGH-LIFT MEASUREMENTS

($Re = (0.70 \text{ to } 0.75) \times 10^6$):

β_F = FOWLER FLAP DEFLECTION,

β_Q = TRAILING-EDGE AILERON DEFLECTION

State	$c_{a_{max}}$
Fowler flap C extended, both slats A and B retracted	(1)
$\beta_F = 52^\circ$, $\beta_Q = 0^\circ$, trailing-edge aileron slot open	2.82
$\beta_F = 52^\circ$, $\beta_Q = 0^\circ$, trailing-edge aileron slot closed	2.79
$\beta_F = 48^\circ$, $\beta_Q = 31^\circ$, trailing-edge aileron slot open	3.12
$\beta_F = 48^\circ$, $\beta_Q = 30^\circ$, trailing-edge aileron slot closed	2.885
Fowler flap C and Fowler flap-slat B extended, slat A at the main wing retracted	
$\beta_F = 69^\circ$, $\beta_Q = 0^\circ$, 15° , trailing-edge aileron slot closed	3.42
$\beta_F = 69^\circ$, $\beta_Q = 18^\circ$, trailing-edge aileron slot open	3.605
Fowler flap C and both slats A and B extended	
$\beta_F = 69^\circ$, $\beta_Q = 0^\circ$, 5° , trailing-edge aileron slot closed	3.93
$\beta_F = 69^\circ$, $\beta_Q = 14^\circ$, trailing-edge aileron slot open	4.05
Fowler flap C and frontal slat A extended, slat B retracted	
$\beta_F = 47^\circ$, $\beta_Q = 0^\circ$, trailing-edge aileron slot closed	3.40
$\beta_F = 47^\circ$, $\beta_Q = 0^\circ$, trailing-edge aileron slot open	3.43
$\beta_F = 44^\circ$, $\beta_Q = 18^\circ$, trailing-edge aileron slot closed	3.49
$\beta_F = 44^\circ$, $\beta_Q = 27^\circ$, trailing-edge aileron slot open	3.68

$l_{c_{a_{max}}}$ is referred to the wing chord for retracted landing flaps.

The effect of the trailing-edge aileron of 12.5-percent t chord was investigated separately for retracted landing aids (three-component and momentum measurements for various control surface deflections β_Q).

c_a and $c_{m_t/4}$ (>0 , α -increasing) were measured for various α by means of three-component measurements, c_{w_c} by momentum measurements 0.15 meter behind the wing at 0.11 meter lateral distance from the wing plane of symmetry. The camber line was chosen as line of reference for α , the point of reference for $c_{m_t/4}$ lies in $t/4$ from the front on this line. The local lift coefficient at the momentum test point was put equal to $1.10c_a$. The Reynolds number in the three-component and momentum measurements was $Re = \frac{U_0 t}{\nu} = 0.80 \times 10^6$ and 1.07×10^6 , respectively. The test results can be seen from figures 14 to 16.

Owing to deflection of the trailing-edge aileron extending over the entire span, a favorable envelope polar with low profile drags results for standard flight conditions in a considerable c_a -range. (See fig. 14.)

The transition-point position in the optimum c_a -range is only slightly shifted forward by moderate deflections of this narrow control surface (observations by stethoscope). At the receding corner on the upper wing surface between main wing and control surface, a local separation on the upper control surface is avoided in the optimum c_a -range up to $\beta_Q = 20^\circ$ according to observations by stethoscope and tufts, hence, a low profile drag for larger positive control surface deflections is attained.

For $\beta_Q = -5^\circ$ and -10° the boundary layer at the nose of the control surface on the lower wing surface was made artificially turbulent by providing a receding step (fig. 13) in order to avoid a more extensive laminar separation on the bottom of the control surface and to obtain a turbulent readhering.

Observations by stethoscope showed that the boundary layer of the lower wing surface for $\beta_Q \leq -5^\circ$ underwent laminar separation unless the boundary layer was artificially controlled, and would not readhere completely turbulently. Correspondingly, there resulted (according to momentum measurements) relatively large profile drags. By providing the receding step F on the lower surface 23 millimeters ahead of the flap nose, the boundary

layer became turbulent at $Re = 1.07 \times 10^6$ 0 to 5 millimeters behind the latter (according to stethoscope observations) and the profile drag decreased (momentum measurements fig. 14).

The variation of c_a and $c_{m_t}/4$ versus α for various control-surface deflections β_Q can be seen from figures 15 and 16.

By deflection of the trailing-edge aileron c_a undergoes a relatively considerable change which will probably cause rolling moments sufficient for normal-flight conditions. For $\beta_Q = 0^\circ$ the maximum lift without landing aids is $c_{a_{max}} = 1.06$. The angle of attack at the stall is rather larger than for conventional profiles of equal thickness. The lift increase is normal for the optimum c_a -range and decreases sharply for larger α , hence, one can attain rather smaller positive gust loads than for earlier conventional profiles of equal thickness and camber. The zero moment for $\beta_Q = 0^\circ$ is $c_{m_0} = -0.027$ and may be kept arbitrarily small by small negative control surface deflections. The pitching-moment distribution for moderate β_Q probably will be sufficiently uniform.

CHAPTER 4

LAMINAR BOUNDARY-LAYER SUCTION, GENERAL REMARKS

1. Aims for Further Development

The tests of chapter 3 showed that the profile drag can be considerably lowered by a suitable profile shape. With increasing profile thickness the drag will increase relatively strongly, the main reason being the earlier transition for greater profile thickness. Considerably lower drags would be possible by maintaining the boundary layer up to the trailing edge completely laminar. For larger Reynolds numbers very low drags would then result even for thicker profiles. (See figs. 1 and 2.)

Thus the following tests were undertaken which aimed at the development of thicker profiles where, for large Reynolds numbers and in flight, the boundary layer remains laminar up to the trailing edge for a sufficient c_a -range. In order to obtain high Mach numbers without compression shocks, slight maximum superstream velocities are desirable, that is, the pressure distribution is supposed to be uniform far toward the rear.

Boundary-layer suction made it possible to maintain in the present tests the boundary layer completely laminar up to the trailing edge.

2. Effect of Suction of Laminar Boundary Layer
on the Flow Characteristics

The suction of a laminar boundary layer has various effects:

(a) Augmentation of the laminar pressure increase: According to chapter 2, 1, the transition occurs for a weak laminar pressure increase caused by laminar separation of the boundary layer. By elimination of the greatly retarded portion of the boundary layer in the neighborhood of the wall with rising pressure, by means of suction (through separate slots or by area suction) the laminar separation and hence the transition could be avoided even for considerable pressure increases. A favorable effect is created in many cases by the so-called sink effect: The location of suction acting as sink produces in its neighborhood an additional pressure field with accelerated flow. Its superposition on the

external flow at the location of suction results in a steeper pressure increase from the flow conditions immediately ahead of the suction point to the stagnation point behind the suction slot. Hence, the remaining pressure increase along the wall is correspondingly reduced.

(b) Attainment of higher Reynolds numbers $Re = \frac{U_0 t}{\nu}$ with laminar boundary layers: According to chapter 2, 2 (influence of an external turbulence on the transition) one obtains for a given external turbulence with a laminar boundary layer, a maximum critical Reynolds number $Re_{\theta, \text{critical}} = \left(\frac{U\theta}{\nu} \right)_{\text{critical}}$ (U = velocity at the edge of the boundary layer.) Since the increasing of θ and Re_{θ} , respectively, along the chord can be reduced by boundary-layer suction, it should be possible to obtain higher $Re = \frac{U_0 t}{\nu}$, for equal admissible maximum Reynolds numbers $Re_{\theta, \text{critical}}$.

(c) By boundary-layer suction and reacceleration of the suction air to free-stream velocity, a part of the relatively large kinetic wake energy of the laminar boundary layer can be recovered and the power required for propulsion can thus be reduced. Professor Ackeret (reference 65) was the first to point out the possibility of reducing the power required for propulsion of airplanes by utilization of the kinetic wake energy.

(d) With the aid of boundary-layer suction the boundary layer could be maintained completely laminar for a larger range of angle of attack in spite of the occurring greater pressure increases which would extend the c_a -range with low drag.

3. Statement of the Problem

A boundary layer on thicker profiles for larger Reynolds number kept completely laminar with the aid of boundary-layer suction is equivalent to the maintenance of laminar boundary layer for high Re with simultaneous strong pressure increase. In order to obtain lowest possible drags the losses in the suction-slots must be reduced. The boundary layer continuing behind the suction slots is not to be additionally disturbed by the suction itself.

Besides, the customary stipulations for wings must be observed. (See chapter 3 and 4.)

A wing with laminar boundary-layer suction of equal strength and rigidity should not become much heavier than customary wings without suction.

In carrying out the tests the problems connected with laminar boundary-layer suction were at first investigated separately, step by step, and then gradually combined. The test sequence was as follows:

1. Test with laminar boundary-layer suction on a slightly cambered profile of 6.75-percent thickness with a single suction slot in 77 percent t from the leading edge on the upper surface to investigate the basic aptitude of boundary-layer suction for maintaining a boundary-layer laminar (chapter 4, 4).

2. Study of the laminar pressure increase with boundary-layer suction in separate slots for smaller to medium Reynolds numbers Re (chapter 5).

3. More detailed investigation of the flow in the suction slots for laminar boundary-layer suction (slot losses, sink effect, slot flow, etc.) (See chapters 5 and 6.)

4. Test for obtaining higher Reynolds numbers with laminar boundary layers with the aid of boundary-layer suction for intentionally small external pressure increase and normal wind-tunnel turbulence (chapter 7, Tests on a Thin Symmetrical Profile with Suction).

5. Investigations of the laminar boundary-layer suction for larger pressure increase and higher Reynolds numbers on a slightly cambered profile of 10.5-percent thickness with conventional thickness distribution (without extended flat pressure distribution ahead of the pressure rise). (See chapter 8.)

4. History of Development of the Laminar

Boundary-Layer Suction

(a) In 1928 the assumption was expressed for the first time, by B. M. Jones, that a boundary layer might perhaps be maintained laminar for a longer time with the aid of boundary-layer suction which would reduce the frictional drag.

(b) L. Prandtl calculated the laminar boundary-layer development with suction for pressure increase, under the supposition $\lambda_{\text{Pohlhausen}} = -12$ (reference 72, pp. 117 and 118).

(c) Laminar suction tests on a slightly cambered profile of 6.75-percent thickness. The first test, made for the purpose of orientation, on a slightly cambered profile of 6.75-percent thickness with a single suction slot in 77 percent t from the leading edge on the upper surface (autumn 1940 and winter 1940-41) showed that it is possible, by boundary-layer suction, to maintain the boundary layer completely laminar and to obtain low profile drags.

The investigated profile (2) with the suction slot can be seen from figure 17. The wing was mounted between end disks in the wind tunnel of the Institute.

Data:

Chord	$t = 0.451$ meter
Profile thickness	$d/t = 0.0675$ in $0.394 t$ from the leading edge
Nose curvature radius	$R_o/t = 0.0035$

Slot in $0.77 t$ from the leading edge on the upper surface, minimum slot width $s = 1.3$ millimeters and $s = 0.9$ millimeter, slot directed toward the rear at an angle of 45° to the surface.

The suction slot was developed as a diffuser with an 8° opening angle in order to convert part of the kinetic energy of the sucked air into pressure and hence obtain smaller negative pressures in the suction chamber and smaller pressures and power requirements for the suction blower. The development of the suction slot as a diffuser for the purpose of a partial conversion of the velocity energy of the sucked air into pressure was for the first time successfully applied in turbulent suction tests by A. Gerber (reference 69) on a suggestion by Professor Ackeret.

The slot inlet was designed on the basis of a thesis by H. Bleuler, investigated by Professor Ackeret. The slot flow was treated by H. Bleuler as a free jet with constant pressure along the jet edge, under the assumption of frictionless flow.

SYMBOLS

Drag measurements:

t wing chord (0.451 m)

- l slot length (0.324 m)
 F area of reference $\cdot (tl)$ (0.146 m²)
 s minimum slot width
 g_0 undisturbed total pressure outside of boundary layer or wake, measured with atmosphere as reference level
 p_0 static pressure in center of side wall of wind tunnel at beginning of test section, measured with atmosphere as reference level
 q_0 free-stream dynamic pressure, kilograms per meter² ($g_0 - p_0$)
 U_0 free-stream velocity meters per second $\left(\sqrt{\frac{2}{\rho} q_0}\right)$
 p_a static pressure in center of suction chamber, measured compared with p_0 , kilograms per meter²
 Δp_g suction blower pressure, kilograms per meter²
 u_L mean velocity of sucked air perpendicular to wing in suction chamber at location of static pressure measurement
 $\left(u_L = \frac{\text{Suction quantity}}{\text{Cross section of the suction chamber}} \text{ at this location}\right)$
 u_A exit velocity of sucked air rearward in free-stream direction, meters per second
 Q_a suction quantity (m³/s) measured by calibrated venturi nozzle of 17.4 millimeters ϕ at narrowest cross section and 28.0 millimeters ϕ ahead of nozzle
 δ^* displacement thickness ahead of suction slot
 Q_δ^* $U\delta^*l$ where U = velocity at edge of boundary layer ahead of slot
 Re Reynolds number $\left(\frac{U_0 t}{\nu}\right)$
 Drags:
 W_∞ total profile drag decisive for propulsion
 W_∞' drag contribution of wake

W_g drag contribution of suction blower

Dimensionless coefficients:

c_Q suction-quantity coefficient $\left(\frac{Q_a}{U_o F} \right)$

c_{p_g} suction-blower pressure coefficient $\left(\frac{\Delta p_g}{q_o} \right)$

$$c_{p_a} = \frac{p_a}{q_o}$$

c_{w_∞} coefficient of total profile drag $\left(\frac{W_\infty}{q_o F} \right)$

c_{w_∞}' coefficient of drag contribution of wake (determined by momentum measurements in wake) $\left(\frac{W_\infty'}{q_o F} \right)$

c_{w_g} coefficient of drag contribution of suction blower $\left(\frac{W_g}{q_o F} \right)$

Measurements: The static pressure p_a was measured, for various $Re = \frac{U_o t}{\nu}$ and suction quantities Q_a , in the center of the suction chamber (with 0.5 millimeter ϕ pressure holes). Momentum measurements were performed 0.173 meter behind the wing. The slot width s was 1.3 millimeters and 0.9 millimeter. The state of the boundary layer on the upper surface behind the slot was verified with a hot wire (references 21 and 61b), by soot coating and acoustically by stethoscope (reference 61c).

Drag evaluation for boundary-layer suction (compare also O. Schrenk (reference 75)).

Let the sucked air be accelerated, rearward in flight direction to the velocity u_A . The motive power L_g of the suction blower (efficiency η_g) then is

$$L_g = \frac{Q_a \left(\frac{\rho}{2} u_A^2 - p_a - \frac{\rho}{2} u_L^2 \right)}{\eta_g}$$

where

$$\frac{\rho}{2} u_A^2 - p_a - \frac{\rho}{2} u_L^2 = \text{Suction-blower pressure}$$

The kinetic energy $\frac{\rho}{2} u_L^2$ of the sucked air in the suction chamber may still be utilized. Pressure losses in the suction ducts were neglected.

When $u_A \neq U_0$, the sucked air far behind the wing has another momentum than far toward the front; the change of momentum is

$$\Delta J = \rho Q_a (U_0 - u_A)$$

(for $u_A < U_0$, ΔJ signifies drag, for $u_A > U_0$ thrust.

The propulsive power requirement for overcoming the drag contribution of the wake W_∞' and $\rho Q_a (U_0 - u_A)$, will be, if a propeller in flight or installed in a tunnel with the efficiency η_p is provided:

$$L_p = \frac{[W_\infty' + \rho Q_a (U_0 - u_A)] U_0}{\eta_p}$$

The entire power requirement for overcoming of the profile drag becomes:

$$L = L_g + L_p = \frac{Q_a \left(\frac{\rho}{2} u_A^2 - p_a - \frac{\rho}{2} u_L^2 \right)}{\eta_g} + \frac{[W_\infty' + \rho Q_a (U_0 - u_A)] U_0}{\eta_p}$$

Depending on the exit velocity u_A of the sucked air, L is distributed unequally between L_g and L_p . The minimum total power requirement L_{\min} results for $\frac{\partial L}{\partial u_A} = 0$, η_g and η_p may, in the general case, also be functions of u_A . It is now assumed that η_g and η_p are independent of u_A . Then there becomes for

$$\frac{\partial L}{\partial u_A} = 0: \quad \frac{u_A}{U_0} = \frac{\eta_g}{\eta_p}$$

Let furthermore an equal efficiency of propeller and suction blower be assumed: $\eta_g = \eta_p = \eta$.

For L_{min} then $u_A = U_o$ and

$$L_{min} = \frac{Q_a \left(\frac{\rho}{2} U_o^2 - p_a - \frac{\rho}{2} u_L^2 \right) + W_\infty' U_o}{\eta} = \frac{W_\infty U_o}{\eta}$$

that is,

$$W_\infty = \frac{Q_a}{U_o} \left(\frac{\rho}{2} U_o^2 - p_a - \frac{\rho}{2} u_L^2 \right) + W_\infty' = -\frac{Q_a \Delta p_g}{U_o} + W_\infty' = W_g + W_\infty'$$

where

$$W_g = -\frac{Q_a \Delta p_g}{U_o}$$

$\Delta p_g = \frac{\rho}{2} U_o^2 - p_a - \frac{\rho}{2} u_L^2$ = Suction-blower pressure for acceleration of the sucked air to U_o

Under the assumptions given above (equal efficiency of suction blower and propeller, acceleration of the sucked air to U_o toward the rear) one may calculate for the drag evaluation precisely as if the suction blower had a 100-percent efficiency. The total drag coefficient decisive for the propulsion becomes:

$$c_{W_\infty} = \frac{W_\infty}{q_o F} = \frac{Q_a \Delta p_g}{U_o q_o F} + c_{W_\infty}' = c_{Q \Delta p_g} + c_{W_\infty}' = c_{W_g} + c_{W_\infty}'$$

The drag measurements with boundary-layer suction were evaluated according to the above formulas under the assumption that propeller and suction blower have equal efficiency and the sucked air is accelerated rearward in flight direction to U_o . For comparison, the minimum profile drag without suction (suction slot closed) of the profile (2), $d/t = 0.067$ and the profile (1), $d/t = 0.09$ was measured by means of the momentum method.

The measurement results can be seen from figures 18 to 25.

$c_{w_{\infty opt}}(Re)$	with $s = 0.9$ mm	Fig. 18
$c_{w_{\infty min}}(Re)$	without suction	
$c_{w_{\infty}}(c_Q)$	$s = 1.3$ mm	Fig. 19
$c_{w_{\infty}}'(c_Q)$		Fig. 20
$c_{Q_{opt}}(Re)$	$s = 0.9$ mm and $s = 1.3$ mm	Fig. 21
$c_{p_{a_{opt}}}(Re)$		

2 hot-wire photographs with and without suction (figs. 22 and 23).

2 photographs with soot coating (laminar and turbulent) (figs. 24 and 25).

By boundary-layer suction it was possible to maintain, for Reynolds numbers up to $Re = \frac{U_{ot}}{v} = 800,000$ on upper and lower surface a completely laminar boundary layer (hot-wire photographs, figs. 22 and 23, and photographs, figs. 24 and 25 with soot coating, confirmation by stethoscope observations). Generally, only weak and slow laminar velocity fluctuations were ascertainable behind the suction slot.

The laminar pressure increase on the upper surface from the pressure minimum to the trailing edge amounted to 35 percent of the pressure difference between stagnation point and pressure minimum.

The lowest total drag was, with $s = 0.9$ -millimeter slot width for $Re = 0.9 \times 10^6$: $c_{w_{\infty min}} = 0.0035$ (power required for suction included). For smaller Re , $c_{w_{\infty}}$ increased somewhat more slowly than the laminar friction of the flat plate. For larger Re , $c_{w_{\infty}}$ increases again since, owing to the influence of the tunnel turbulence, the transitions on the upper side occur already ahead of the suction slot (as was shown by stethoscope and soot-coating observations). Hence, the boundary layer remains

turbulent behind the slot in spite of increased suction. The drag is definitely larger without suction than with it.

The suction quantities c_q required for keeping the boundary layer laminar were very small particularly for a slot width $s = 0.9$ millimeter; in general only a fraction of the displacement thickness δ^* had to be sucked off the laminar boundary layer ahead of the slot (15 percent to 50 percent for $Re = 0.2 \times 10^6$ to 0.9×10^6). (See fig. 21 $C_{q_{opt}}(Re)$ for $s = 0.9$ mm and $s = 1.3$ mm.) The required minimum suction quantity for a suction slot of the width $s = 1.3$ millimeters was larger than the one for $s = 0.9$ millimeter (fig. 21). If the suction is too weak, a local laminar separation occurs at the suction point and the boundary layer behind the slot becomes rapidly turbulent (according to observations by stethoscope, soot coating, and hot wire). Correspondingly, for very weak suction c_{w_∞} increases again (fig. 19). For an optimum suction quantity $c_{q_{opt}}$ results the lowest drag $c_{w_{min}}$, $c_{q_{opt}}$ increases with increasing Reynolds number (fig. 21). For $c_q > c_{q_{opt}}$ the skin friction increases behind the slot (thinner boundary layer), hence, c_{w_∞} increases with c_q .

In general, the corresponding negative suction pressures $c_{p_{a_{opt}}}$ in the suction chamber were small (fig. 21) although, for laminar suction, the conversion of the velocity energy of the sucked air into pressure in the slot diffuser was not particularly good (compare, later tests).

(d) In connection with these laminar suction tests with a single slot, M. Ras performed, on the suggestion of Professor Ackert, in the Institute for Aerodynamics, Zurich, tests with laminar boundary suction by means of a sort of area suction consisting of 35 narrow slots arranged one after the other. With this area suction one obtained laminar pressure increases of about 53 percent to 55 percent of the pressure difference between stagnation point and pressure minimum for smaller Reynolds numbers (references 66, 67, and 68).

(e) H. Schlichting calculated the laminar boundary-layer development on a flat plate with area suction for constant suction intensity (reference 70). Furthermore, Schlichting calculated recently the laminar boundary-layer development with area suction on a Joukowski profile (reference 71).

CHAPTER 5

INVESTIGATION OF THE LAMINAR PRESSURE INCREASE
WITH BOUNDARY-LAYER SUCTION FOR SMALLER AND
MEDIUM REYNOLDS NUMBERS

1. Laminar Suction Tests with Three Suction Slots

Arranged One After the Other

The suction tests with the laminar profile of 6.75-percent thickness for $Re = 0.8 \times 10^6$, showed a laminar pressure increase of 35 percent with a single suction slot. With area suction a laminar pressure increase of 53 percent to 55 percent was attained. More laminar suction tests were performed with three suction slots lying one after the other in the suction tunnel used by M. Ras with the aim to obtain larger laminar pressure increases with relatively few slots.

Definitions for the suction tests with single slots in the suction tunnel (chapter 5, 1, chapter 5, 2b, 2c, and 2d, chapter 6, 1 and 6, 2).

q dynamic pressure at edge of boundary layer

q_m maximum dynamic pressure at edge of boundary layer at narrowest section of tunnel

$$\frac{q}{q_m} = 1 - \frac{\Delta p}{q_m}$$

Δp static pressure at test plate or at walls of slot diffuser, measured with 0.5 millimeter ϕ bore holes with static pressure at test plate at narrowest place of tunnel as reference level

p_A static pressure in suction chamber, measured with 0.5 millimeter ϕ bore holes with static pressure at test plate at narrowest place of tunnel as reference level

l slot length (0.40 m)

- s minimum slot width
- δ^* displacement thickness ahead of slot (δ^* was calculated every time from measured pressure distribution for mean suction quantity according to Pohlhausen (reference 43)).
- $Q_{\delta^*} = U\delta^*$, with U = velocity at edge of boundary layer ahead of suction slot
- h displacement of slot trailing edge with respect to slot inlet,
h > 0 for inward displacement
- Q_a suction quantity measured with calibrated measuring nozzles
- V_a velocity of sucked air at end of slot diffuser, determined from difference of total g at slot exit (measured with 1.0 mm ϕ total head tube) and static pressure p_a in suction chamber in neighborhood of test point for velocity distribution. (The test arrangement can be seen from fig. 26.)

The flat test plate was provided with three suction slots the shape of which can be seen from figure 27.

The slots were perpendicular to the surface and were developed as diffusers with small opening angle (slot shape a) By adjustment of the opposite wall Nr. V the internal width of the tunnel and the pressure distribution at the test plate could be changed. The boundary layer of the opposite wall also was kept laminar by suction. The width of the test plate and the slot length were 400 millimeters.

The pressure distribution along the test plate was determined for various suction quantities Q_a and tunnel widths. The state of the boundary layer behind the slot was verified by hot wire and stethoscope. The test results can be seen from figures 28 and 29.

At the arrow behind the third slot the boundary layer was still laminar. Considerably larger laminar pressure increases resulted with boundary-layer suction than without it (maximum 63 percent with 40 mm tunnel width).

The sink effect makes an essential contribution to the laminar pressure increase, particularly for stronger external pressure increase. The significance of the sink effect for turbulent boundary-layer suction was pointed out repeatedly (Ackeret, Prandtl, O. Schrenk, Gerber (references 69, 72, 73, 74, and 75)).

2. Tests with Laminar Boundary-Layer Suction with a Single Suction Slot

The purpose of these tests was a more detailed study of the flow phenomena in the neighborhood of a suction slot for laminar boundary-layer suction (sink effect, laminar pressure increase down to the transition; flow in the suction slot and pressure losses in the slot).

(a) Tests with laminar boundary-layer suction in the water tank.- (α) Tests on a single slot: A few laminar suction tests for the purpose of orientation were performed with various slot shapes. The suction slot was placed on a symmetrical profile of 10-percent thickness (at 0.43 t from the leading edge) and $t = 1.21$ m chord at a distance of 0.71 m from the leading edge. The slot was developed as diffuser with small opening angle.

The model was towed through the water with a velocity of 0.1 to 0.2 meter per second. The flow in the region of the suction slot was made visible by sprinkled-on aluminum powder and photographed. (Compare the flow pictures figs. 30 to 34.)

In general, the laminar boundary-layer suction operated faultlessly even for very different slot shapes and suction of various strength. The laminar boundary layer, continuing behind the slot to which no suction was applied, was mostly undisturbed by the suction. The flow in the suction slot separated on one side of the slot.

With increasing suction quantity the slot must be made wider in order to avoid high velocities at the slot exit and correspondingly large slot losses.

For smaller suction quantities the slot width must be reduced since otherwise a local laminar separation occurs at the slot inlet (fig. 31(g)). The tests with the suction wing of 6.75-percent thickness (chapter 4, 4) and later laminar suction tests showed that in such cases the boundary layer behind the slot became rapidly turbulent (observation by stethoscope). Due to outward curvature of the profile surface ahead of the suction slot (fig. 31) and a stronger local pressure increase ahead of the slot, a laminar separation may occur for weak suction; thereby the boundary layer behind the slot also becomes rapidly turbulent. Forward-curved suction slots (figs. 30(e), 30(f), 31(a), 31(b), and 31(c)) are especially sensitive in this respect.

In a few cases the slot trailing edge was shifted various degrees toward the outside and the inside, respectively. (See figs. 30(c), 31(d), and 31(e).)

A too great inward shifting may eventually also lead to a local laminar separation at the slot inlet (fig. 38) and thus render the laminar suction ineffective. (See later tests chapter 5, 2 test F with slot (b) with $h = 1.3$ mm inward shifting.)

(β) A test with several narrow suction slots placed one after another (a sort of area suction) shows how the laminar boundary layer oozes into the wing interior (fig. 32).

(γ) On a thin symmetrical profile, suction was applied to the laminar boundary layer at the trailing edge of the wing. The first suction tests were performed without a partition wall in the suction slot and gave a negative result: for starting conditions a stagnation point originated in the free stream behind the suction point which traveled at the slightest disturbance toward one or the other wing side. (See fig. 33(b).)

By means of a partition wall in the slot, the rear stagnation point was fixed on that wall. (See figs. 33(a) and 33(c).)

The boundary layer behind the slot was mostly very thin.

By rotation of the partitioning metal sheet and by suction of different magnitude on upper and lower surface one may shift the rear stagnation point and thus (as remarked by Professor Ackert) change the circulation around the wing.

The laminar suction of the trailing edge is very sensitive to the shape of the wing surface shortly ahead of the slot. For a slot inlet which is too round the boundary layer ahead of the slot undergoes a laminar separation; if the inlet is too pointed there result large negative pressures at the slot inlet, high velocities in the suction slot, and large slot losses.

(δ) Another test with laminar boundary-layer suction was performed in the water tank with a slotted flap wing of chord $t = 0.61$ m ($d/t = 0.153$). The boundary layer could be maintained completely laminar by means of suction on main wing and flap for various flap deflections (fig. 34). The Reynolds number was $Re_t \approx 100,000$ to $120,000$.

(b) Laminar suction tests with the slot (a) (see fig. 27 and for definitions see beginning of chapter 5). - With the test apparatus used for the laminar suction tests with three slots (chapter 5, 1), laminar suction tests with only the suction slot farthest to the front were performed (slot shape(a)). The test plate was plane. Suction was applied over the width of the tunnel of 400 millimeters.

The pressure distribution on the test plate was measured, with the minimum slot width s , suction quantity Q_a , tunnel width and free-stream velocity being varied. The trailing edge of the slot could be adjusted at different heights with respect to the slot inlet (displacements $h > 0$ for inward shifted trailing edge of the slot).

The influence of the suction quantities Q_a and Q_a/δ^* , respectively, (δ^* = displacement thickness ahead of the slot) of the slot width and of the shifting of the slot trailing edge on the sink effect were investigated. Figures 35 and 36 show a few pressure distributions on the test plate in the region of the suction slot. In the investigated cases, the boundary layer remained laminar behind the slot (according to stethoscope observations).

The laminar pressure increase due to sink effect increases with growing suction quantity Q_a and increasing inward shifting of the slot trailing edge and vice versa, whereas a change in the slot width produces practically no effect. With increasing slot width, stronger suction must be applied in order to avoid a local laminar separation at the suction point and a rapidly becoming turbulence of the boundary layer behind the slot (according to stethoscope observations).

The measured laminar pressure increase due to sink effect is considerably larger than it would be under the assumption of frictionless flow; by the boundary-layer suction the displacement thickness δ^* becomes suddenly smaller behind the suction slot, and, correspondingly, the effective surface (at the distance δ^* from the wall) is shifted nearer toward the wall. With an effective surface of such wavy development a stronger local pressure increase would result as shown in respective calculations by A. Betz (reference 77) and pressure-distribution measurements at transition due to external pressure increase, where the displacement thickness also decreases suddenly. (See figs. 3, 4, 5, etc.) By superposition of a sink at the suction point, there originates a considerably larger pressure increase due to sink effect than for frictionless flow. By inward or outward shifting

of the trailing edge of the slot this effect may be still increased or decreased.

In further measurements (c) the attempt was made to increase the laminar pressure increase, due to sink effect, still further by wavy development of the wall in the neighborhood of the suction point, particularly for larger suction quantities Q_a/Q_{S*} . It is true that the required minimum suction quantities, for which the boundary layer behind the suction slot still remains completely laminar, will probably increase: the slowest boundary layer parts to which no suction was applied can be retarded at the most to the velocity zero at the stagnation point behind the slot. For larger external pressure increase (for instance, due to stronger sink effect because of waviness of the surface at the suction slot) and for smaller suction quantities sometimes a strong local pressure increase and a rapid transition of the boundary layer occurs behind the slot. (See later measurements: fig. 39, test 8A, fig. 40, test 160.9.)

(c) Investigation of the suction slot (b) with the test plate (b) for laminar boundary-layer suction.- The form of the test plate (b) and the suction slot (b) can be seen from figures 37 and 38. (See beginning of chapter 5 for definitions.)

The slot (b) was perpendicular to the surface and was also designed as diffuser with small opening angle. The external pressure distribution could be varied by adjustment of the opposite wall V, the boundary layer of which was maintained laminar by suction. To the test plate, suction was applied over the tunnel width of 400 millimeters.

The pressure distribution at the test plate and the transition-point position were determined for various suction quantities Q_a and Q_a/Q_{S*} , respectively, for various free-stream velocities and tunnel widths.

The transition-point position evidenced by the break in the pressure-distribution curve which in turn was caused by the sudden reduction in displacement thickness due to the transition, was also determined from observations by stethoscope.

At the transition, considerable fluctuations in static pressure could be ascertained by means of a sensitive manometer.

The results of the pressure distribution and transition measurements can be seen from the figures 39 to 44.

The experiences described in the last section with regard to sink effect were confirmed: increase of the laminar pressure increase, due to sink effect, with growing suction quantity Q_a and Q_a/Q_{δ^*} , respectively, and with increasing inward shifting of the trailing edge of the slot, and vice versa. An excessive inward shifting ($h = 1.3$ mm) did not augment the sink effect any further.

Higher laminar pressure increases due to sink effect result for larger external pressure increase (40-mm tunnel width) than for 80-millimeter tunnel width; however, the minimum suction quantities Q_a/Q_{δ^*} were increased.

With increasing Reynolds number, the pressure increase due to sink effect decreases slightly and vice versa, for equal suction quantity Q_a/Q_{δ^*} (compare figs. 40 and 41).

$$\begin{cases} q_m = 16.3 \text{ kg/m}^2 \\ q_m = 32.6 \text{ kg/m}^2 \end{cases} \quad \text{Fig. 39,} \quad q_m = \begin{cases} 8.15 \text{ kg/m}^2 \\ 16.28 \text{ kg/m}^2 \end{cases}$$

The sink effect is increased by the waviness of the surface in the region of the suction slot. Of course, as was to be expected, larger minimum suction quantities Q_a/Q_{δ^*} are required to maintain a laminar boundary layer behind the slot.

The total laminar pressure increase up to the transition point is, generally, considerably larger than without suction. It increases with growing suction quantity as well as with rising external pressure increase (comparison of the tests with 40-mm and 80-mm tunnel width).

For equal Q_a/Q_{δ^*} the transition occurs earlier with growing Reynolds number, similar to the case without boundary-layer suction (compare fig. 40 and 41)

$$q_m = 16.3 \text{ kg/m}^2 \text{ and } 32.6 \text{ kg/m}^2$$

also figure 39

$$q_m = \begin{cases} 8.15 \text{ kg/m}^2 \\ 16.3 \text{ kg/m}^2 \end{cases}$$

By inward shifting of the trailing edge of the slot (stronger sink effect), the laminar pressure increase before the transition is slightly augmented and vice versa, under the assumption of equal suction power.

Tests 14 with $h = 0.9$ to $h = -0.3$ see fig. 42

Tests 17 with $h = 0.9$ and $h = -0.3$ see figs 40, 43

Tests 18 with $h = 0.9$ and $h = -0.3$ see figs. 40, 43

An excessive inward shifting of the trailing edge of the slot ($h = 1.3$) deteriorates the laminar pressure increase again (figs. 42 and 44).

Increasing of the sink effect and the laminar pressure increase by a slightly wavy formation of the surface in the region of the suction slot, similar to the form of the test plate (b), is useful probably only for larger suction quantities Q_a/Q_{s*} ; it is less so for smaller ones.

(d) Laminar suction tests with slot (b) and test plate (d)
(See fig. 37.) - By increasing the waviness in the region of the suction slot (b) (see form of the test plate (d)) the sink effect and the laminar pressure increase before the transition was augmented still further for stronger suction; see the pressure distribution at the test plate (fig. 45).

Of course, still larger minimum suction quantities than for slot (b) with test plate (b) are required in order to keep the boundary layer behind the slot completely laminar.

Further laminar suction tests with the single slot (g) (fig. 46) gave similar results (fig. 47).

The suction tests with the plate (d) showed that a boundary layer for a flow around a slightly protruding corner may be maintained laminar by means of the boundary-layer suction, if a suction slot is placed in the corner.

Summary Regarding Laminar Pressure Increase with Boundary

Layer Suction for Small up to Medium Reynolds Numbers

For small up to medium Re ($N = 1/3 R_{\delta^*}^2$ ahead of the slot varied between 0.4 and 0.8×10^6) laminar boundary-layer suction makes high laminar pressure increases with relatively few suction slots possible; generally, only a fraction of the respective displacement thickness δ^* ahead of the slots must be sucked off.

In most cases the sink effect makes a considerable contribution toward the laminar pressure increase. For larger suction quantities Q_s/Q_{δ^*} , an augmenting of the pressure increase due to sink effect by suitable shaping of the surface is useful; it is less so for small ones.

CHAPTER 6

INVESTIGATION OF THE SLOT FLOW FOR LAMINAR BOUNDARY-
LAYER SUCTION WITH SINGLE SLOTS

1. Laminar Suction Tests with Straight Suction Slot

The test apparatus for the tests of chapter 6 was the same as for the tests of chapter 5.

(a) Tests with slot (a) (see fig. 27 and for definitions see beginning of chapter 5)..- The test plate was plane. Suction was applied over the tunnel width of 400 millimeters.

Measurements: The static pressure in the suction tank was measured for various suction quantities Q_a and Q_a/Q_{δ^*} , respectively, (δ^* = displacement thickness ahead of the slot), slot widths s and stagnation pressures or Reynolds numbers, respectively. Furthermore, the trailing edge of the slot was made to shift to various extents outward or inward with respect to the slot inlet. The distribution of the static pressure in the suction chamber with the varying suction quantity can be seen from figures 48 to 53.

With growing suction quantity, the negative pressure in the suction tank increase. For larger Re , the suction quantity Q_a/Q_{δ^*} being equal, they are smaller; the same holds true for wider suction slots.

If the trailing edge of the slot is shifted inward, larger negative pressures result at the slot inlet and in the suction tank due to the stronger sink effect. Inward or outward shifting of the trailing edge of the slot causes, conditions otherwise being equal, only unessential changes in the pressure difference between suction chamber and the place directly ahead of the suction slot.

In order to obtain a uniform suction along the span, the slot width and the extent of the inward or outward shift of the trailing edge of the slot along the span must, as far as possible, remain constant. If the trailing edge of the slot is somewhere shifted further inward, less air is sucked there; sometimes this fact may cause a local laminar separation shortly ahead of the slot; also, the boundary layer behind the slot may become rapidly turbulent at that location, as was shown in observations by stethoscope

(confirmed in the laminar suction tests of chapters 7 and 8). From the point of transition a turbulent wedge spreads toward the rear in the usual manner. If the slot is slightly narrower in some place, less boundary-layer air is sucked there. The laminar boundary layer behind the slot then thickens; sometimes an earlier turbulence^c may occur, unless the preceding or the following slot is widened accordingly.

(b) Tests with slots (b), test plate (b) (figs. 37 and 38).-
The static pressures in the suction tank and along the slot diffuser were measured, together with the velocity distribution at the slot exit for various suction quantities, slot widths, and stagnation pressures.

Other conditions being equal, practically the same pressure differences between suction chamber and the place directly ahead of the slot resulted as for the slot (a).

By lengthening the slot diffuser from 16 millimeters to 24 millimeters, the negative pressure in the suction tank was slight reduced and the pressure increase in the slot diffuser slightly augmented (fig. 54; see also later tests with suction slot curve rearward, chapter 6, 3).

For a slot width of $s = 0.8$ mm and $q_m = 16.3$ kg/m², a weak uniform pressure increase occurs in the slot diffuser which increases with growing suction quantity (fig. 54).

The velocity distributions at the slot exit for slot width $s = 0.83$ mm, $q_m = 8.15$ kg/m², 16.3 kg/m², 32.6 kg/m², and various suction quantities can be seen from figures 55 to 57.

For weak suction the velocity distribution at the slot exit is laminar with a weak reverse flow on the front side of the slot. For stronger suction the slot flow separates on the rear side of the slot and the suction air flows, at a relatively high velocity, into the suction tank near the front side of the slot. Accordingly, the conversion of the kinetic energy of the suction air into pressure is not particularly favorable in the slot diffuser (see figure: Distribution of the static pressure in the slot diffuser). The minimum slot losses result for small suction quantities Q_a/Q_{δ^*} ; suction is applied only to the innermost slowest parts of the boundary layer.

The conversion of the velocity energy of the suction air into pressure in the slot diffuser would improve if the slot flow would

^cThis fact was, in cases of inaccurately adjusted suction slots, established by observation by stethoscope repeatedly.

readhere turbulently before the end of the slot and the velocity distribution at the slot exit would become uniform. Further laminar suction tests with the slot (b) showed that this aim was attained by increased slot width, larger suction quantities, and stagnation pressures, that is, for larger Reynolds numbers, referred to the slot flow (tests K, L, $s = 1.3$ -mm slot width, $q_m = 32.5 \text{ kg/m}^2$).

The velocity distribution at the slot exit was for $s = 1.3 \text{ mm}$ and $q_m = 32.5 \text{ kg/m}^2$ relatively uniform. (See fig. 58.)

The transition-point position behind the slot shows that the boundary layer ahead of and behind the slot was laminar.

The pressure distributions along the slot diffuser (fig. 59) show at the presumable transition point of the slot flow a rapid pressure increase and strong fluctuations in the static pressure, similarly to the conditions found at the transition of a laminar boundary layer for increasing pressure.

For $s = 1.3$ -mm slot width and $q_m = 32.5 \text{ kg/m}^2$, the slot losses and negative pressures in the suction tank are slight. (See fig. 60.)

Summary Regarding the Losses in the Straight Suction Slot

for Laminar Boundary Layer Suction

Design of the suction slots as diffusers will make it possible to convert part of the kinetic energy of the suction air in them into pressure. For weak suction or small Reynolds numbers, the slot flow separates and the pressure increase in the slot diffuser is correspondingly small. For stronger suction, wider slots and higher stagnation pressures, that is, for larger Reynolds numbers of the slot flow, it becomes turbulent and adheres, thereby causing a considerable pressure increase in the slot diffuser. The slot losses then become low.

2. Investigation of the Slot Flow for Laminar Boundary-

Layer Suction with the Suction Slot (i) Curved

Forward (Definitions, See Beginning of Chapter 5)

With the suction slot (i) curved forward (see fig. 38), laminar suction tests were performed in the same manner as with slot (a).

and (b). The static pressure in the suction tank and the velocity distribution at the slot exit were determined.

The velocity distributions at the slot exit for $s = 1.45$ -mm slot width and $q_m = 32.7 \text{ kg/m}^2$ and the corresponding static pressures in the suction tank for various suction quantities can be seen from the figures 62 and 63.

For weak suction, that is, smaller Re of the slot flow, the slot (i) behaved like the straight slot (a) or (b).

For stronger suction, that is, larger Re of the slot flow, the flow continued in the investigated cases on the front side of the slot flow under laminar separation; accordingly, the resulting slot losses and negative pressures in the suction tank were larger than for the straight slot (a) or (b).

The transition of the slot flow is probably retarded by the stabilizing effect of the outward curved front side of the slot.

3. Investigation of the Slot Flow for Laminar

Boundary-Layer Suction with the Rearward

Curved Suction Slot (h)

On the basis of the laminar suction tests with straight and forward curved suction slots, one may assume that the slot flow for a rearward curved suction slot (h) (fig. 64) becomes sooner turbulent than for the straight slot, due to the concave curvature of the front side of the slot. A laminar boundary layer for concave or convex curvature becomes turbulent sooner or later, respectively, than on a plane surface; measurements by F. and M. Clauser (reference 33) and M. Fauconnet at the Institute for Aerodynamics, E. T. H. Zurich (not yet published) demonstrated this fact.

In order to examine the assumption above, laminar suction tests were performed with a single rearward curved suction slot (h) (fig. 64) which was located on the bottom of a slightly cambered profile of 10.5-percent thickness (chapter 8). The suction slot was placed at a distance of 0.73 meter from the wing nose. Provisions were made for auxiliary suction on both sides of the test suction, which had a length of 0.18 meter.

Measurements: The static pressure p_a in the suction tank and p on the front side of the suction slot were measured for

various stagnation pressures and suction quantities for $s = 1.0$ -mm and $s = 1.25$ -mm slot width, with the wing angle of attack remaining constant. p_a and p were ascertained by means of 0.5-millimeter ϕ pressure holes with the static pressure p_0 as reference level (see chapter 8, determination of U_0).

The distribution of the static pressure ahead of the slot and in the slot diffuser for various slot widths, stagnation pressures, and suction quantities $Q_a/Q\delta^*$ can be seen from figures 66 to 72. δ^* = boundary layer displacement thickness ahead of the suction slot calculated according to Pohlhausen from the measured pressure distribution (fig. 65).

The static pressure increased sharply at the presumable transition point in the straight rear part of the slot diffuser; adjoining, a further weak pressure increase took place. Lengthening of the slot diffuser proved generally favorable.

The pressure increase in the slot diffuser and hence the conversion of the kinetic energy of the suction air into pressure are for the slot (h) superior to those for the straight slot (a) or (b), particularly for smaller Re of the slot flow. Correspondingly, the resulting negative pressures in the suction tank are smaller. (See figs. 73 and 74.)

CHAPTER 7

TESTS ABOUT KEEPING A BOUNDARY LAYER FOR HIGH REYNOLDS
NUMBERS LAMINAR WITH THE AID OF BOUNDARY-LAYER SUCTION

1. Purpose of the Tests

The purpose of the tests is study of the laminar boundary-layer development with suction for larger Reynolds numbers, normal wind-tunnel turbulence and - at first - slight external pressure increase on a symmetrical profile of 3.35-percent thickness for zero angle of attack (profile shape see fig. 75(a)). The laminar boundary layer was sucked off through eight consecutive slots.

Furthermore, the problem had to be investigated, whether one could attain, for similar external pressure distribution, equal maximum Reynolds numbers for laminar flow Re_0 or Re_0^* referred to the momentum loss or displacement thickness with or without boundary-layer suction.

2. Test Apparatus

The wing, constructed of wood of $t = 2.032$ m chord, was erected vertically in the closed wind-tunnel test section. The span was equal to the height of the test section (2.12 m). For reasons of measuring technique, suction was applied to one wing surface only; the comparison for conditions without suction was gained from the measurements on the opposite side without suction.

The suction slots I - VIII may be seen from the slot drawing 76. They are straight and have a rearward inclination of 60° .

As before, they were designed as diffusers with small opening angle. In order to intensify the sink effect, the surface was made slightly wavy in the slot region, according to the tests of chapter 5 (fig. 76). In the first tests the waviness was exaggerated; consequently, the boundary layer remained laminar only with very strong suction. Slot width and relative position of slot inlet and slot trailing edge were adjusted along the span as constant as possible.

The laminar boundary-layer development with suction was investigated at the wing center, the location of the suction slots

with the pertinent suction chambers (fig. 75(b)). Auxiliary suction laterally to the test suction made it possible to keep the boundary layer in the entire test section laminar.

Suction was applied separately through each suction slot. The appertaining auxiliary suction were adjusted in the best possible agreement with the test slots. The length of the test suction slots was for the slots I - VI 0.620 meter, for the slots VII, VIII 0.208 meter. All suction chambers are conical and at an angle to the wing and have an amply dimensioned cross section. Hence the pressure losses in the suction chambers are slight and the suction along the span uniform. The suction quantity for each test suction slot was determined by calibrated measuring nozzles which were attached to the lower end of the respective suction chamber. The measuring nozzles used may be seen from figure 75(c). They were calibrated by measurement of the velocity distribution at the nozzle end by means of a flat total-head tube of 0.12-millimeter by 2-millimeter inner opening and 0.2-millimeter outer height and of a 1.0-millimeter ϕ static pressure tube; the two lateral 0.4-millimeter ϕ test holes of the latter were at a distance of 9 millimeters from the semicircular head and of 90 millimeters from the sting (2 mm ϕ). Nozzle diameter d in the cylindrical part: for the slots I - VI (d) = 17 mm, for VII, VIII d = 13 mm. The static pressure in the suction chambers was measured at their lower end at sufficient distance from the measuring nozzles. The suction air was guided through ducts (hose) from the measuring nozzles to the suction ventilator. The suction quantity of the slots was adjusted by throttling of these hose and by varying the rpm of the ventilator.

3. Measurements

I. Suction side:

1. Pressure distribution along the wing chord, measured by static pressure holes of 0.5 millimeter ϕ up to the slot VIII, from there to the trailing edge with 1.0-millimeter ϕ static-pressure tube⁴

2. Suction quantity of the eight test suction slots, measured with 17-millimeter ϕ nozzles for the slots I to VI and with 13-millimeter ϕ nozzles for the slots VII and VIII

⁴The static pressure tube of 1.0 millimeter ϕ used here was built like the one used for the calibrations of the measuring nozzles. Control measurements with connecting pressure holes showed that the static pressure p/q_0 had been measured within an accuracy of ± 0.005 .

3. Static pressure in the eight test suction chambers, measured with 0.5-millimeter ϕ pressure orifices

4. Boundary-layer profile at the point G 9 millimeters behind the slot VIII in 1.790 meters distance from the wing nose

5. Transition-point position by stethoscope and from the break in the pressure-distribution curve at transition

The suction was regulated in such a manner that the boundary layer remained laminar as long as possible with a minimum of total suction power. The measurements were performed for various Reynolds numbers and, accordingly, different suction quantities. Some measurements were repeated with wider suction slots.

TABLE ON SLOT WIDTHS

Slot	Tests 8 to 37, 19*	Tests 38 to 71, 14*, 62*
I	s = 0.5 to 0.55 mm	s = 0.65 mm
II	s = 0.30 mm	s = 0.35 mm
III	s = 0.36 mm	s = 0.40 to 0.45 mm
IV	s = 0.45 to 0.48 mm	s = 0.45 to 0.50 mm
V	s = 0.35 to 0.4 mm	s = 0.4 mm
VI	s = 0.4 to 0.45 mm	s = 0.4 to 0.45 mm
VII	s = 0.38 to 0.4 mm	s = 0.4 mm
VIII	s = 0.3 mm	s = 0.35 mm

II. Opposite wall without suction

1. Boundary-layer profile at the trailing edge for various Re
2. Transition measurement by stethoscope for various Re

The boundary-layer profile at the point G on the suction side was measured by means of a flat total-head tube of 0.12-millimeter by 2-millimeter inner opening and 0.2-millimeter outer height from the side where no suction was applied. By a micrometer the wall distance of the static tube could be adjusted within an accuracy of 0.01 millimeter. The static pressure at the point G was measured by a 0.5-millimeter ϕ pressure hole which was located next to the total-head tube.

The boundary-layer profile at the trailing edge of the opposite wall, to which no suction had been applied, was determined by measurement of the total head and the static pressure by means of a total-head tube and a static-pressure tube; the profile drag of the opposite side without suction calculated for both wing surfaces, results therefrom according to known methods (Squire-Young, RM 1838 (reference 4)).

4. Symbols and Evaluation of the Suction Tests

Symbols

t wing chord (2.032 m)

b span of test suction, for slots I to VI: b = 0.620 m, for VII, VIII: b = 0.208 m, area of reference

- F projected area of wing (bt)
- g_0 undisturbed total head outside of boundary layer or wake, measured with respect to atmosphere, kilograms per meter²
- p_0 static pressure in center of one of side walls at beginning of closed test section, 0.90 meter ahead of wing nose, kilograms per meter²
- q_0 free-stream dynamic pressure, kilograms per meter² ($g_0 - p_0$)
- U_0 free-stream velocity $\left(\sqrt{\frac{2q_0}{\rho}}\right)$
- p static pressure at surface of profile, measured with respect to p_0 , kilograms per meter²
- p_a static pressure in suction chambers, measured with respect to p_0 , kilograms per meter²
- Δp_g suction-blower pressure, for acceleration of suction air to U_0 , kilograms per meter²
- u_L mean air velocity in suction chamber at angle to wing at point of static-pressure measurement, meters per second
- u velocity in boundary layer or wake, meters per second
- U velocity at edge of boundary layer or wake, meters per second
- Displacement thickness $\delta^* = \int_0^\delta \left(1 - \frac{u}{U}\right) dy$, with y = wall distance
- δ total boundary-layer thickness
- Momentum-loss thickness $\theta = \int_0^\delta \left(\frac{u}{U}\right) \left(1 - \frac{u}{U}\right) dy$
- $H = \frac{\delta^*}{\theta}$
- θ_∞ momentum loss thickness of one of wing sides far toward rear at static pressure p_0
- $Re = \frac{U_0 t}{\nu}$
- $Re_\theta = \frac{U\theta}{\nu}$

Q_{a_i} suction quantity of different test suction slots (i) = I to VIII
for one wing side

W_{∞} total profile drag significant for propulsion

W_{∞}' drag contribution of wake

W_g drag contribution of suction blowers

Dimensionless coefficients:

Suction-quantity coefficient of the slot

$$ic_{Q_i} = 2 \frac{Q_{a_i}}{U_0 F}$$

calculated for both wing surfaces.

Total suction-quantity coefficient for both wing surfaces:

$$c_{Q_t} = \sum_{i=1}^{VIII} c_{Q_i}$$

Suction blower-pressure coefficient

$$c_{p_{g_i}} = \frac{\Delta p_{g_i}}{q_0}$$

$$c_{W_{\infty}} = \frac{W_{\infty}}{q_0 F}, \quad c_{W_{\infty}'} = \frac{W_{\infty}'}{q_0 F}, \quad c_{W_g} = \frac{W_g}{q_0 F}$$

The drags and coefficients, respectively, were calculated for both wing surfaces.

Evaluation of the Suction Tests

For evaluating the drag, one assumes that the suction blowers (efficiency η_g) accelerate the suction air to the free-stream velocity U_o in flight direction toward the rear. A propeller (in flight or installed in the tunnel) (efficiency η_p) is pre-supposed for overcoming the drag contribution of the wake. The efficiencies of the suction blowers and of the propeller are to be equal: $\eta_g = \eta_p = \eta$.

Then the total profile drag significant for the propulsion becomes, according to chapter 4, 4(c)

$$W_{\infty} = 2 \sum_{i=1}^{VIII} \left[\frac{Q_a}{U_o} \left(\frac{\rho}{2} U_o^2 - p_a - \frac{\rho}{2} u_L^2 \right) \right]_i + W_{\infty}' \quad (1)$$

$$= 2 \sum_{i=1}^{VIII} \left(\frac{Q_a}{U_o} \Delta p_g \right)_i + W_{\infty}' \quad (2)$$

where

$$\Delta p_g = \frac{\rho}{2} U_o^2 - p_a - \frac{\rho}{2} u_L^2 \quad (3)$$

The factor 2 in the first term stems from the fact that Q_a was measured for one wing side only.

Dimensionless:

$$c_{W_{\infty}} = \frac{W_{\infty}}{q_o F} = \sum_{i=1}^{VIII} \left(\frac{2Q_a}{U_o F} \frac{\Delta p_g}{q_o} \right)_i + c_{W_{\infty}}' \quad (4)$$

where

$$c_{W_{\infty}}' = 2 \frac{2\theta_{\infty}}{t} = \text{drag contribution of the wake} \quad (5)$$

(θ_{∞} for one wing side)

With the suction-quantity coefficient

$$c_{Qi} = \frac{2Q_{a_i}}{U_o F} \quad (6)$$

and the suction blower-pressure coefficient

$$c_{p_{gi}} = \frac{\Delta p_{gi}}{q_o} \quad (7)$$

there becomes:

$$c_{w_{\infty}} = \sum_{i=1}^{VIII} c_{Qi} c_{p_{gi}} + c_{w_{\infty}}' = c_{w_g} + c_{w_{\infty}}' \quad (8)$$

where

$$c_{w_g} = \sum_{i=1}^{VIII} c_{Qi} c_{p_{gi}} = \text{drag contribution of the suction blowers} \quad (9)$$

In order to determine $c_{w_{\infty}}$ the drag contributions c_{w_g} of the suction blowers and $c_{w_{\infty}}'$ of the wake were ascertained.

c_{w_g} : For the various tests, the values c_{Qi} and $c_{p_{gi}}$ of the slots I to VIII were determined according to (6), (7), (3) and hence c_{w_g} according to (9). $\rho/2u_{\infty}^2$ was in most cases negligibly small compared to $\rho/2U_o^2 - p_a$.

In order to determine $c_{w_{\infty}}' = \frac{4\theta}{t}$, θ_{∞} was ascertained as follows:

The boundary-layer profile was measured at station G 9 millimeters behind the slot VIII at a distance of 1.790 meters from the front.

From G on, the laminar boundary-layer development (momentum-loss thickness θ and $Re_\theta = \frac{U\theta}{\nu}$ was calculated with the measured pressure distribution up to the experimentally determined transition point according to Falkner and Howarth (references 45, 46 and 48)). At the transition point θ was assumed constant. From the transition to the trailing edge θ was determined by means of a method of differences according to Squire-Young (reference 4); a wall shearing stress τ_o equal to the one of the turbulent flat plate without pressure gradient for equal $Re_\theta = \frac{U\theta}{\nu}$ (U = velocity at the boundary-layer edge) and with $H = \frac{\delta^*}{\theta} = 1.40$ = constant was presupposed:

$$\frac{d\theta}{ds} = \frac{\tau_o}{\rho U^2} - \frac{U'}{U} \theta (H + 2) \quad (\text{boundary-layer momentum equation})$$

where

$$H + 2 = 3.4; \quad U' = \frac{dU}{ds}, \quad s \text{ along surface.}$$

The wall shearing stress is

$$\frac{\tau_o}{\rho U^2} = \frac{1}{\xi^2} = f(Re_\theta)$$

where $\xi = 2.557 \times \ln(4.075 Re_\theta)$ according to Squire-Young (reference 4).

TABLE FOR ξ (Re_θ) ACCORDING TO SQUIRE-YOUNG

Re_θ ξ	400 18.91	600 19.94	800 20.68	1000 21.26	1500 22.29	2000 23.02	
Re_θ ξ	3000 24.06	4000 24.80	5000 25.36	7000 26.23	10000 27.14	15000 28.18	
Re_θ ξ	20000 28.91	30000 29.99	40000 30.70	50000 31.27	2×10^5 33.05	5×10^5 34.83	10^6 38.94

The variation of θ in the wake from the trailing edge to very far toward the rear was determined also according to Squire-Young (reference 4), with the assumption that in the wake

$$\ln \left(\frac{U_o}{U} \right) = k \frac{\delta^*}{\theta}$$

(see also reference 61c).

The momentum loss thickness θ_∞ far toward the rear becomes:

$$\theta_\infty = \theta_h \left(\frac{U_h}{U_o} \right)^{\frac{H_h+5}{2}}$$

with the index h referring to the trailing edge. With $H_h = 1.4$, θ_∞ becomes

$$\theta_\infty = \theta_h \left(\frac{U_h}{U_o} \right)^{3.2}$$

hence follow c_{w_∞}' and c_{w_∞} .

5. Test Results

The test results can be seen from the figures 77 to 90 and the test tables which contain the following data (see at the end of the report).

Test-Nos.

$$q_0, U_0, v, Re = \frac{U_0 t}{v}, c_{Qt}, c_{wG}$$

c_Q and c_{pG} for the eight suction slots, the momentum-loss thickness θ and the static pressure at the boundary-layer test point G.

The pressure distributions along the chord, the static pressures in the suction chambers and the transition-point positions (arrows) for various Re and suction quantities are plotted in figures 77 to 80.

The pressure distributions are flat and show a slight pressure increase only in the rear part of the profile. The laminar pressure increase before the transition amounts to 17 to 21.5 percent of the pressure difference between stagnation point and pressure minimum. At the suction points appears the typical pressure increase due to sink effect which increases with growing suction quantity. Generally, the boundary layer is accelerated between the slots. Only behind slot VIII occurs a stronger laminar pressure increase which finally leads to the transition in general shortly ahead of the trailing edge. In most cases the pressure distribution curves show the typical break during transition.

The negative pressures in the suction chambers increase with growing suction quantity. They are smaller for larger Re , also for wider suction slots.

In the cases of larger Re or of smaller suction quantities the transition point travels forward. The suction quantities c_{Qt} required to keep the boundary layer laminar up to a place shortly ahead of the trailing edge are generally small. With increasing suction quantity more suction has to be applied, see optimum curve $c_{Qt_{opt}}(Re)$ for the minimum total drag. (See fig. 81.)

For suction quantities smaller than $c_{Qt_{opt}}$ one may ascertain by stethoscope, isolated turbulent bursts in the rear part of the

profile, which, with decreasing suction quantity rapidly become more frequent and start farther toward the front. The transition starts earlier and takes place in a more or less wide transition region which is no longer sharply defined. In these cases the boundary layer becomes turbulent by the effect of the wind-tunnel turbulence.

The critical Reynolds numbers $Re_\theta = \frac{U\theta}{\nu}$ during transition, where the boundary layer under the effect of the external turbulence barely remained laminar, were for

$$Re = 2 \text{ to } 4 \times 10^6, Re_{\theta_{kr}} = 930 \text{ to } 880$$

with the narrower suction slots as well as with the wider ones. For larger Re resulted somewhat lower $Re_{\theta_{cr}}$.

The critical Re_θ -values are slightly larger on the suction side than on the opposite wall to which no suction had been applied and are practically of the same magnitude as for the laminar profile 14-percent thickness in figure 12.

It may be concluded that a laminar boundary layer with suction reaches the transition point, due to an external turbulence, for equal Re_θ -values, as without suction for identical flat external pressure distribution if the slots are correctly adjusted.

Smaller $Re_{\theta_{cr}}$ resulted only for very weak suction. The suction slots probably were too wide for very small suction quantities (as was shown by a verifying calculation of the laminar boundary-layer development with suction); hence, a local laminar separation occurs at the slot inlet thus causing the boundary layer continuing behind the slots to be disturbed (observation by stethoscope).

The boundary-layer profiles at the station G 9 millimeters behind the slot VIII for various suction quantities and dynamic pressures can be seen from figures 82 to 87.

For weak suction, the boundary-layer profiles are similar as on a flat plate without pressure gradient (Blasius (reference 42)) and become fuller with increasing suction quantity. (See also measurements by M. Ras (references 66 to 68) with laminar area suction and calculations by H. Schlichting (reference 70) about laminar area suction on a flat plate.)

In figure 88 the optimum total drag $c_{w\infty}$ with suction (curve b) is plotted versus $Re = \frac{U_0 t}{\nu}$ and compared with the opposite side (curve a) to which no suction had been applied.

For larger Re the drag is considerably reduced by the laminar boundary-layer suction. The increase of the drag due to tunnel turbulence starts with suction for considerably larger Re . Without suction $c_{w\infty}$ decreases with Re similarly to the laminar plate friction to $Re = 10^6$ and increases again for larger Re , owing to the forward travel of the transition due to the wind-tunnel turbulence (fig. 89).

Up to $Re = 4 \times 10^6$ the drag with boundary-layer suction was only slightly larger than the laminar plate friction; the Reynolds numbers Re_θ were relatively low. For $Re = 4 \times 10^6$ resulted $c_{w\infty} = 0.00167$. For larger Re ($> 4 \times 10^6$) c_w increased again due to the effect of the tunnel turbulence: The suction in the suction slots must be made stronger and stronger, in order to avoid - at larger Re - turbulent discontinuities which increase the skin friction and start at $Re_{\theta_{cr}}$. Hence, larger slot losses and very thin laminar boundary layers result directly behind the suction slots, causing an increase of the surface friction. Thereby the drag $c_{w\infty}$ for larger Re , again increases, although it was by means of suction possible to maintain the boundary layer laminar up to $Re = 5.4 \times 10^6$. For larger Re the lowest drags resulted precisely with the start of a few isolated turbulent bursts which did not yet cause a large increase in skin friction.

The plot of the variation of $c_{w_{cs}}$ and c_{w_s} versus the suction quantity c_{Q_t} for $Re = 3.0 \times 10^6$ can be seen from figure 90.

$c_{w_{cs}}$ varies with c_{Q_t} similarly as for the first laminar suction wing of 6.75-percent thickness (chapter 4, 4):

$c_{w_{cs}}$ is smallest for the optimum suction quantity $c_{Q_{t, opt}}$. For smaller c_{Q_t} -values turbulent discontinuities appear in the rear part of the profile, increasing $c_{w_{cs}}$. For larger c_{Q_t} the laminar boundary layer becomes thinner (see boundary-layer measurements figs. 82 to 87) causing an increase in skin friction and $c_{w_{cs}}$.

Widening of the slots resulted in smaller negative pressures in the suction tank and thus in somewhat lower c_w and $c_{w_{cs}}$ (test 38, 14*, 54).

The drag could be decreased still farther by placing more suction slots behind slot VIII, thus

1. Maintaining the boundary layer laminar up to the trailing edge
2. Recovering a considerable part of the kinetic-wake energy of the boundary layer at the trailing edge (presupposition: acceleration of the suction air to U_0)

The dashed curve c (fig. 88) shows the drags which may be attained by placing two more slots near the trailing edge. The curve c was calculated from the test values with the aid of a theory of the laminar boundary-layer development with suction.

The fact that the drag significant for the propulsion can be lower than the laminar plate friction can be explained by the partial recovery of relatively large kinetic wake energy of the laminar boundary layer. By wake utilization the drag of the laminar flat plate could be decreased, on principle, by 21.3 percent (fig. 88, curve d).

6. Extension of Schlichting's Theory on the Laminar

Boundary-Layer Development with Area Suction

in the Case of Acceleration of the Sucked Air

to the Undisturbed Free-Stream Velocity U_0

H. Schlichting calculated the laminar boundary-layer development on a flat plate with area suction at constant suction velocity $-v_0$ perpendicularly to the plate (reference 70). Schlichting made the following formulation for the velocity distribution in the boundary layer:

$$\frac{u}{U} = 1 - e^{-\eta} + K\eta e^{-\eta}, \quad \eta = \frac{y}{\delta_1(x)}$$

thus, he obtained the distribution of the skin friction c_{wR} shown in figure 91 for various Re and suction intensities $-\frac{v_0}{U_0}$ (U_0 = undisturbed free-stream velocity).

The condition on the plate infinitely far toward the rear is given with strict accuracy whereas for smaller Re , c_{wR} is overestimated. Without suction the result is, according to Schlichting,

$$c_{wR} = \frac{1.66}{\sqrt{Re}} \quad \text{instead of} \quad \frac{1.328}{\sqrt{Re}} \quad \text{according to Blasius}$$

If the suction air is accelerated to U_0 without loss, the drag c_{w2} which is significant for the propulsion becomes considerably lower than the skin friction c_{wR} , the reason is the recovery of the kinetic wake energy of the sucked air which otherwise moves forward with the plate, (See fig. 92.) For an infinitely long plate c_{w2} becomes $c_{w2} = \frac{1}{2}c_{wR}$.

The drag c_{w2} for acceleration of the suction air to U_0 decreases with Re considerably more strongly than the surface friction c_{wR} (under the assumption of uniform suction intensity - $\frac{v_0}{U}$). Hence, low drags c_{w2} become possible at larger Re for relatively thin laminar boundary layers which are, with respect to stability, better controllable.

Conversely, it is probably possible to obtain, for higher admissible laminar Re -values (with weak external turbulence) with the aid of the laminar boundary-layer suction very large Re under laminar conditions; the drag c_{w2} would become only slightly larger than the laminar-plate friction.

A further drag reduction would result if one would, moreover, accelerate the boundary layer at the end of the plate without loss to U_0 , thus possibly recovering its wake energy. (See fig. 93.)

The utilization of the wake energy of the boundary layer on a laminar suction profile could be attained with relatively small losses by gradual suction of the boundary layer in the rear part of the profile through several suction slots placed one behind the other for a static pressure increasing toward the rear, and by reacceleration of the sucked air to U_0 . In each slot, suction need be applied only to a fraction of the respective boundary layer, so that small slot losses result. In this manner a thin laminar boundary layer would result at the trailing edge of the wing; its

wake energy would now be only slight; moreover, it is partially recovered during the following acceleration in the wake. An arrangement of pressure propellers also would make it possible to recover a small part of the boundary-layer wake energy (as in the similar case of wake propellers of ships).

CHAPTER 8

INVESTIGATION OF A SLIGHTLY CAMBERED LAMINAR SUCTION

PROFILE OF 10.5-PERCENT THICKNESS

1. Purpose of the Investigation

The laminar pressure increase with boundary-layer suction was studied for higher Re , at normal wind-tunnel turbulence and for various c_a , on a slightly cambered profile of 10.5-percent thickness and conventional thickness distribution. Furthermore, the drag reduction by the laminar boundary-layer suction was investigated.

2. Profile, Test Arrangement

The investigated profile with the suction slots can be seen from figure 94.

Profile thickness $d/t = 0.105$

Curvature of the mean line $f/t = 0.019$

Nose curvature radius $R_o/t = 0.0097$

With the selected thickness distribution, the pressure increase on the upper surface starts relatively far to the front.

The wing which was made of wood was erected vertically between floor and ceiling of the closed wind-tunnel test section. In the central wing section were the test suction slots of 0.18 meter length with auxiliary suction slots on both sides. Suction was applied to the boundary layer on the upper surface through 14 slots and on the lower surface through 10 slots. For most tests the foremost slots of the upper surface were sealed with putty and no suction was applied to them (see test tables). A separate suction chamber, in which the static pressure was measured, was connected to each suction slot. The suction quantity of each test suction slot was determined by calibrated measuring nozzles attached to the lower end of the suction chamber. The suction chambers were conically developed in suction direction and had a cross section with ample dimensions. The auxiliary suction slots were adjusted as similarly as possible to the test suction.

Form and position of the suction slots can be seen from figure 94. The narrow slots which are developed as diffusers have a rearward inclination of 60° . The forward or rearward curvature of the slots served only for deflection of the suction air, not for an artificial production of turbulence of the slot flow.

In order to intensify the laminar pressure increase by sink effect, the surface in the slot region was made slightly wavy on the basis of earlier tests, for test 21 considerably less than for the test 27 to 55 (see profile sketch).

The suction slots along the span were as far as possible identically adjusted (constant slot width and shifting of the trailing edge of the slot relative to the slot inlet along the slot).

3. Measurement with Laminar Boundary-Layer Suction

(a) Pressure distribution along the chord, measured with 0.5-millimeter ϕ pressure holes and with 1.0 millimeter ϕ static-pressure tube; (b), (c) suction quantity and static pressure in the different test-suction chambers (with calibrated measuring nozzles and with 0.5 mm ϕ bore holes); (d) momentum measurements in the wake.

The boundary-layer condition in the suction region was verified by stethoscope. The boundary-layer suction was regulated to the lowest possible total drag.

The tests were performed for various c_a (from pressure distribution) and $Re = \frac{U_\infty t}{\nu}$; in a few cases the suction quantity was varied. For the tests 27 to 55 the slot widths were enlarged as compared to test 21.

For comparison, $c_{w_{min}}$ without suction in the part of the wings to which no suction had been applied was determined for various Re by means of the momentum method. (See fig. 95.)

Symbols and Evaluation of the Suction Tests

Wing chord $t = 1.035$ m

Span of the test suction $b = 0.18$ m

Reference area $F = bt = 0.186$ m²

The investigated wing was relatively large, compared to the cross-sectional area of the test section (3×2.12 m, octagonal). The profile then operates between side walls or in a wing cascade (mirrored wings). In order to obtain from the test values the properties of the investigated wing as individual profile in the unlimited air stream, the undisturbed free-stream dynamic pressure q_0 and the free-stream velocity U_0 , respectively, and the static pressures at the profile evaluated as follows: The tunnel side walls and the wings mirrored on them, respectively, cause the test wing in the center of the tunnel to be subjected to a stream of air with a velocity which is by ΔU larger than the free-stream velocity U_{cG} far toward the front: $U_0 = U_{cG} + \Delta U$. (The index G refers to the cascade.) ΔU is the incremental velocity due to the mirrored wings at the location of the test wing. The undisturbed static pressure p_0 at the location of the test wing is by $\rho/2 (U_0^2 - U_{cG}^2)$ lower than the static pressure p_{cG} far ahead of the wing.

The incremental velocity ΔU at the location of the test wing under the influence of the mirrored wings was calculated by replacing each of them by a source and sink at 0.8-meter distance in free-stream direction and a vortex. The strength was chosen so that the maximum thickness of the mirrored wings equalled the one of the test wing. The mirrored vortices do not cause an incremental velocity in free-stream direction in the tunnel center at the test wing location, on the other hand, with growing c_a the effective profile camber is increased by Δf (see Prandtl-Betz (reference 85):

$\Delta f/t = 0.0023c_a$. There resulted $\frac{\Delta U}{U_{cG}} = 0.006$, thus $U_0 = 1.006U_{cG}$.

The following quantities were measured: the static pressures p_{w1} and p_{w2} on both tunnel side walls at the location of the maximum profile thickness for installed test wing, furthermore, the total head g_0 and the static pressure p_{oG}' at the location of the test wing (for "empty-tunnel" condition) ($p_{w1,2}'$, p_{oG}' , and g_0 were measured with the atmosphere as reference level). In general, p_{w1} and p_{w2} are different due to the circulation around the wing. Because of the displacement effect of the wake behind the wing p_{oG}' is slightly different from p_{oG} .

The static pressures p at the profile surface and p_a in the suction chambers were determined with p_0 as reference level.

Evaluation of p_0 , q_0 , U_0 from p_{w1} , p_{w2} .- The incremental velocity ΔU_w at the tunnel side walls at the location of the maximum profile thickness under the influence of the test wing and the mirrored wings together was calculated, all wings were replaced by a source and a sink at 0.8 meter distance each. From ΔU_w , ΔU , and $p_w = \frac{p_{w1} + p_{w2}}{2}$ follows the undisturbed static pressure p_0 at the location of the test wing (squared terms of ΔU and ΔU_w neglected):

$$\frac{p_0 - p_w}{q_{0G}} \cong \frac{2(\Delta U_w - \Delta U)}{U_{0G}}$$

with

$$\frac{\Delta U_w}{U_{0G}} = 0.015$$

$$q_0 = \epsilon_0 - p_0$$

$$U_0 = \sqrt{\frac{2}{\rho} q_0}$$

The further symbols and the drag evaluation are the same as in chapter 4, 4. Acceleration of the sucked air to U_0 and equal efficiency of propeller and suction blower were presupposed. The kinetic energy $\frac{\rho}{2} u_L^2$ of the sucked air in the suction chamber was included in the blower pressure Δp_g .

q_{ai} suction quantity of slot (i), measured with calibrated measuring nozzles of same shape as in tests of chapter 7

Δp_{gi} suction blower pressure for slot (i) $\left(q_0 - p_{ai} - \frac{\rho}{2} u_L^2 \right)$

p_{ai} static pressure in the suction chamber (i), measured with 0.5-millimeter ϕ holes

p static pressure at the surface

$$Re = \frac{U_o t}{\nu}$$

Suction-quantity coefficient $c_{Q_1} = \frac{Q_{a_1}}{U_o F}$ of the slot (i). Total suction-quantity coefficient

$$c_Q = \sum_{i=1-14}^{1'-10'} c_{Q_1}$$

for upper side,

$$c_{Q_0} = \sum_{i=1}^{14} c_{Q_i}$$

for the lower side,

$$c_{Q_{11}} = \sum_{i=1''}^{10'} c_{Q_i}$$

Drag contribution of the suction blower:

$$c_{w_g} = \sum_{i=1-14}^{1'-10'} (c_Q c_{p_g})_i$$

Drag contribution of the wake $c_{w_{co}}' = \frac{2\theta_{\infty}}{t}$, determined by momentum measurements. Total profile drag significant for the lift

$$c_{w_{co}} = c_{w_{co}}' + c_{w_g}$$

c_a was evaluated from the pressure-distribution measurements.

The test results can be seen from the test tables and the figures 95 to 103.

4. Test Results

The minimum drag with laminar boundary-layer suction (power required for suction included) is plotted versus Re for various c_a in figure 95 and is compared with the measurement without suction.

In spite of the thickness distribution which is not particularly favorable with respect to drag, the resulting total drag for $Re = 2.2 \times 10^6$ is $c_{w_{\infty}} = 0.0023$ with suction, compared to $c_{w_{\infty}} = 0.00535$ without suction for $Re = 1.4 \times 10^6$. With suction $c_{w_{\infty}}$ decreases with Re up to 2×10^6 similarly to the laminar friction of the flat plate and is only slightly larger than the latter.

For $Re > 2.2 \times 10^6$, $c_{w_{\infty}}$ increases again due to the wind-tunnel turbulence (starting of isolated turbulent bursts similarly as in the suction tests of chapter 7).

By widening of the suction slots (tests 27 to 55) the slot losses and $c_{w_{\infty}}$ were reduced (comparison of the tests 27 and 21).

Figure 96 shows the optimum profile drag polars with laminar boundary-layer suction for various Re .

Since the boundary layer was kept completely laminar up to the trailing edge on both wing surfaces, $c_{w_{\infty}}$ remains low in a considerable c_a -range, thus causing favorable profile-drag lift ratios. In order to maintain, for larger c_a , the boundary layer still laminar up to the trailing edge in spite of the growing pressure increase, stronger suction must be applied on the upper side, whereas the suction of the lower side may be correspondingly reduced, and vice versa.

For still larger (or smaller, respectively) c_a one wing side finally becomes turbulent in spite of stronger suction, due to the incipient suction peak at the wing nose, hence, the drag increases accordingly.

The influence of the suction quantity c_Q on $c_{w_{\infty}}$, $c_{w_{\infty}}'$, and c_{w_g} can be seen from figure 97 ($Re = 2.2 \times 10^6$).

For $c_{w_{\infty}} = c_{w_{\infty}opt}$ the boundary layer remains laminar down to the trailing edge with small suction quantities c_{Qopt} on both wing surfaces. For larger suction quantities ($c_Q > c_{Qopt}$) the laminar skin friction and the total drag $c_{w_{\infty}}$ increase. For weaker suction ($c_Q < c_{Qopt}$) isolated turbulent bursts start in the boundary layer, in the region of the pressure increase, which become rapidly more frequent with decreasing suction quantity and increase the skin friction and $c_{w_{\infty}}$.

The percent-drag contribution of the suction blowers to the total drag is considerable, particularly for larger Re .

Figure 98 shows a comparison of the wakes with and without suction. The drag contribution of the wake with suction is very much smaller than the drag without suction.

The pressure distributions along the chord can be seen from figures 99 to 103. The test points obtained by pressure holes and the static pressures in the suction chambers are plotted. The pressure-distribution curves were supplemented by measurements with a 1.0 ϕ static-pressure tube; the corresponding test points do not appear in the plot.

For larger Re considerable laminar pressure increases were obtained with the aid of boundary-layer suction, for instance, in test

No.	c_a	Re	Laminar pressure increase (percent)
27.1	0.232	2.16×10^6	49
44	.477	2.22	56
55.3	.587	1.45	63.3

The sink effect makes an essential contribution to the laminar pressure increase.

For a few cases the laminar boundary-layer development was determined along the chord down to the trailing edge. The boundary-layer development along the wall between the slots was calculated according to Pohlhausen (reference 43). The boundary-layer momentum-loss thickness θ directly behind the locations of suction was determined according to Bernoulli from the momentum-loss thickness of the boundary-layer part ahead of the suction point to which no suction had been applied (mixing within the boundary layer with pressure increase as a result of sink effect neglected). There-

from resulted θ along the chord and $Re_\theta = \frac{U\theta}{\nu}$, respectively

(U = velocity at the edge of the boundary layer at the particular station). Those critical Reynolds numbers Re_θ were designated by $Re_{\theta_{cr}}$ where the boundary layer just remained laminar on both surfaces down to the trailing edge.

Influence of the external pressure distribution on $Re_{\theta_{cr}}$:
For not too small c_a -values ($c_a \geq 0.27$) similar $Re_{\theta_{cr}}$ resulted

on the lower wing surface (flat pressure distribution) as for the symmetrical suction profile of 3.35-percent thickness of chapter 7 ($Re_{\theta_{cr}} = 800$ to 850). On the other hand $Re_{\theta_{cr}}$ on the upper surface in the pressure-increase region was essentially lower, particularly for larger c_a ($Re_{\theta_{cr}} = 550$ (at start of pressure increase) to 400 to 450 at the end of the pressure increase in the neighborhood of the trailing edge). Thus, similarly to the case without suction, higher (or essentially lower) $Re_{\theta_{cr}}$ than for pressure gradient zero result for accelerated (or retarded) external flow for laminar boundary-layer suction.

Influence of the sink effect on $Re_{\theta_{cr}}$. The tests 21 and 27 with sink effect of different strength resulted in practically equal Re_{θ} -values, with $c_{\theta_{opt}}$ remaining the same. Thus it seems that primarily the total external pressure increase is decisive for the stability of a laminar boundary layer with suction with increasing pressure. Whether this total external pressure increase is to a larger or smaller extent created by sink effect or by the flow along the wall seems, within certain limits, of lesser importance.

If one calculates from the velocity gradient u' of the external pressure distribution as it would result without sink effect a quantity $\lambda = \delta^2/\nu u'$ (which corresponds to the Pohlhausen method), the following values result in the region of increasing pressure on upper and lower side: $\lambda = -2$ (start of the pressure increase) to -8 (at the end of the pressure increase). Therefore, similar negative λ -values are obtained for laminar pressure increase with boundary-layer suction as without suction, under the assumption of equal external turbulence and equal Re_{θ} .

5. Conclusions from the Tests of Chapters 7 and 8 for the

Design of Laminar Suction Profiles with the Lowest

Possible Drag for High Reynolds Numbers

In order to obtain for laminar suction profiles highest possible Re_{θ} over a large range of the wing chord, and thus a low surface friction and small drag for larger Re , one should use profile shapes with uniform pressure distribution and a pressure increase occurring far toward the rear, as they were developed for laminar profiles without suction (chapter 3). This corresponds to the combination of the test of chapters 7 and 8.

Weak suction only would have to be applied in the region of flat pressure distribution. Boundary-layer thickness and Re_θ would have to be reduced by suction ahead of the pressure increase. So much suction would have to be applied in the region of pressure increase that, for the present turbulence $\frac{u'}{U_0} = 0.004$, Re_θ remains $Re_\theta \leq 500$ and $\lambda = \frac{\delta^2}{\nu} u'$ does not become excessively negative ($\lambda \geq -6$). (u' = velocity gradient of the external pressure distribution without sink effect).

6. Prospects for Application of Laminar Boundary-Layer

Suction in Flight for High Reynolds Numbers

The calculation for flight measurements on a laminar profile of 15.9-percent thickness (15) resulted, ahead of the transition, in a Reynolds number $Re_\theta = \frac{U_0 \theta}{\nu} = 2600$ in the region of the point of laminar separation (chapter 2, 2), that is, about three times more than for the present wind-tunnel tests. Hence, presumably, for laminar suction profiles in flight, with a boundary layer kept completely laminar, about three times smaller drags for nine times higher $Re = \frac{U_0 t}{\nu}$ are possible than had been measured in the wind tunnel.

For higher flight velocities the percent atmospheric turbulence $\frac{u'}{U_0}$ decreases; thus one could then expect higher laminar flow Re and lower drags, at least as long as no compressibility disturbances appear.

The drags of fuselage and tail unit also could be considerably reduced by maintaining the boundary layer laminar with the aid of suction. The fairings from wing to fuselage, etc., also could, in principle, be kept laminar by boundary-layer suction.

The induced drag which now gains renewed importance may be reduced by enlarging of the span and increasing of the flight velocity, possibly by staggered flight arrangement (as used by migratory birds). The optimum drag/lift ratio would result for small c_a , that is, for high flight speed at not extreme altitudes. Large spans require wings with sufficiently thick profiles and

adroit design of the wing structure. In order to obtain high Mach numbers without compression shocks, the superstream velocities ought to remain as small as possible.

For laminar suction profiles in flight exists the possibility to adapt the boundary-layer thickness and Re_θ , respectively, by means of boundary-layer suction to the respective state of turbulence of the atmosphere. For higher atmospheric turbulence stronger suction would have to be applied farther toward the front in order to keep Re_θ sufficiently low and to obtain a lower sensitivity with respect to variations in angle of attack due to gusts, etc. Conversely, weaker suction could be applied in case of the air being very calm, resulting in larger Re_θ and correspondingly lower drags.

Translated by Mary L. Mahler
National Advisory Committee
for Aeronautics

APPENDIX

REDUCTION OF THE PROFILE DRAG FOR SMALL Re BY ARTIFICIALLY
PRODUCED TURBULENCE OF THE BOUNDARY LAYER IN THE REGION
OF THE POINT OF LAMINAR SEPARATION

It had been shown on the propeller profile number 11 of 9-percent thickness (fig. 11, chapter 3, 3) that the boundary layer of the upper wing surface undergoes, for small Re and smooth inflow, laminar separation and does not turbulently readhere (stethoscope); hence, the profile drag is sometimes considerably increased. Only for larger c_a the boundary layer of the upper wing surface is disturbed so much that the transition occurs in time to obtain here a turbulent readhering of the boundary layer for smaller Re .

A report on tests on a medium-cambered profile of 6-percent thickness (fig. 104) follows. The profile-drag polars on this profile were, for smaller Re , improved by artificially produced turbulence of the boundary layer on the upper wing surface in the region of the point of laminar separation with the aid of surface disturbances (steps in the surface, see fig. 104: disturbances 1 and 2).

For various Re and c_a momentum measurements were performed on the smooth wing and with the disturbances 1 and 2. (See profile-drag polars figs. 104 to 107.) For low Re the profile-drag polars are definitely improved by use of the disturbances, the boundary layer after the disturbance generally turbulently readhering and undergoing laminar separation only for very small Re (observation by stethoscope). The disturbance then would have to extend farther to the front.

The weaker or stronger disturbance 1 or 2, respectively, improves the drag polar mainly in the Re -region of 250,000 to 300,000 (or 200,000, respectively). For larger Re the boundary layer becomes unnecessarily early turbulent due to the disturbance (observations by stethoscope), thereby correspondingly increasing the profile drag. The Reynolds number $Re_l = \frac{U_l}{\nu}$ referred to the distance l from the start of the disturbance to the start of transition resulted for the present case as $Re_l = 48,000$

(l = distance from start of disturbance to start of transition;
 U = mean velocity at the boundary-layer edge between start of
disturbance and start of transition).

The method of producing an artificial turbulence of a laminar boundary layer in the region of the point of laminar separation is, in general, successfully applicable if otherwise a stronger laminar separation occurs and the boundary layer does not turbulently readhere.

REFERENCES

1. Jones, B. M.: Skin Friction and the Drag of Streamline Bodies. R.M. 1199, 1928, 1929.
2. Jones, B. M.: Flight Experiments on the Boundary Layer. J. A. Sciences 1938, Jan., vol. 5, no. 3, p. 81.
3. Serby, J., Morgan, M., and Cooper, E.: Flight Tests on the Profile Drag of 14 Percent and 25 Percent Thick Wings. R.M. 1826, 1937.
4. Squire, H. B., and Young, A. D.: The Calculation of the Profile Drag of Aerofoils. R.M. 1838, 1938.
5. Pretsch, J.: Zur theoretischen Berechnung des Profilwiderstandes. Jahrbuch 1938 der Deutschen Luftfahrtforschung, pp. 1-60.
6. Lewis, G. W.: Some Modern Methods of Research in the Problems of Flight, Low Turbulence Wind Tunnel. The Journal of the Royal Aeronautical Society 1939, p. 779.
7. Tani, I., and Mituisi, S.: Contributions to the Design of Aerofoils Suitable for High Speeds Rep. of the Aeronautical Research Institute Tokyo, No. 198, Sept. 1940.
8. Pfenninger, W.: Über die aerodynamische Durchbildung von Flügelstrebenanschlüssen. Flugwehr und-Technik, Sept. 1942.
9. Jacobs, Eastman, and von Doenhoff, A. E.: Transition as it Occurs Associated with and Following Laminar Separation. 5th Intern. Congr. for appl. Mech., Cambr., Mass. 1938, p. 311.
10. Hall, A., and Hislop, G.: Experiments on the Transition of the Laminar Boundary Layer on a Flat Plate. R.M. 1843, 1938.
11. Taylor, G. I.: Some Recent Developments in the Study of Turbulence. Proc. 5th Intern. Congr. for appl. Mech., Cambr., Mass. 1938.
12. Fage, A., and Preston, H.: Experiments on Transition from Laminar to Turbulent Flow in the Boundary Layer. Proc. Roy. Soc. A, vol. 178, 1941.
13. Schubauer, G.: Airflow in the Boundary Layer of an Elliptic Cylinder. NACA Rep. No. 652, 1939.

14. Fage, A.: The Airflow Around a Circular Cylinder in the Region where the Boundary Layer Separates from the Surface. R.M. 1179, 1928.

Fage, A.: On Reynolds Numbers of Transition. R.M. 1765, 1937.

Fage, A.: Experiments on a Sphere at Critical Reynolds Numbers. R.M. 1766, 1937.

15. Amerikanische Profilwiderstandsmessungen im Fluge an einem 15.9 percent dicken Laminarprofil mit einer "King Cobra" (nach Reiseberichten).

16. Lyon, H. M.: Flow in the Boundary Layer of Streamline Bodies. R.M. 1622, 1934.

- 17, 18. Taylor, G. I.: Statistical Theory of Turbulence, Parts I - IV, Proc. Roy. Soc. A, vol. 151, no. 873, Sept. 1935, Part V, Proc. Roy. Soc. A, vol. 156, no. 888, Aug. 1936.

19. Von Kármán, Th.: Turbulence and Skin Friction. Journal of the Aeron. Sciences Jan. 1934.

20. Von Kármán, Th.: Turbulence. Journal of the Royal Aeron. Soc., vol. 41, no. 324, p. 1109, Dec. 1937.

Von Kármán, Th.: Some remarks on the Statistical Theory of Turbulence. Proc. of the 5th. Int. Congr. for Appl. Mech. Cambr., Mass. 1938.

21. Dryden, H. L.: Airflow in the Boundary Layer near a Plate. N.A.C.A. Rep. 562, 1936.

22. Dryden, H. L.: Turbulence and the Boundary Layer. Journal of the Aeron. Sciences Jan. 1939.

23. Dryden, H. L.: Turbulence, Companion of Reynolds number. Journal of the Aeron. Sciences, April 1934.

24. Dryden, H. L.: Turbulence Investigations at the National Bureau of Standards. Proc. of the 5th Intern. Congr. for Appl. Mech. Cambr., Mass. 1938.

25. Prandtl, L.: Beiträge zum Turbulenzsymposium. Proc. of the 5th Intern. Congr. for Appl. Mech. Cambr., Mass. 1938.

Prandtl, L.: Über die Entstehung der Turbulenz. ZAMM 1931, p. 407.

26. Schlichting, H.: Berechnung der Anfachung kleiner Störungen bei der Plattenströmung. Z.A.M.M. 1933, Bd. 13, Heft 3.
27. Schlichting, H.: Zur Entstehung der Turbulenz bei der Plattenströmung. Nachr. Ges. Wiss. Göttingen, Math.-Phys. Klasse 1933, p. 181.
- 28a. Tollmien, W.: Über die Entstehung der Turbulenz Nachr. Ges. Wiss. Göttingen, Math.-Phys. Klasse 1929, p. 21.
- 28b. Tollmien, W.: Über die Korrelation der Geschwindigkeitskomponenten in periodisch schwankenden Wirbelverteilungen. Z.A.M.M. 1935, p. 96.
29. Tollmien, W.: Ein allgemeines Kriterium der Instabilität laminarer Geschwindigkeitsverteilungen. Nachr. Ges. Wiss. Göttingen, Math.-Phys. Klasse 1935, Fachgruppe 1, p. 79.
30. Fage, A.: Transition in the Boundary Layer Caused by Turbulence. R.M. 1896, 1942.
31. Peters, H.: A Study in Boundary Layers. 5th Intern. Congr. for Appl. Mech. Cambr., Mass. 1938, p. 393.
32. Stephens, A. V. and Hall, A.: Hot-Wires in Flight. Proc. 5th Intern. Congr. for Appl. Mech. Cambr., Mass. 1938, p. 336.
33. Clauser, M. and F.: The Effect of Curvature on the Transition from Laminar to Turbulent Boundary Layer. N.A.C.A. T.N. 613, 1937.
34. Görtler, H.: Instabilität laminarer Grenzschichten an konkaven Wänden gegenüber gewissen 3-dimensionalen Störungen. Z.A.M.M. 1941, p. 250. Nachr. Ges. Wiss. Göttingen, Math.-Phys. Klasse 1940, p. 1.
35. Prandtl, L.: Einfluss stabilisierender Kräfte auf die Turbulenz. Vorträge aus dem Gebiet der Aerodynamik und verwandter Gebiete. Aachen 1929, p. 1.
36. Young, A. D.: Surface Finish and Performance. Aircraft Eng. Sept. 1939.
37. Hood, M. J.: Surface Roughness and Wing Drag. N.A.C.A. T.N. 695. Aircraft Eng. Sept. 1939.

38. Tanf, I., Hama, R, and Mituisi, S.: On the Permissible Roughness in the Laminar Boundary Layer. Rep. of the Aeron. Research Institute Tokio, No. 199, Oct. 1940.
39. Theodorsen, T. and Garrick, I.: General Potential Theory of Arbitrary Wing Sections. N.A.C.A. Rep. 452, 1933.
40. Kochanowsky, W.: Zur Berechnung der Druckverteilung über den Umfang beliebig geformter Flügelschnitte. Jahrb. 1937 der Deutschen Luftfahrtforschung, pp. 1-58. D.V.L. - Jahrbuch 1937, p. 139.
41. Kochanowsky, W.: Weitere Ergebnisse von Druckverteilungsrechnungen an beliebigen Flügelschnitten. Jahrbuch 1938 der Deutschen Luftfahrtforschung, pp. 1- 82.
42. Pinkerton, R. M.: Calculated and Measured Pressure Distribution over the Midspan Section of N.A.C.A. 4412 Airfoil. N.A.C.A. Rep. 563, 1936.
43. Pohlhausen, K.: Zur näherungsweise Integration der Differentialgleichung der laminaren Grenzschicht. Z.A.M.M. 1921, p. 252.
44. Falkner, V. M. and Skan, S. W.: Some Approximate Solutions of the Boundary Layer Equations. R.M. 1314, 1930.
45. Falkner, V. M.: A Further Investigation of Solutions of the Boundary Layer Equations. R.M. 1884, 1939.
46. Falkner, V. M.: Simplified Calculation of the Laminar Boundary Layer. R.M. 1895, 1941.
47. Blasius, H.: Grenzschichten in Flüssigkeiten mit kleiner Reibung. Zeitschr. f. Math. u. Phys. Bd. 56, p. 1, 1908. Diss. Göttingen 1907.
48. Howarth, L.: On the Solution of the Laminar Boundary Layer Equations. Proc. Roy. Soc. A, No. 919, vol. 164, 1938.
49. Prandtl, L.: Zur Berechnung der Grenzschichten. Z.A.M.M. 1938, p. 77.
50. Görtler, H.: Weiterentwicklung eines Grenzschichtprofils bei gegebenem Druckverlauf. Z.A.M.M. 1939, p. 129.

51. Howarth, L.: Steady Flow in the Boundary Layer near the Surface of a Cylinder in a Stream. R.M. 1632, July 1934.
52. Tomotika, S.: The Laminar Boundary Layer on the Surface of a Sphere in a Uniform Stream. R.M. 1673, 1935.
53. Buri, A.: Eine Berechnungsgrundlage für die turbulente Grenzschicht bei beschleunigter und verzögerter Grundströmung. Diss. Zürich 1931.
54. Gruschwitz, E.: Die turbulente Reibungsschicht in ebener Strömung bei Druckabfall und Druckanstieg. Ing. Archiv, 1931, p. 321.
55. Kehl, A.: Untersuchungen über konvergente und divergente turbulente Reibungsschichten. Ing. Archiv, 1943, p. 293.
56. Young, A. D.: The Calculation of the Total and Skin Friction Drags of Bodies of Revolution at 0° Incidence. R.M. 1874, 1939.
57. Von Kármán, Th.: Über laminare und turbulente Reibung. Zeitschr. f. angew. Math. u. Mech. 1, 1921, p. 233.
58. Göttinger Nachrichten 1930, p. 58, Vortrag auf dem 3. Int. Kongr. f. techn. Mech. in Stockholm 1930 (Verhandlungen dieses Kongr. Bd 1, p. 85).
- Von Kármán, Th.: Theorie des Reibungswiderstandes. In Hydromech. Probleme des Schiffsantriebs 1932.
59. Prandtl, L.: Ergebnisse der A.V.A. Göttingen No. 3 (1927), p. 1.
60. Von Doenhoff, A.: A Preliminary Investigation of Boundary Layer Transition Along a Flat Plate with Adverse Pressure Gradient. N.A.C.A. T.N. 639, 1938.
- 61a. Ackeret, J.: Das Institut für Aerodynamik an der Eidg. Techn. Hochschule.
- 61b. Datwyler, G.: Eine Apparatur zur Messung turbulenter Schwankungen in Strömungen.
- 61c. Pfenninger, W.: Vergleich der Impulsmethode mit der Wägung bei Profilwiderstandsmessungen. Mitteilung No. 8 des Inst. f. Aerodyn. E.T.H. Zürich, 1943.

62. Lord Rayleigh: On the Instability of Certain Fluid Motions.
Proc. London Math. Soc. 11, p. 57, 1880 und 19, p. 67, 1887.
(Scientific Papers vol. I, p. 474 und vol. III, p. 17.)
- 63a. Prandtl, L.: Bemerkungen über die Entstehung der Turbulenz.
Z.A.M.M. 1921, p. 431.
- 63b. Tietjens, O.: Beiträge über die Entstehung der Turbulenz. Diss.
Göttingen, 1922. Z.A.M.M. 1925, p. 200.
64. Patry, J.: Instabilité d'une rangée de tourbillons de long d'une
paroi. Helvetica Physica Acta 1943, p. 83.
65. Ackeret, J.: Probleme des Flugzeugantriebs in Gegenwart und
Zukunft. Schweiz. Bauzeitung, Bd. 112, No. 1, 1938.
66. Ackeret, J., Ras, M., and Pfenninger, W.: Verhinderung des
Turbulentwerdens einer Grenzschicht durch Absaugung. Die
Naturwissenschaften 1941, 29. Jahrg., Heft 41, p. 622.
67. Ras, M., and Ackeret, J.: Über Verhinderung der Grenzschicht-
turbulenz durch Absaugung. Helvetica Physica Acta 1941.
68. Ras, M.: Diss. Paris: Contributions à l'étude de la couche
limite aspirée, 1945.
69. Gerber, A.: Untersuchungen über Grenzschichtabsaugung. Mitteilung
No. 6 des Inst. für Aerodynamik E. T. H. Zürich, 1938.
70. Schlichting, H.: Die Grenzschicht an der ebenen Platte mit
Absaugung und Ausblasen, Luftfahrtforschung 1942, p. 179,
p. 293.
71. Schlichting, H.: Berechnung der laminaren Grenzschichtentwicklung
mit Absaugung an einem Joukowskyprofil. Cahiers d'Aérodynamique,
No. 3, Oct.-Nov. 1945.
72. Prandtl, L.: The Mechanics of Viscous Fluids. Aerodynamic Theory,
Durand, vol. III, Div. G.
73. Prandtl, L.: Strömungslehre, 1942.
74. Schrenk, O.: Grenzschichtabsaugung und Senkenwirkung. Z.A.M.M.,
Bd. 13, 1933, p. 180.
75. Schrenk, O.: Versuche mit Absaugeflügeln. Z.f.M. 1931, Heft 9.
Luftfahrtforschung 1935, p. 10.

76. Ackeret, J.: Grenzschnittabsaugung. Zeitschrift des V.D.I., No. 35, p. 1153, Sept. 1926.
77. Betz, A.: Verlauf der Strömungsgeschwindigkeit in der Nähe einer Wand bei un stetiger Änderung der Krümmung. Luftfahrtforschung 1942, Liefg. 4, p. 129.
78. Jordan, P.: Auftriebsberechnung und Strömungsvorgänge beim Überschreiten des Maximalauftriebs. Diss. Göttingen 1939 (Luftfahrtforschung, Bd. 16, 1939, p. 184).
79. Schiller, L.: Verh. des 3. intern. Kongr. für techn. Mechanik I, p. 226, 1931. Z.A.M.M. 14, p. 36, 1934. Proc. of the 5th Intern. Congr. for Applied Mechanics, p. 315, 1938.
80. Ergebnisse der Aerodyn. Versuchsanstalt zu Göttingen, Lieferungen I, III, IV.
81. Schmitz, F. W.: Aerodynamik des Flugmodells (Tragflügel-messungen I).
82. Jacobs, E. N., and Sherman, A.: Airfoil Section Characteristics as Affected by Variations of the Reynolds Number. NACA Rep. No. 586, 1937.
83. Schiller, L.: Untersuchungen über laminare und turbulente Strömung, Forschungsarbeiten auf dem Gebiet des Ing.-Wesens No. 248, 1922.
84. Haller, P. de: L'influence des limites de la veine fluide sur les caractéristiques aérodynamiques d'une surface portante. Mitteilung des Inst. f. Aerodynamik E.T.H. Zürich, No. 3, 1934.
85. Prandtl and Betz: 4 Abhandlungen zur Hydrodynamik und Aerodynamik, Göttingen 1927.
86. Rayleigh: Proc. Roy. Soc. A, 1916, p. 148.

TABLE OF COORDINATES

Propeller profile No. 11 $R_o/t = 0.008$			Laminar profile $d/t = 0.10$ in $0.49 t$ from the front $f/t = 0.00525$ in $0.50 t$ from the front			Laminar profile* $d/t = 0.140$ in $0.44 t$ from the front $f/t = 0.0245$ in $0.41 t$ from the front		
x/t	y_o/t	$-y_u/t$	x/t	y_o/t	$-y_u/t$	x/t	y_o/t	$-y_u/t$
0	0	0	0	0.00107	-0.00107	0	0.0030	-0.0030
.025	.0190	.0116	.025	.019	.014	.025	.0324	.0180
.05	.0285	.0142	.05	.02567	.01954	.05	.0443	.0224
.1	.0419	.0174	.1	.03435	.0272	.1	.0600	.0284
.2	.0581	.0190	.15	.0404	.03235	.2	.0788	.0380
.3	.0680	.0182	.2	.0446	.0364	.3	.0892	.0420
.4	.0723	.0166	.3	.0511	.0411	.4	.0940	.0436
.5	.0723	.0142	.4	.0547	.0431	.5	.0936	.0436
.6	.0692	.0126	.5	.0556	.0443	.6	.0868	.0416
.7	.0617	.0095	.6	.0660	.04275	.7	.0736	.0360
.8	.0486	.0071	.7	.0502	.0394	.8	.0492	.0284
.9	.0288	.0032	.8	.0393	.0329	.9	.0140	.0148
.95	.0154	.0012	.85	.0309	.0267	.95	.0040	.0068
.975	.0087	.0000	.9	.0194	.01926	1	0	0
0	0	0	.925	.01334	.0144			
			.96	.0078	.0088			
			.975	.00405	.0031			
			1	0	0			
			$R_o/t = 0.009$			$R_o/t = 0.019$		

*To the laminar profile $d/t = 0.14$ (fig. 12). According to measurements of F. Feldmann in the high-speed tunnel of the Institute (description, 61 a) compression shocks for this profile start, for shockless entrance, at a Mach number $M = 0.71$. For $M = 0.76 - 0.77$ and shockless entrance the lift decreases and disturbances in longitudinal stability appear. ($Re = 570,000$)

No.	14 [*]	53	12	38	13
q_0	32.3	32.3	32.2	32.4	32.2
U_0	23.68	23.60	23.76	23.84	23.73
$\sqrt{}$	16.00×10^{-6}	15.85×10^{-6}	16.10×10^{-6}	16.25×10^{-6}	
Re	3.004×10^6	3.015×10^6	2.998×10^6	2.981×10^6	2.982×10^6
θ_{mm}	0.487	0.532	0.557	0.584	0.524
for p/q_0	.033	.026	.020	.013	.028

Slot	$C_Q/2^\circ/\text{oo}$ ¹	C_{p_g}	$C_Q/2^\circ/\text{oo}$	C_{p_g}	$C_Q \times 10^{-3}/2$	C_{p_g}	$C_Q/2^\circ/\text{oo}$	C_{p_g}	$C_Q/2^\circ/\text{oo}$	C_{p_g}
1	0.0752	1.102	0.0643	1.098	0.0552	1.106	0.0466	1.092	0.0637	1.111
2	.0376	1.143	.0318	1.127	.0267	1.142	.0233	1.110	.0308	1.153
3	.0342	1.105	.0293	1.096	.0243	1.117	.0216	1.083	.0286	1.125
4	.0342	1.078	.0294	1.074	.0254	1.074	.0220	1.063	.0292	1.079
5	.0352	1.165	.0303	1.149	.0258	1.150	.0220	1.119	.0298	1.166
6	.0453	1.118	.0395	1.107	.0336	1.102	.0290	1.089	.0389	1.115
7	.0344	1.120	.0283	1.105	.0237	1.097	.0207	1.085	.0288	1.109
8	.0288	1.123	.0242	1.106	.0198	1.092	.0173	1.059	.0226	1.117

$C_{Q_t}^\circ/\text{oo}$	0.648	0.556	0.4690	0.404	0.544
$C_{w_g}^\circ/\text{oo}$.725	.613	.522	.441	.612

No.	14	16	17	18	15
q_0	32.2	32.0	32.0	32.0	32.2
U_0	23.73	23.63	23.66	23.63	23.73
$\sqrt{}$		16.20×10^{-6}	16.30×10^{-6}	16.15×10^{-6}	16.10×10^{-6}
Re	2.982×10^6	2.960×10^6	2.942×10^6	2.964×10^6	2.998×10^6
θ_{mm}	0.494	0.416	0.372	0.308	0.456
for p/q_0	.036	.049	.050	.056	.043

Slot	$C_Q/2^\circ/\text{oo}$	C_{p_g}	$C_Q/2^\circ/\text{oo}$	C_{p_g}	$C_Q/2^\circ/\text{oo}$	C_{p_g}	$C_Q/2^\circ/\text{oo}$	C_{p_g}	$C_Q/2^\circ/\text{oo}$	C_{p_g}
1	0.0750	1.118	0.1084	1.145	0.1282	1.165	0.1703	1.225	0.0912	1.128
2	.0351	1.182	.0534	1.243	.0651	1.276	.0843	1.386	.0449	1.207
3	.0335	1.146	.0491	1.190	.0591	1.207	.0773	1.276	.0412	1.167
4	.0338	1.083	.0498	1.094	.0598	1.101	.0770	1.116	.0419	1.088
5	.0353	1.191	.0521	1.259	.0628	1.299	.0817	1.393	.0429	1.222
6	.0462	1.125	.0672	1.160	.0809	1.194	.1042	1.263	.0560	1.140
7	.0341	1.125	.0481	1.175	.0581	1.211	.0740	1.369	.0399	1.149
8	.0286	1.140	.0393	1.229	.0497	1.297	.0602	1.444	.0352	1.179

$C_{Q_t}^\circ/\text{oo}$	0.644	0.936	1.130	1.458	0.786
$C_{w_g}^\circ/\text{oo}$.732	1.104	1.370	1.885	.908

¹Translator's note: A value of $C_Q/2^\circ/\text{oo}$ or $C_Q \cdot 10^{-3}/2$ of 0.0752 denotes a value of C_Q of 0.0000752.

No.	20		19*		33		34		36	
q_0	45.07		45.6		45.0		45.1		45.3	
U_0	28.22		28.32		28.19		28.22		28.17	
$\sqrt{\nu}$	16.43×10^{-6}		16.30×10^{-6}		16.41×10^{-6}		16.41×10^{-6}		16.01×10^{-6}	
Re	3.488×10^6		3.530×10^6		3.49×10^6		3.496×10^6		3.575×10^6	
θ_{mm}	0.422		0.472		0.456		0.376		0.276	
for p/q_0	.035		.028		.032		.037		.049	
Slot	$C_Q/2^\circ/oo$	C_{p_g}	$C_Q/2^\circ/oo$	C_{p_g}	$C_Q/2^\circ/oo$	C_{p_g}	$C_Q/2^\circ/oo$	C_{p_g}	$C_Q/2^\circ/oo$	C_{p_g}
1	0.0807	1.107	0.0645	1.094	0.0713	1.097	0.1032	1.113	0.1554	1.152
2	.0402	1.155	.0317	1.127	.0358	1.134	.0506	1.174	.0764	1.232
3	.0366	1.122	.0292	1.098	.0327	1.101	.0470	1.121	.0696	1.146
4	.0369	1.077	.0292	1.070	.0330	1.073	.0467	1.080	.0691	1.089
5	.0388	1.174	.0303	1.144	.0344	1.152	.0495	1.195	.0736	1.258
6	.0495	1.122	.0393	1.100	.0434	1.109	.0633	1.141	.0942	1.208
7	.0360	1.119	.0286	1.097	.0316	1.104	.0470	1.139	.0691	1.212
8	.0290	1.139	.0238	1.094	.0260	1.115	.0394	1.188	.0575	1.320
C_{Qt}°/oo	0.696		0.552		0.616		0.894		1.328	
C_{wg}°/oo	.785		.611		.684		1.018		1.585	

No.	37		39		41		43		40	
q_0	45.4		11.15		10.96		11.29		11.40	
U_0	28.20		13.93		13.81		14.01		14.12	
$\sqrt{\nu}$	16.01×10^{-6}		16.00×10^{-6}		16.00×10^{-6}		16.00×10^{-6}		16.15×10^{-6}	
Re	3.580×10^6		1.768×10^6		1.753×10^6		1.779×10^6		1.775×10^6	
θ_{mm}	0.230		0.870		0.830		0.760		0.842	
for p/q_0	.051		.001		.009		.019		.004	
Slots	$C_Q/2^\circ/oo$	C_{p_g}	$C_Q/2^\circ/oo$	C_{p_g}	$C_Q/2^\circ/oo$	C_{p_g}	$C_Q/2^\circ/oo$	C_{p_g}	$C_Q/2^\circ/oo$	C_{p_g}
1	0.1958	1.202	0.0268	1.094	0.0428	1.111	0.0623	1.126	0.0314	1.099
2	.0963	1.297	.0144	1.115	.0213	1.140	.0306	1.177	.0164	1.121
3	.0876	1.176	.0137	1.089	.0200	1.104	.0286	1.129	.0160	1.091
4	.0867	1.100	.0137	1.073	.0200	1.082	.0286	1.093	.0151	1.075
5	.0929	1.321	.0137	1.116	.0200	1.146	.0293	1.190	.0151	1.125
6	.1172	1.283	.0175	1.099	.0261	1.118	.0385	1.135	.0203	1.105
7	.0862	1.289	.0138	1.083	.0200	1.105	.0274	1.136	.0163	1.089
8	.0752	1.463	.0113	1.071	.0157	1.099	.0226	1.136	.0124	1.081
C_{Qt}°/oo	1.676		0.250		0.372		0.536		0.286	
C_{wg}°/oo	2.104		.273		.414		.610		.315	

No.	44		46		45		42		32	
q_o	11.31		11.49		11.30		11.37		45.3	
U_o	14.03		14.13		14.03		14.04		28.22	
ν	16.00×10^{-6}		16.00×10^{-6}		16.00×10^{-6}		16.00×10^{-6}		16.30×10^{-6}	
Re	1.780×10^6		1.793×10^6		1.780×10^6		1.783×10^6		3.515×10^6	
θ_{mm}	0.700		0.598		0.668		0.780		0.486	
for p/q_o	.027		.048		.035		.015		.024	
Slot	$C_Q/2^\circ/oo$	C_{p_g}	$C_Q/2^\circ/oo$	C_{p_g}	$C_Q/2^\circ/oo$	C_{p_g}	$C_Q/2^\circ/oo$	C_{p_g}	$C_Q/2^\circ/oo$	C_{p_g}
1	0.0812	1.143	0.1258	1.184	0.1010	1.162	0.0514	1.117	0.0571	1.094
2	.0399	1.217	.0618	1.316	.0500	1.260	.0257	1.160	.0282	1.122
3	.0374	1.153	.0573	1.209	.0464	1.177	.0245	1.117	.0258	1.097
4	.0377	1.104	.0579	1.129	.0461	1.115	.0238	1.086	.0263	1.066
5	.0393	1.239	.0601	1.347	.0484	1.285	.0245	1.164	.0271	1.133
6	.0508	1.157	.0772	1.216	.0629	1.181	.0316	1.123	.0352	1.088
7	.0363	1.174	.0584	1.265	.0457	1.212	.0232	1.119	.0256	1.089
8	.0292	1.186	.0466	1.326	.0373	1.248	.0183	1.112	.0220	1.070
$C_{Q_t} o/oo$	0.702		1.088		0.872		0.444		0.494	
$C_{w_g} o/oo$.822		1.352		1.048		.501		.543	

No.	55		54		35		56		57	
q_o	45.4		32.5		45.5		45.1		57.8	
U_o	27.97		23.64		28.23		27.87		31.73	
ν	15.85×10^{-6}		15.85×10^{-6}		16.01×10^{-6}		15.85×10^{-6}		16.03×10^{-6}	
Re	3.582×10^6		3.030×10^6		3.580×10^6		3.570×10^6		4.02×10^6	
θ_{mm}	0.420		0.440		0.316		0.328		0.442	
for p/q_o	.034		.038		.046		.045		.031	
Slot	$C_Q/2^\circ/oo$	C_{p_g}	$C_Q/2^\circ/oo$	C_{p_g}	$C_Q/2^\circ/oo$	C_{p_g}	$C_Q/2^\circ/oo$	C_{p_g}	$C_Q/2^\circ/oo$	C_{p_g}
1	0.0792	1.095	0.0931	1.110	0.1284	1.126	0.1228	1.118	0.0678	1.087
2	.0400	1.133	.0463	1.166	.0638	1.193	.0610	1.187	.0336	1.112
3	.0364	1.097	.0426	1.117	.0587	1.128	.0559	1.123	.0308	1.084
4	.0366	1.073	.0430	1.081	.0581	1.084	.0559	1.082	.0310	1.064
5	.0384	1.157	.0447	1.193	.0618	1.219	.0590	1.215	.0326	1.128
6	.0487	1.115	.0573	1.133	.0775	1.169	.0748	1.154	.0423	1.090
7	.0344	1.112	.0407	1.141	.0573	1.172	.0536	1.164	.0305	1.086
8	.0298	1.123	.0353	1.166	.0469	1.238	.0456	1.224	.0268	1.072
$C_{Q_t} o/oo$	0.686		0.806		1.104		1.056		0.592	
$C_{w_g} o/oo$.763		.916		1.284		1.217		.645	

No.	58		60		61		59		62 [*]	
q_o	57.9		58.3		58.1		57.9		78.9	
U_o	31.75		31.71		31.68		31.76		37.02	
$\sqrt{}$	16.03×10^{-6}		15.90×10^{-6}		15.90×10^{-6}		16.03×10^{-6}		16.06×10^{-6}	
Re	4.02×10^6		4.05×10^6		4.045×10^6		4.02×10^6		4.68×10^6	
θ_{mm}	0.385		0.276		0.218		0.327		0.219	
for p/q_o	0.036		.047		.053		.043		.047	
Slot	$C_{Q/2^\circ/oo}$	C_{p_g}	$C_{Q/2^\circ/oo}$	C_{p_g}	$C_{Q/2^\circ/oo}$	C_{p_g}	$C_{Q/2^\circ/oo}$	C_{p_g}	$C_{Q/2^\circ/oo}$	C_{p_g}
1	0.0786	1.090	0.1338	1.127	0.1708	1.163	0.1025	1.100	0.1452	1.132
2	.0390	1.122	.0662	1.207	.0818	1.258	.0515	1.147	.0649	1.186
3	.0360	1.091	.0606	1.129	.0760	1.157	.0468	1.100	.0645	1.121
4	.0363	1.069	.0604	1.079	.0753	1.087	.0464	1.072	.0637	1.076
5	.0373	1.144	.0634	1.232	.0863	1.308	.0490	1.171	.0728	1.237
6	.0483	1.105	.0822	1.152	.1091	1.204	.0628	1.127	.0922	1.166
7	.0348	1.098	.0601	1.161	.0775	1.225	.0437	1.126	.0653	1.165
8	.0305	1.099	.0511	1.224	.0647	1.336	.0385	1.163	.0542	1.226
$C_{Q_t}^\circ/oo$	0.682		1.154		1.480		0.882		1.246	
$C_{w_g}^\circ/oo$.749		1.338		1.791		.989		1.443	

No.	64		70 ¹		65 ²		66 ³		71 ⁴	
q_o	79.3		109.1		79.5		79.6		109.9	
U_o	37.27		44.07		37.32		37.34		43.97	
$\sqrt{}$	16.32×10^{-6}		16.80×10^{-6}		16.32×10^{-6}		16.32×10^{-6}		16.38×10^{-6}	
Re	4.63×10^6		5.33×10^6		4.64×10^6		4.645×10^6		5.45×10^6	
θ_{mm}	0.259		0.231		0.294		0.328		0.186	
for p/q_o	.044		.038		.041		.036		.039	
Slot	$C_{Q/2^\circ/oo}$	C_{p_g}	$C_{Q/2^\circ/oo}$	C_{p_g}	$C_{Q/2^\circ/oo}$	C_{p_g}	$C_{Q/2^\circ/oo}$	C_{p_g}	$C_{Q/2^\circ/oo}$	C_{p_g}
1	0.1216	1.111	0.1356	1.114	0.1017	1.099	0.0895	1.093	0.1903	1.151
2	.0544	1.152	.0611	1.126	.0464	1.132	.0411	1.120	.0833	1.166
3	.0544	1.106	.0626	1.090	.0462	1.095	.0406	1.088	.0864	1.103
4	.0537	1.074	.0632	1.069	.0460	1.071	.0409	1.068	.0868	1.079
5	.0610	1.199	.0678	1.161	.0512	1.175	.0458	1.157	.0938	1.211
6	.0772	1.143	.0857	1.126	.0651	1.123	.0575	1.110	.1204	1.177
7	.0542	1.133	.0609	1.110	.0453	1.109	.0403	1.102	.0860	1.167
8	.0444	1.173	.0496	1.166	.0383	1.130	.0334	1.101	.0690	1.262
$C_{Q_t}^\circ/oo$	1.076		1.172		0.880		0.778		1.632	
$C_{w_g}^\circ/oo$	1.173		1.310		.982		.858		1.894	

¹Transition 10 millimeters ahead of trailing edge, individual turbulent bursts earlier.²Individual turbulent bursts further forward.³Frequent turbulent bursts further forward.⁴Transition 5 millimeters ahead of trailing edge, individual turbulent bursts earlier.

No.	21				27				30.1				32				34			
q_o	69.8				69.5				85.0				54.8				103.8			
v_o	35.15				35.3				39.0				31.2				42.8			
\sqrt{v}	16.60×10^{-6}				16.88×10^{-6}				16.93×10^{-6}				16.55×10^{-6}				16.45×10^{-6}			
Re	2.188×10^6				2.160×10^6				2.382×10^6				1.948×10^6				2.690×10^6			
C_a	0.232				0.232				0.232				0.232				0.232			
Slot	$Q_a \times 10^{-3}$		C_{p_g}		$Q_a \times 10^{-3}$		C_{p_g}		$Q_a \times 10^{-3}$		C_{p_g}		$Q_a \times 10^{-3}$		C_{p_g}		$Q_a \times 10^{-3}$		C_{p_g}	
1	0				0				0				0				0			
2	0.070		1.258		0				0				0				0			
3	0.287		1.483		0.332		1.477		0.403		1.477		0.260		1.472		0.496		1.488	
4	0.254		1.553		0.260		1.550		0.313		1.546		0.202		1.527		0.383		1.551	
5	0.279		1.521		0.323		1.503		0.391		1.510		0.260		1.600		0.474		1.508	
6	0.480		1.483		0.548		1.454		0.667		1.460		0.445		1.449		0.807		1.463	
7	0.647		1.443		0.661		1.457		0.800		1.457		0.538		1.447		0.968		1.458	
8	0.377		1.389		0.471		1.358		0.581		1.361		0.391		1.357		0.701		1.355	
9	0.654		1.317		0.680		1.292		0.828		1.301		0.560		1.292		0.988		1.300	
10	0.335		1.230		0.346		1.227		0.410		1.228		0.279		1.223		0.497		1.224	
11	0.522		1.151		0.510		1.139		0.781		1.148		0.531		1.144		0.930		1.149	
12	0.315		1.121		0.312		1.113		0.393		1.117		0.261		1.118		0.480		1.113	
13	0.387		1.024		0.374		1.020		0.544		1.038		0.374		1.032		0.635		1.036	
14	0.506		0.972		0.390		0.950		0.457		0.954		0.321		0.944		0.544		0.956	
1'	0.083		1.189		0.043		1.167		0.084		1.176		0.055		1.181		0.116		1.188	
2'	0.288		1.209		0.295		1.189		0.390		1.198		0.260		1.195		0.471		1.194	
3'	0.166		1.175		0.149		1.123		0.192		1.133		0.138		1.136		0.236		1.134	
4'	0.191		1.160		0.133		1.120		0.169		1.134		0.118		1.133		0.204		1.131	
5'	0.225		1.158		0.234		1.108		0.312		1.115		0.218		1.114		0.374		1.112	
6'	0.368		1.127		0.331		1.107		0.430		1.119		0.297		1.117		0.516		1.119	
7'	0.315		1.100		0.382		1.075		0.520		1.082		0.363		1.079		0.621		1.079	
8'	0.503		1.021		0.534		1.015		0.682		1.018		0.473		1.016		0.810		1.012	
9'	0.359		1.007		0.375		1.006		0.502		1.018		0.350		1.017		0.301		1.018	
10'	0.809		0.989		0.824		0.971		0.906		0.984		0.725		0.980		1.210		0.983	
$C_{Q_o}^{o/oo}$	0.784				0.792				0.907				0.782				0.990			
$C_{Q_u}^n$	0.508 21.1 21.2 21.3				0.503				0.576 No. 30.2				0.516 No. 32.3				0.610 No. 34.2			
C_Q^n	1.290 1.340 1.470 1.572				1.295				1.483 1.574				1.278 1.253				1.600 1.890			
$C_{w_g}^n$	1.557 1.622 1.790 1.928				1.560				1.790 1.905				1.626 1.490				1.938 2.045			
$C_{w_\infty}^n$	0.838 0.755 0.678 0.657				0.720				0.590 0.520				0.880 0.930				0.590 0.650			
$C_{w_o}^n$	2.395 2.377 2.468 2.685				2.280				2.380 2.425				2.406 2.420				2.526 2.695			

On both sides laminar up to the trailing edge

No.	35		36.2		38.1		39		40	
Q_o	39.1		25.0		65.4		70.4		39.7	
V_o	26.4		21.1		31.32		35.3		26.6	
$\sqrt{V_o}$	16.60×10^{-6}		16.62×10^{-6}		16.45×10^{-6}		18.52×10^{-6}		16.55×10^{-6}	
Re	1.639×10^6		1.309×10^6		1.965×10^6		2.206×10^6		1.655×10^6	
C_a	0.232		0.232		0.372		0.372		0.372	
Slot	$Q_a \times 10^{-3}$ C_{p_g}		$Q_a \times 10^{-3}$ C_{p_g}		$Q_a \times 10^{-3}$ C_{p_g}		$Q_a \times 10^{-3}$ C_{p_g}		$Q_a \times 10^{-3}$ C_{p_g}	
1	0		0		0		0		0	
2	0		0		0		0		0	
3	0.192	1.467	0.168	1.480	0.396	1.624	0.488	1.630	0.302	1.616
4	0.147	1.527	0.131	1.552	0.276	1.636	0.343	1.651	0.216	1.636
5	0.193	1.601	0.170	1.534	0.359	1.576	0.440	1.580	0.285	1.674
6	0.335	1.448	0.296	1.467	0.568	1.511	0.694	1.511	0.449	1.505
7	0.398	1.454	0.356	1.480	0.691	1.487	0.840	1.490	0.542	1.487
8	0.297	1.360	0.260	1.378	0.472	1.365	0.574	1.385	0.374	1.386
9	0.428	1.290	0.376	1.304	0.683	1.311	0.822	1.318	0.543	1.307
10	0.254	1.229	0.218	1.246	0.393	1.236	0.472	1.235	0.323	1.236
11	0.403	1.145	0.323	1.164	0.618	1.154	0.754	1.155	0.496	1.155
12	0.253	1.126	0.210	1.146	0.288	1.116	0.360	1.118	0.267	1.124
13	0.300	1.036	0.270	1.063	0.403	1.019	0.484	1.027	0.361	1.027
14	0.400	0.981	0.424	1.019	0.335	0.939	0.400	0.941	0.386	0.965
1'	0.048	1.189	0.038	1.212	0.026	1.025	0.032	1.028	0.022	1.023
2'	0.146	1.172	0.124	1.203	0.121	1.049	0.292	1.048	0.095	1.048
3'	0.104	1.138	0.090	1.156	0.064	1.050	0.076	1.051	0.056	1.053
4'	0.093	1.138	0.081	1.162	0.060	1.052	0.072	1.053	0.053	1.053
5'	0.170	1.113	0.148	1.135	0.099	1.058	0.119	1.049	0.080	1.056
6'	0.228	1.119	0.198	1.143	0.149	1.043	0.180	1.043	0.119	1.042
7'	0.281	1.078	0.242	1.095	0.217	1.028	0.262	1.028	0.176	1.027
8'	0.366	1.018	0.316	1.035	0.355	0.981	0.410	0.979	0.310	0.882
9'	0.256	1.019	0.220	1.043	0.262	0.979	0.314	0.978	0.239	0.989
10'	0.726	1.006	0.642	1.030	0.756	0.960	0.858	0.954	0.708	0.975
$C_{Q_o}^{\circ}/\infty$	0.733		0.616		0.940 1.052 1.009		1.014		0.922	
$C_{Q_u}^{\circ}$	0.492 No. 35.2		0.534		0.362 0.396 0.331		0.398 No. 38.2 39.3		0.377	
$C_{Q_l}^{\circ}$	1.225 1.300		1.350		1.302 1.468 1.390 1.340		1.412 1.375 1.486		1.299	
$C_{w_g}^{\circ}$	1.454 1.556		1.632		1.618 1.828 1.737 1.681		1.761 1.710 1.857		1.594	
$C_{w_g}^{\circ}$	1.020 0.910		1.110		0.748 0.668 0.693 0.707		0.657 0.692 0.636		0.90	
$C_{w_b}^{\circ}$	2.472 2.465		2.742		2.366 2.496 2.430 2.388		2.418 2.402 2.492		2.494	

On both sides laminar up to the trailing edge

No. 38.2 38.3 38.4

No.	41		43.1		44		46		47	
q_o	25.5		55.8		71.80		39.9		25.8	
V_o	21.2		31.4		35.70		26.46		21.24	
\sqrt{Re}	16.36×10^{-6}		16.47×10^{-6}		16.60×10^{-6}		16.25×10^{-6}		16.25×10^{-6}	
Re	1.337×10^6		1.968×10^6		2.220×10^6		1.682×10^6		1.352×10^6	
C_a	0.372		0.480		0.480		0.480		0.480	
Slot	$Q_a \times 10^{-3}$	C_{p_g}	$Q_a \times 10^{-3}$	C_{p_g}	$Q_a \times 10^{-3}$	C_{p_g}	$Q_a \times 10^{-3}$	C_{p_g}	$Q_a \times 10^{-3}$	C_{p_g}
1	0		0		0		0		0	
2	0		0		0		0		0	
3	0.218	1.617	0.461	1.736	0.530	1.718	0.354	1.736	0.257	1.726
4	.157	1.657	.324	1.769	.372	1.736	.251	1.749	.184	1.745
5	.208	1.593	.439	1.668	.500	1.645	.345	1.665	.258	1.664
6	.338	1.510	.662	1.577	.754	1.563	.518	1.568	.392	1.564
7	.406	1.505	.806	1.558	.920	1.536	.610	1.549	.471	1.552
8	.283	1.397	.548	1.431	.628	1.413	.430	1.429	.325	1.427
9	.411	1.315	.786	1.353	.894	1.342	.622	1.348	.470	1.347
10	.245	1.246	.465	1.268	.526	1.255	.367	1.266	.281	1.268
11	.374	1.163	.630	1.166	.718	1.159	.494	1.165	.370	1.171
12	.215	1.140	.310	1.134	.345	1.122	.263	1.136	.220	1.144
13	.280	1.047	.426	1.045	.454	1.033	.370	1.046	.300	1.053
14	.392	1.008	.322	0.940	.330	0.934	.404	0.964	.400	1.004
1'	.015	1.036	.017	.953	.020	.940	.012	.945	.009	0.950
2'	.069	1.058	.082	.993	.092	.988	.063	.990	.048	.994
3'	.020	1.061	.050	.993	.057	.987	.036	.996	.027	.999
4'	.018	1.062	.031	1.011	.036	1.005	.017	1.010	.011	1.010
5'	.060	1.056	.063	1.007	.074	1.004	.053	1.013	.043	1.018
6'	.090	1.047	.103	1.015	.115	1.010	.078	1.013	.061	1.013
7'	.133	1.033	.125	1.007	.141	1.004	.120	1.005	.093	1.005
8'	.256	0.991	.227	0.967	.257	0.963	.280	0.967	.249	0.976
9'	.195	1.005	.219	.975	.248	.960	.232	.976	.193	.988
10'	.580	0.988	.794	.948	.887	.943	.660	.953	.535	.964
$C_{Q_o} \%$	0.896		1.057		1.050		1.020		0.993	
C_{Q_u} "	.364	No. 41.2	0.293	No. 43.2	0.290		0.315	No. 45	.287	.320
C_{Q_g} "	1.260	1.315	1.350	1.390	1.340	1.362	1.335	1.266	1.313	
C_{w_g} "	1.551	1.624	1.770	1.828	1.740	1.772	1.717	1.650	1.678	
C_{w_g} "	1.13	1.10	0.735	0.695	0.710	0.680	0.850	0.935	1.075	
C_{w_∞} "	2.681	2.724	2.505	2.523	2.450	2.452	2.567	2.585	2.753	

On both sides laminar up to the trailing edge

No.	54		55.3		56.1		57.3	
q_o	22.2		29.3		40.4		18.05	
V_o	19.63		22.58		26.56		17.75	
ν	16.07×10^{-6}		16.07×10^{-6}		16.17×10^{-6}		16.17×10^{-6}	
Re	1.260×10^6		1.450×10^6		1.696×10^6		1.134×10^6	
C_a	0.163		0.587		0.587		0.587	
Slot	$Q_a \times 10^{-3}$	C_{p_g}	$Q_a \times 10^{-3}$	C_{p_g}	$Q_a \times 10^{-3}$	C_{p_g}	$Q_a \times 10^{-3}$	C_{p_g}
1	0		0.328	1.748	0.424	1.761	0.220	1.732
2	0		.187	1.792	.243	1.804	.125	1.792
3	0.121	1.399	.404	1.820	.522	1.819	.276	1.823
4	.116	1.489	.169	1.796	.218	1.795	.116	1.797
5	.166	1.466	.273	1.750	.349	1.749	.187	1.769
6	.247	1.420	.492	1.661	.624	1.664	.344	1.661
7	.301	1.424	.543	1.624	.697	1.619	.379	1.636
8	.209	1.339	.390	1.487	.496	1.484	.275	1.504
9	.305	1.271	.580	1.401	.736	1.404	.407	1.412
10	.123	1.196	.333	1.307	.426	1.299	.236	1.320
11	.266	1.146	.436	1.182	.560	1.178	.296	1.200
12	.245	1.131	.213	1.170	.272	1.165	.146	1.190
13	.287	1.057	.298	1.074	.378	1.075	.286	1.135
14	.476	1.044	.351	0.979	.439	0.983	.558	1.157
1'	.087	1.255	0		0		0	
2'	.144	1.268	0		0		0	
3'	.075	1.205	0		0		0	
4'	.116	1.156	0		0		0	
5'	.276	1.213	.028	.971	.036	.970	.021	0.980
6'	.210	1.155	.059	.988	.070	.988	.042	.995
7'	.261	1.096	.072	.987	.086	.988	.073	1.001
8'	.295	1.018	.158	.950	.197	.949	.116	0.959
9'	.252	1.042	.146	.956	.185	.960	.096	.970
10'	.518	0.972	.548	.928	.681	.931	.555	.977
C_{Q_o}/∞	0.784				1.286		1.167	
C_{Q_u}	.611		No. 55.2 55.4		0.264 No. 56.2		0.273	
C_Q	1.395		1.430	1.405 1.480	1.550	1.597	1.440	
C_{w_g}	1.644		1.985	1.936 2.045	2.154	2.221	1.975	
$C_{w'}$	1.360		0.95	0.97 0.92	0.730	0.710	1.145	
C_{w_∞}	3.004		2.935	2.906 2.965	2.884	2.931	3.120	

On both sides laminar up to the trailing edge

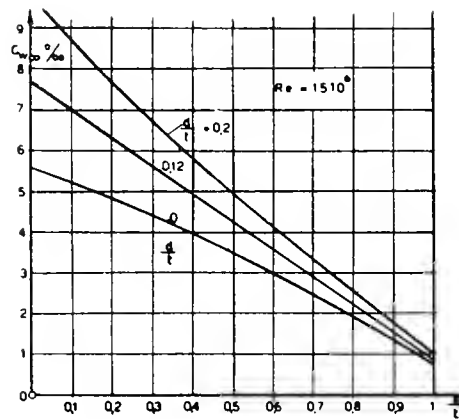


Figure 1.- Influence of the transition-point position on the profile drag for various profile thicknesses; $Re = 15 \times 10^6$.

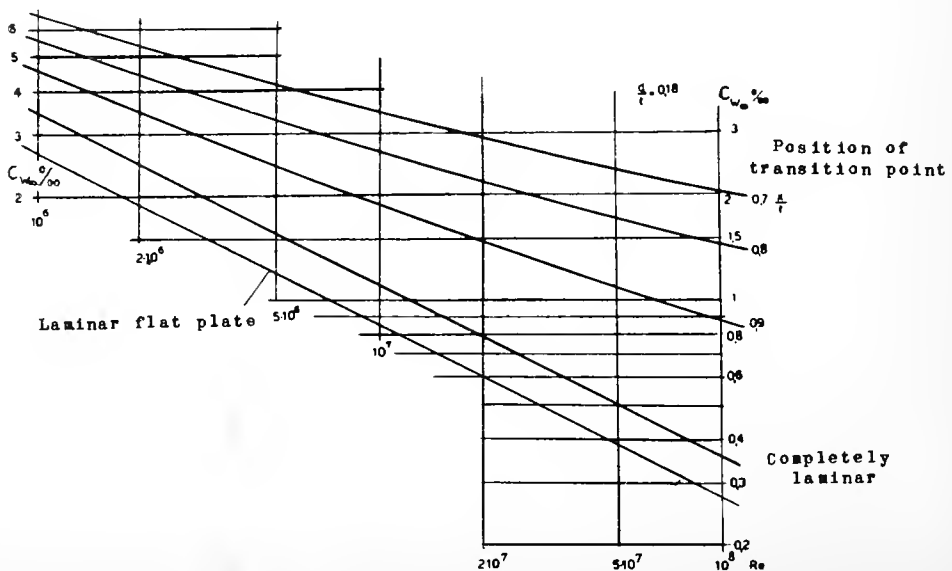


Figure 2.- Influence of the transition-point position on the profile drag for various Re ; $d/t = 0.16$.

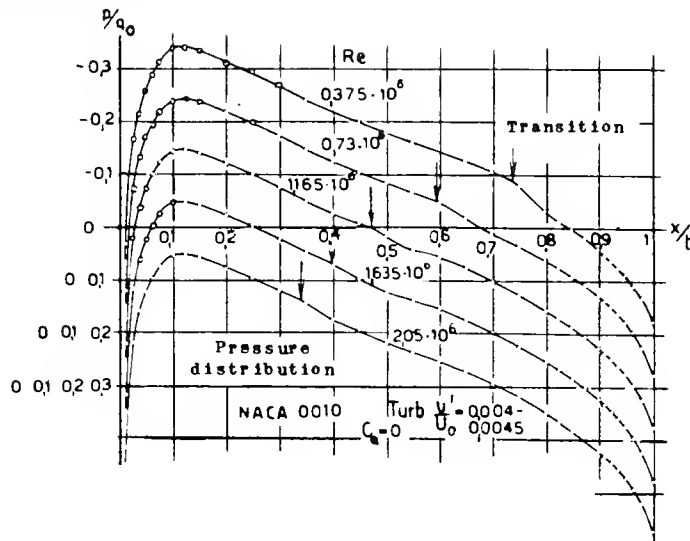


Figure 3.- Pressure distributions along the chord on the profile NACA 0010 for various Re ; $c_a = 0$. (The pressure distributions for the different Re are every time shifted vertically downward by $\Delta p/a_0 = 0.1$.) The start of transition is denoted by arrows, $t = 0.60$ m.

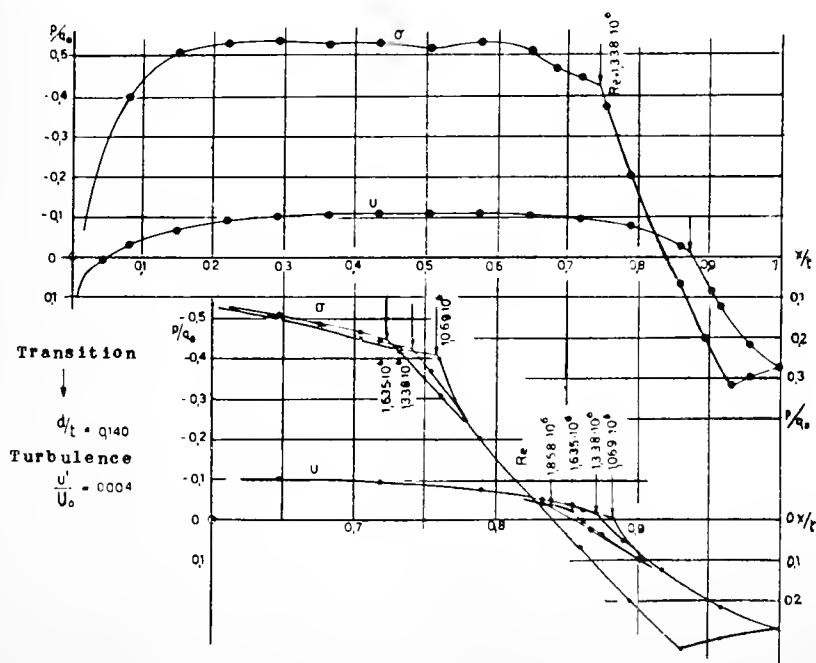


Figure 4.- Laminar profile $d/t = 0.140$ (fig. 12), $t = 0.70$ m. Pressure distributions along the chord and transition start (vertical arrows) for smooth inflow. The lower figure shows the pressure distributions in the rear part of the profile for various Re on an enlarged scale.

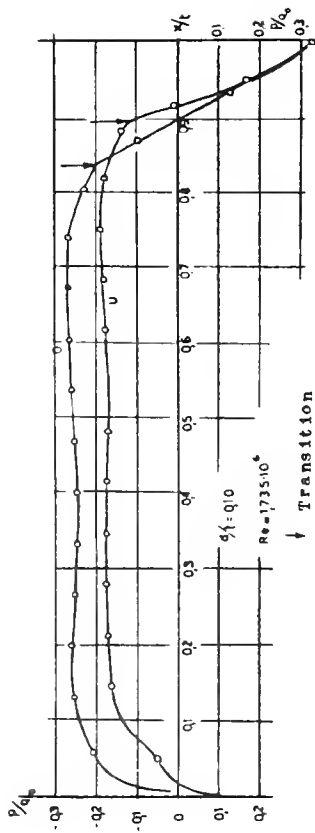


Figure 5.- Laminar profile $d/t = 0.10$ (fig. 12), $t = 0.74$ m. Pressure distribution along the chord and transition start (vertical arrows) for smooth inflow, $Re = 1.735 \times 10^6$.

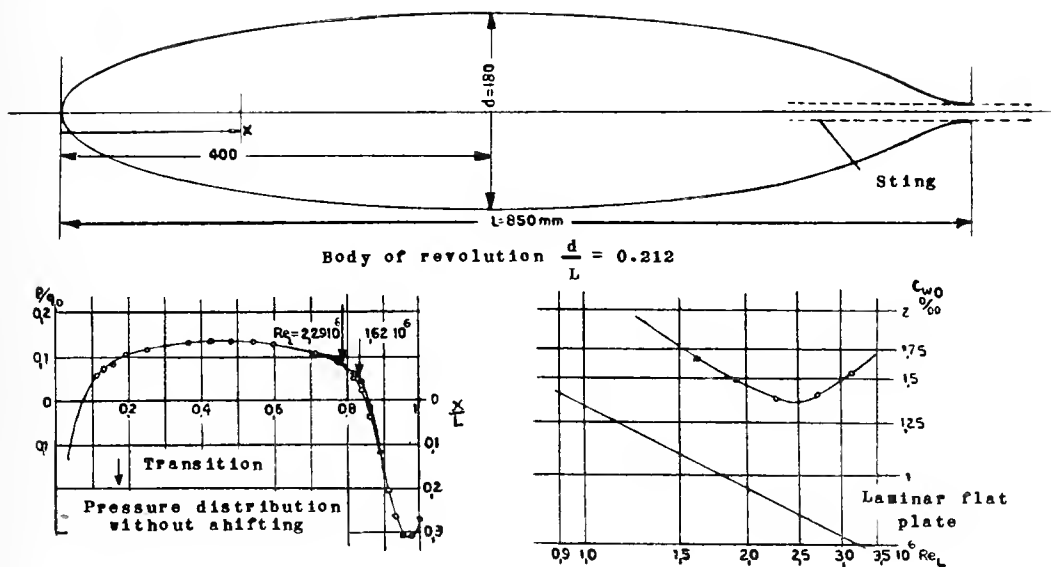


Figure 6.- Body of revolution $d/L = 0.212$, angle of attack $= 0^\circ$. Pressure distribution and transition start (vertical arrow) at $Re_L = 1.62 \times 10^6$ and 2.29×10^6 . Drag variation c_{w0} as a function of $Re_L = \frac{U L}{\nu}$ (c_{w0} is referred to the surface of the body). The drag increase for larger Re is caused by the wind-tunnel turbulence.

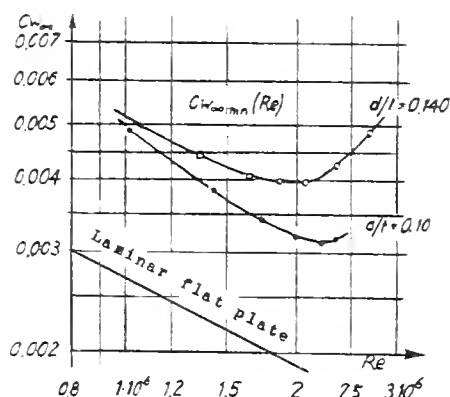


Figure 7.- Laminar profile $d/t = 0.140$, $t = 0.70$ m (fig. 12); $d/t = 0.10$, $t = 0.74$ m (fig. 12); minimum profile drag $c_{w_{\infty min}}(Re)$ (momentum measurements). The drag increase for larger Re is caused by the wind-tunnel turbulence. (See also fig. 8.)

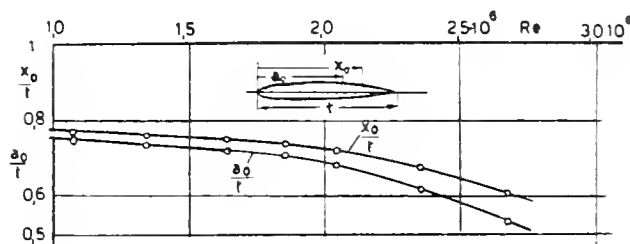


Figure 8.- Laminar profile $d/t = 0.140$, $t = 0.70$ m (fig. 12). Transition-point position on the upper surface for various Re (observations by stethoscope). a_0 = transition start, x_0 = start of the developed turbulent boundary layer measured from the front.

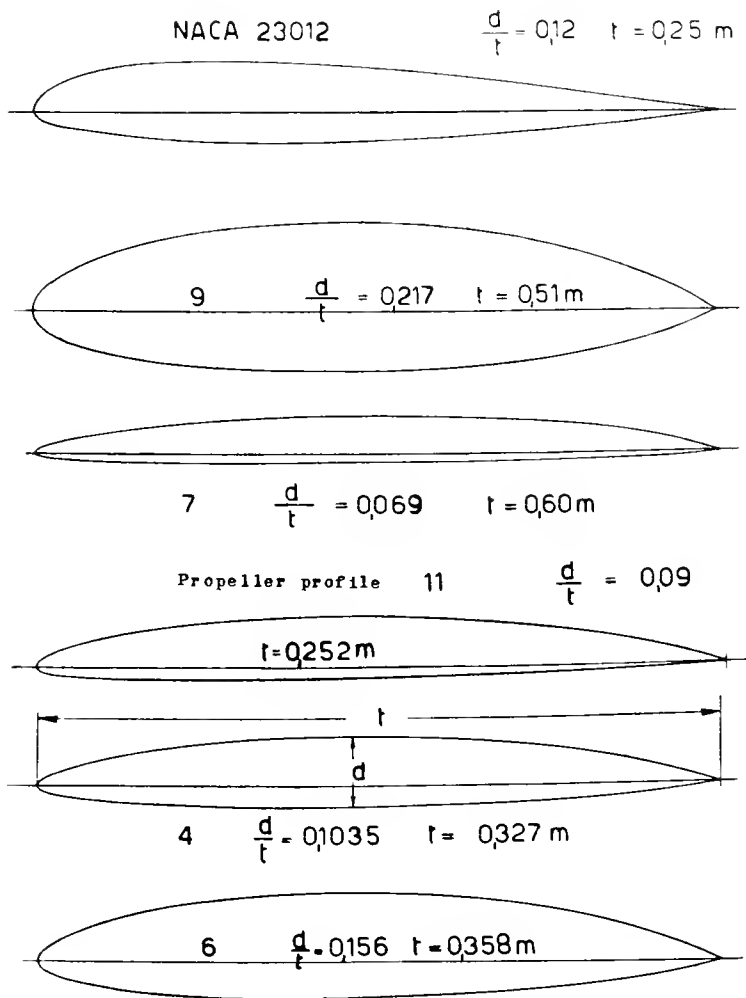


Figure 9.- Laminar profiles for various thicknesses and NACA profile 23012.

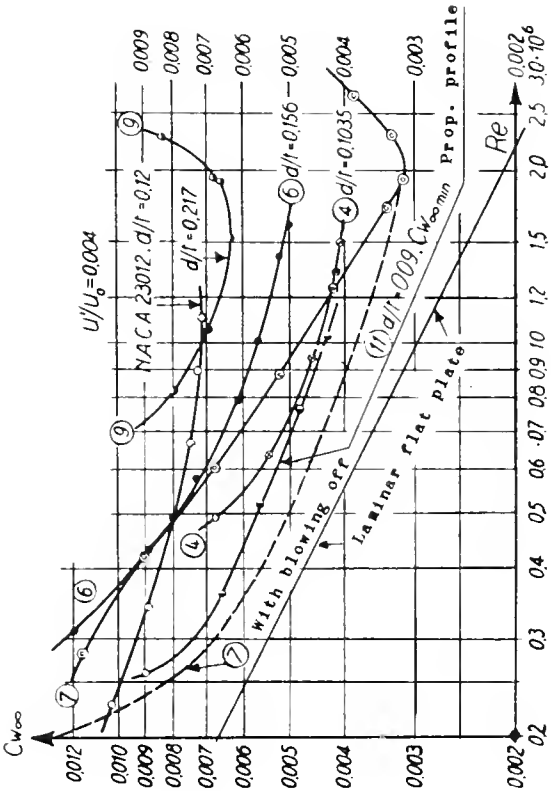


Figure 10.- Profile drag $c_{w\infty}$ (Re) (momentum measurements) of the laminar profiles of figure 9 and of the NACA profile 23012 for smooth inflow. The drag increase for larger Re is caused by the wind-tunnel turbulence.

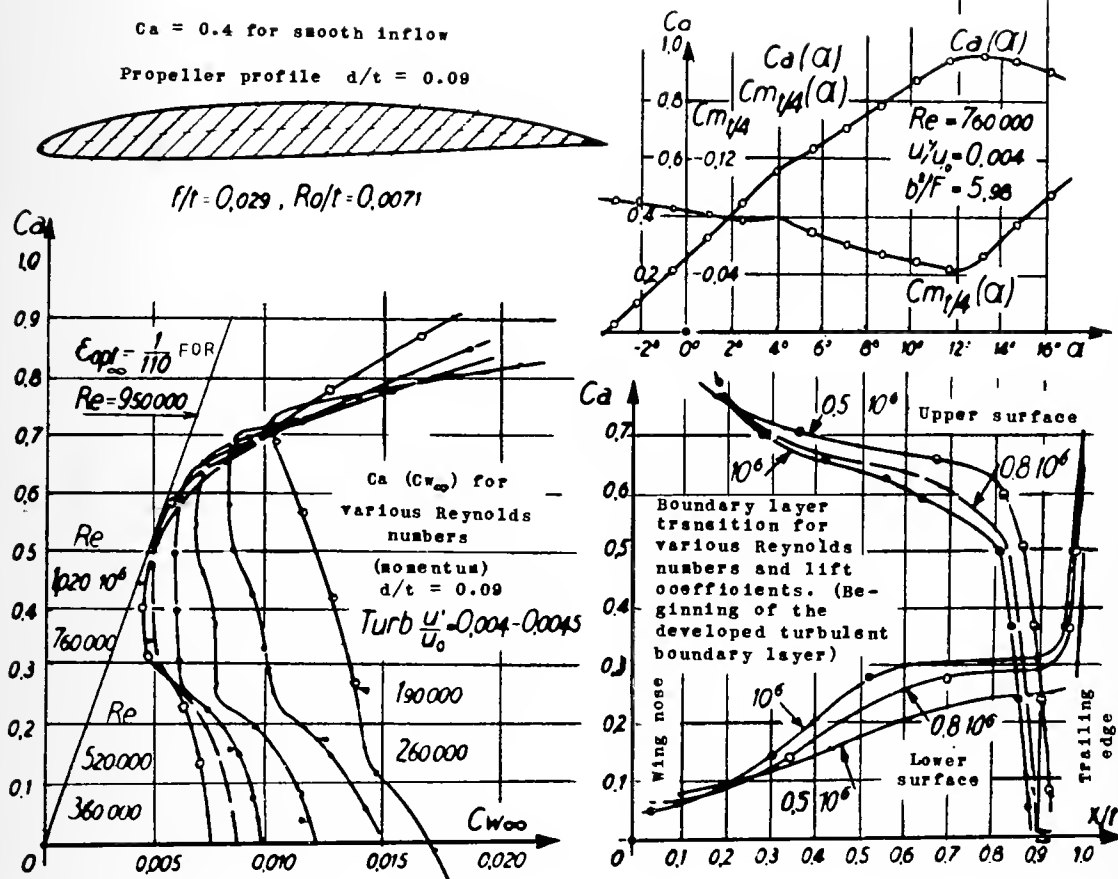


Figure 11.- Propeller profile 11, $d/t = 0.90$, $t = 0.25$ m. Profile-drag polars (momentum measurements) for various Re ; transition point positions (observations by stethoscope) for various c_a and Re ; $c_a(\alpha)$ and $c_{m_{t/4}}(\alpha)$.

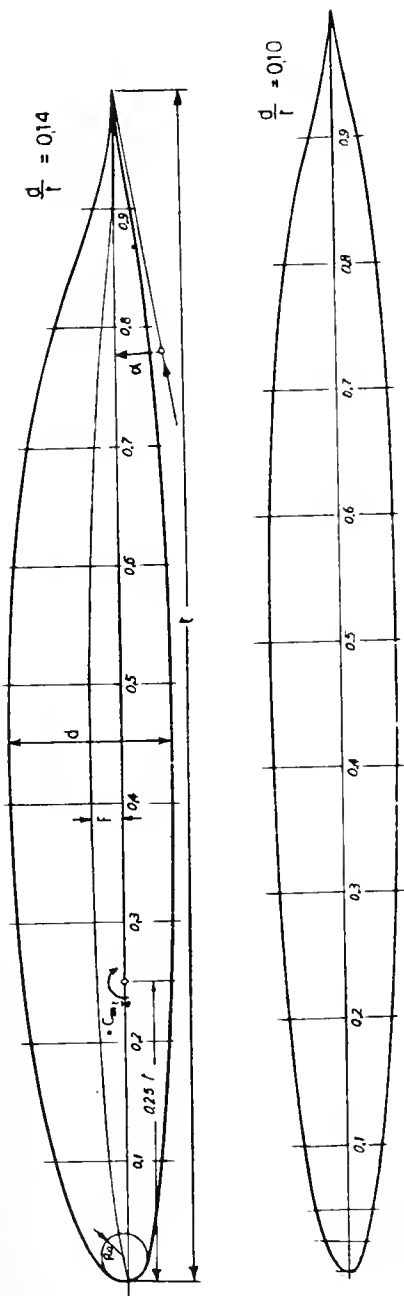


Figure 12.- Laminar profiles for wings, $d/t = 0.10$, $t = 0.74$ m; $d/t = 0.14$, $t = 0.70$ m.

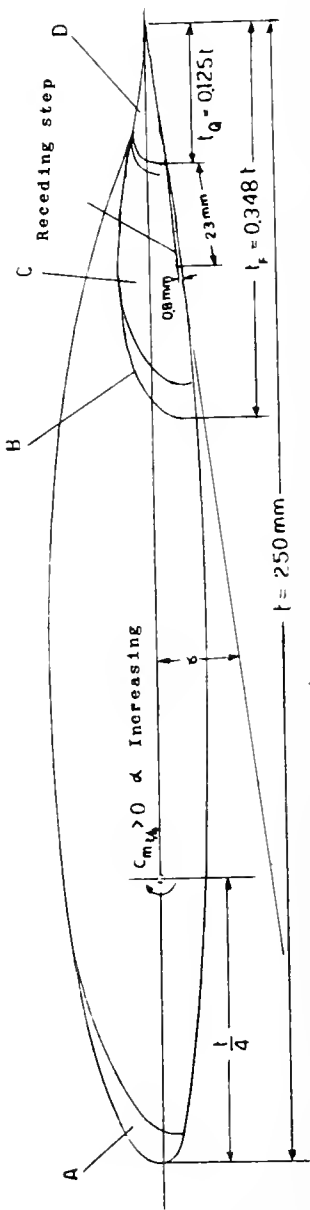


Figure 13.- Laminar profile for wing with landing aid (retracted), $d/t = 0.14$, $t = 0.250$ m. A = front slat on the main profile. B = slat on the Fowler flap, C = Fowler flap ($t_F = 0.348t$). D = trailing edge aileron ($t_Q = 0.125t$).

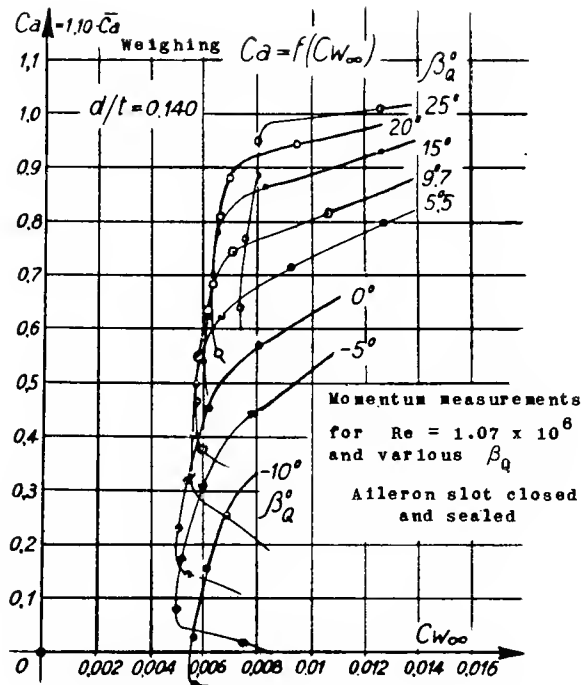
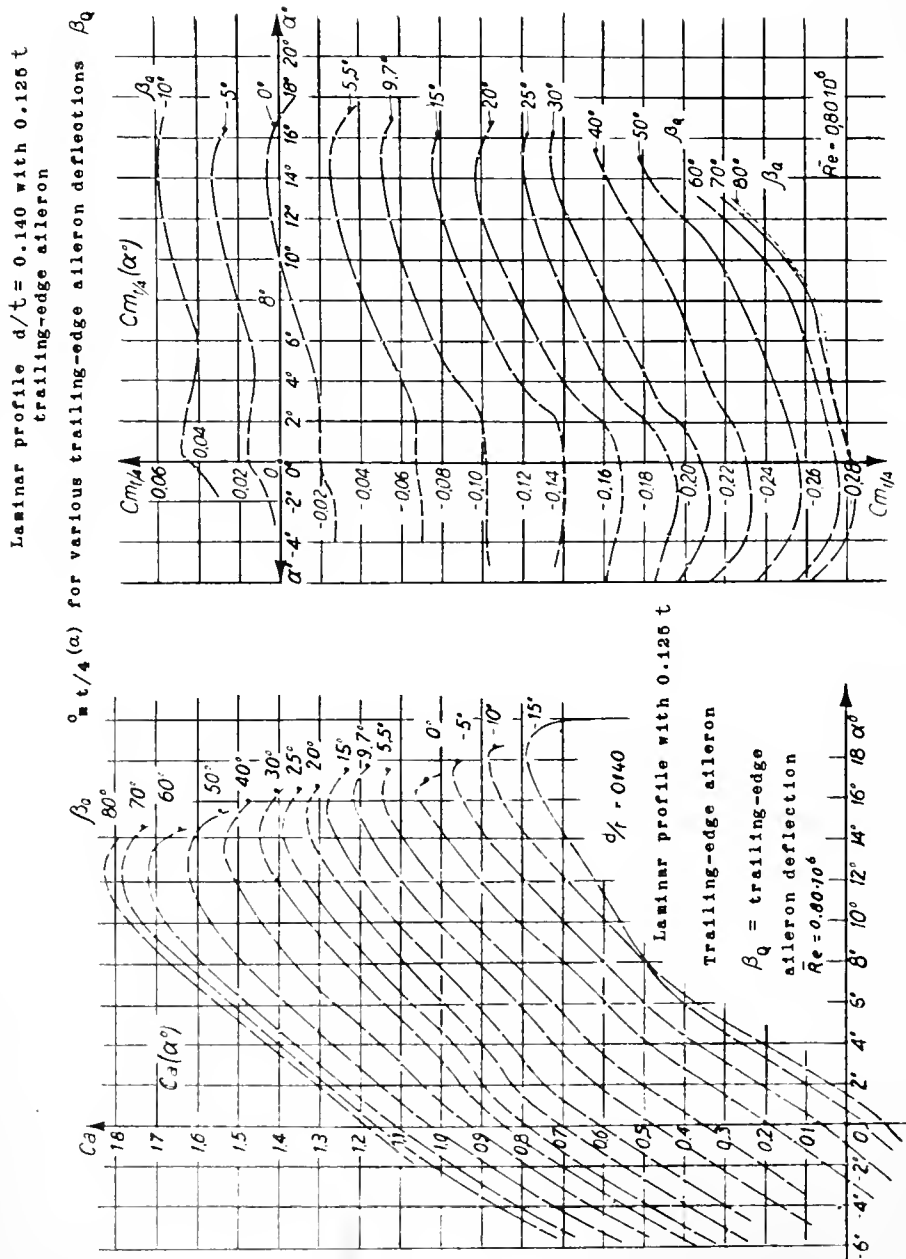


Figure 14.- Laminar profile for wing, $d/t = 0.14$, $t = 0.250$ m (fig. 13).
 Profile-drag polars (momentum measurements) for various trailing-edge aileron deflections β_Q . Aileron slot between upper and lower surface sealed. $Re = 1.07 \times 10^6$.



Figures 15,16.- Laminar profile for wing, $d/t = 0.14$, $t = 0.250 m$ (fig. 13), $b = 1.50 m$, $b^2/F = 6.04$; rectangular wing with rounded ends, $c_a(\alpha)$ and $C_{m_t/4}(\alpha)$ for various trailing-edge aileron deflections β_Q . Aileron slot between upper and lower surface sealed.

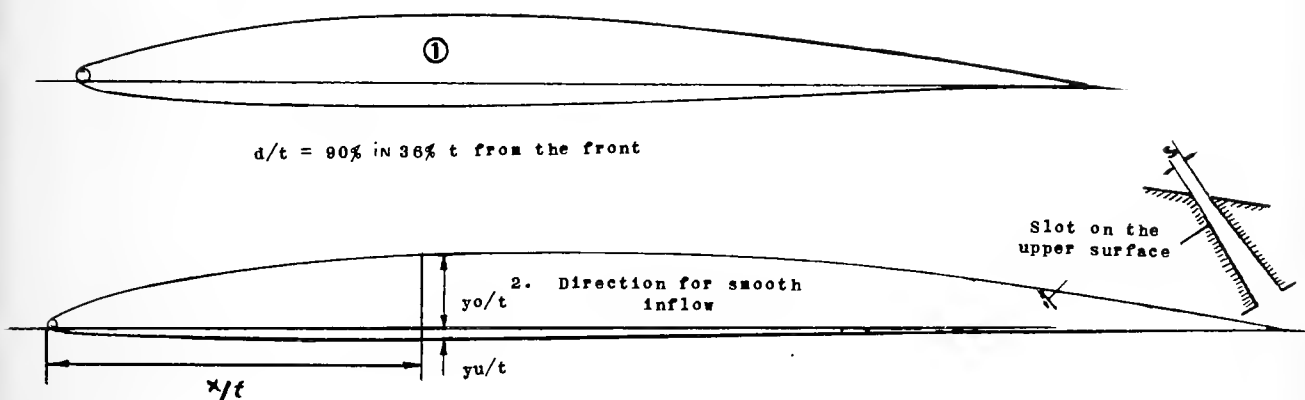


Figure 17.- Laminar suction profile 2 with a single suction slot on the upper surface. $d/t = 0.0675$ in $0.394 t$ from the front. Profile 1, $d/t = 0.09$, without suction.

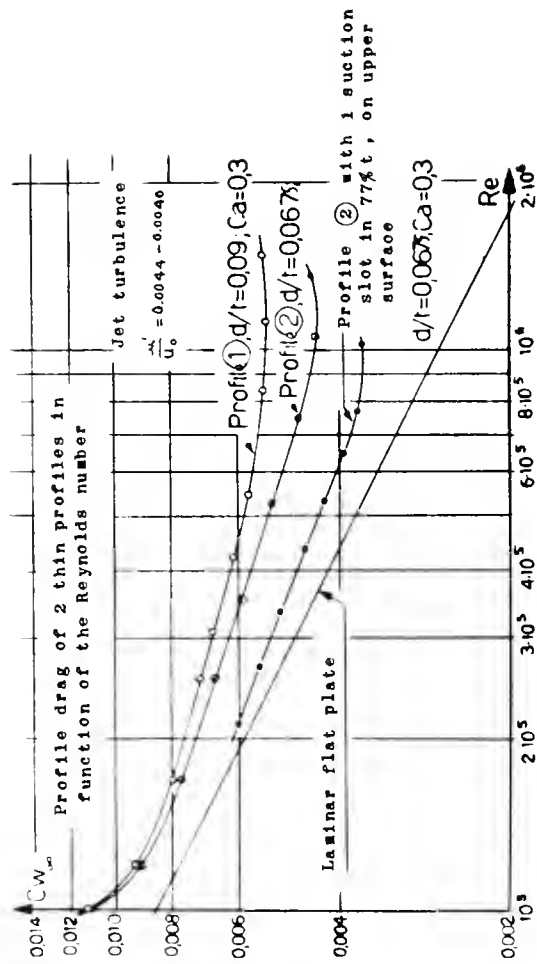
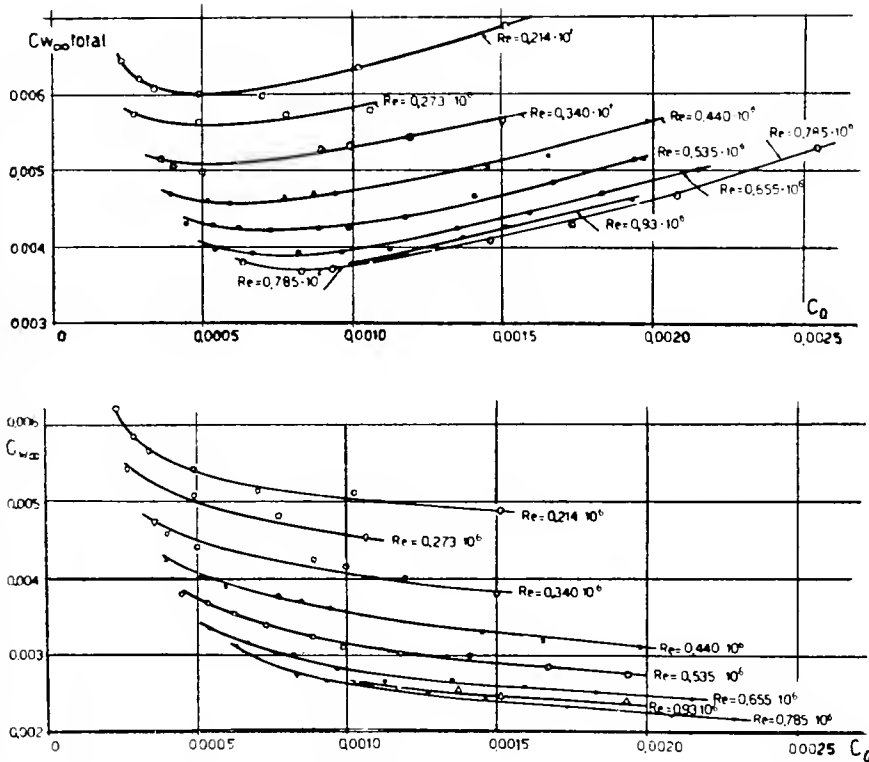


Figure 18.- Laminar suction profile 2 (fig. 17). Minimum slot width $s = 0.9$ millimeter $C_{w_{\infty}}(Re)$ without and with boundary-layer suction, $C_{w_{\infty}}(Re)$ of profile 1.



Figures 19,20.- Laminar suction profile 2. Total drag $c_{w\infty}(c_Q)$ and drag contribution of the wake $c_{w\infty}'(c_Q)$ for various Re , $s = 1.3$ millimeters.

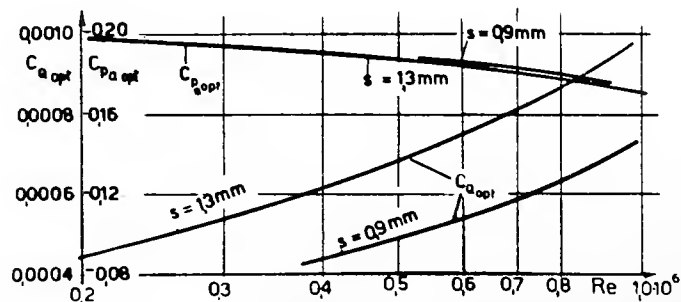


Figure 21.- Laminar suction profile 2. Optimum suction quantity c_{Qopt} and pertaining static pressure cp_{aopt} in the suction chamber for optimum total drag, $s = 0.9$ millimeter and 1.3 millimeters.

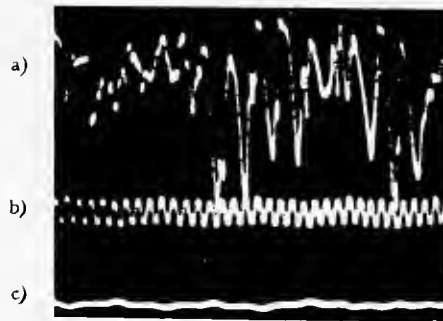


Figure 22.- Hot-wire photograph, 30 millimeters ahead of the trailing edge on upper side 0.2 millimeter over the surface. (a) Without suction, slot closed: turbulent; (b) time trace ($f = 400/\text{sec}$); (c) with suction: laminar, $c_Q = 0.0009$ $Re = 275,000$, $u'/U_0 = 0.0044$.

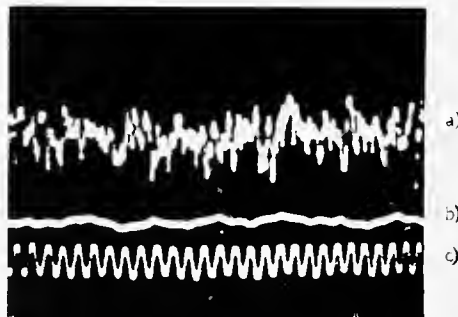


Figure 23.- Hot-wire photograph, 30 millimeters ahead of the trailing edge on upper side 0.2 millimeter over the surface. (a) Without suction, slot closed: turbulent; (b) with suction ($c_Q = 0.0016$): laminar; (c) time trace (500/sec), $Re = 790,000$, $u'/U_0 = 0.0040$.

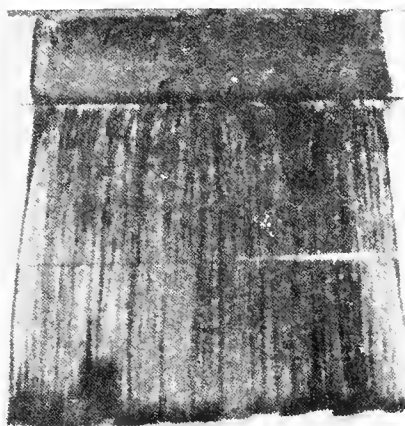


Figure 24.- Boundary-layer observation with soot coating for laminar suction (everything laminar with the exception of the edge of the boundary layer).

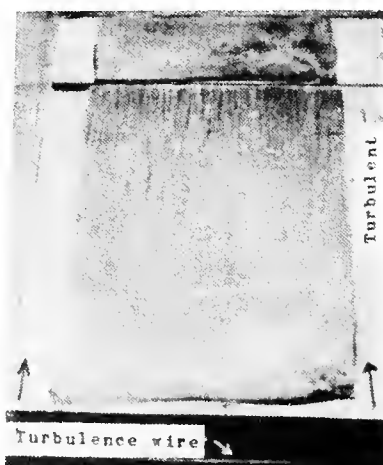


Figure 25.- Boundary-layer observation with soot coating with horizontal turbulence wire (greatest part turbulent).

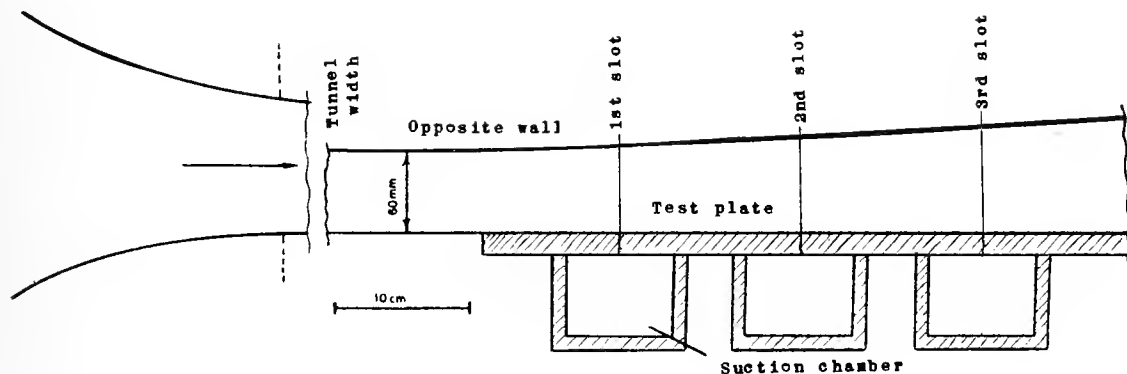


Figure 26.- Laminar suction tests with three single suction slots arranged one after another. Test arrangement.

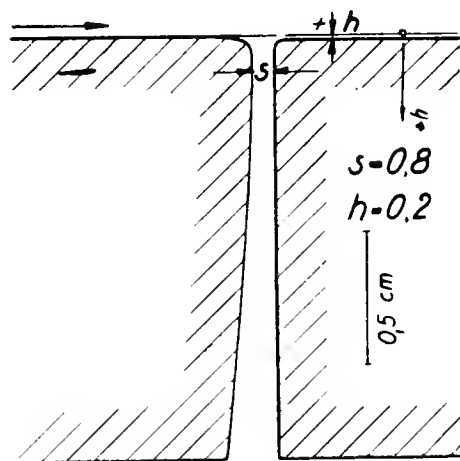


Figure 27.- Shape of the suction slot (a).

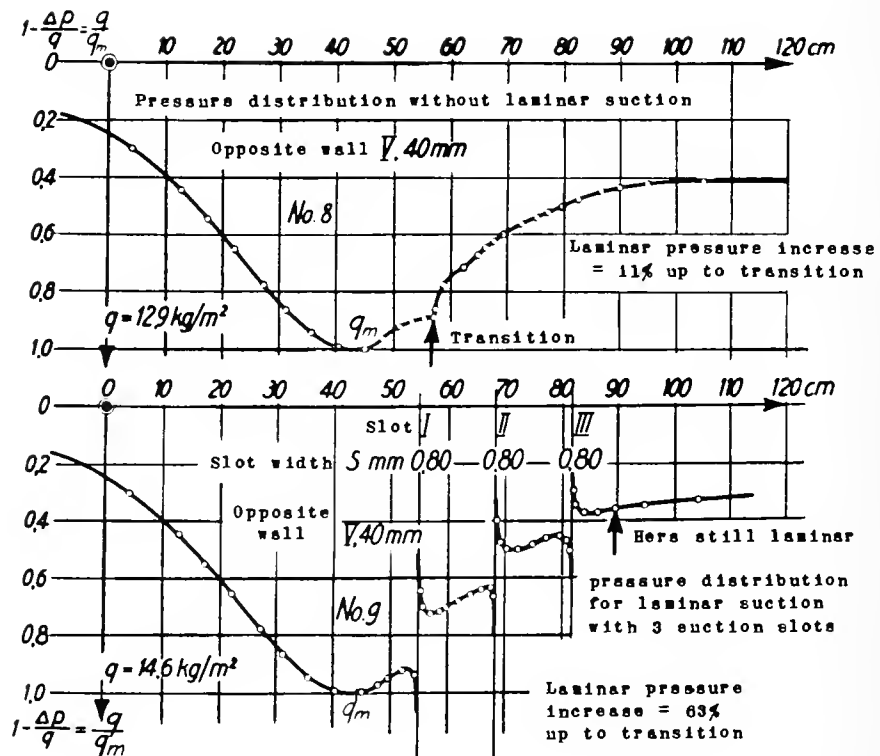


Figure 28.- Laminar suction tests with three suction slots. Static pressure at the test plate for various suction quantities and tunnel widths.

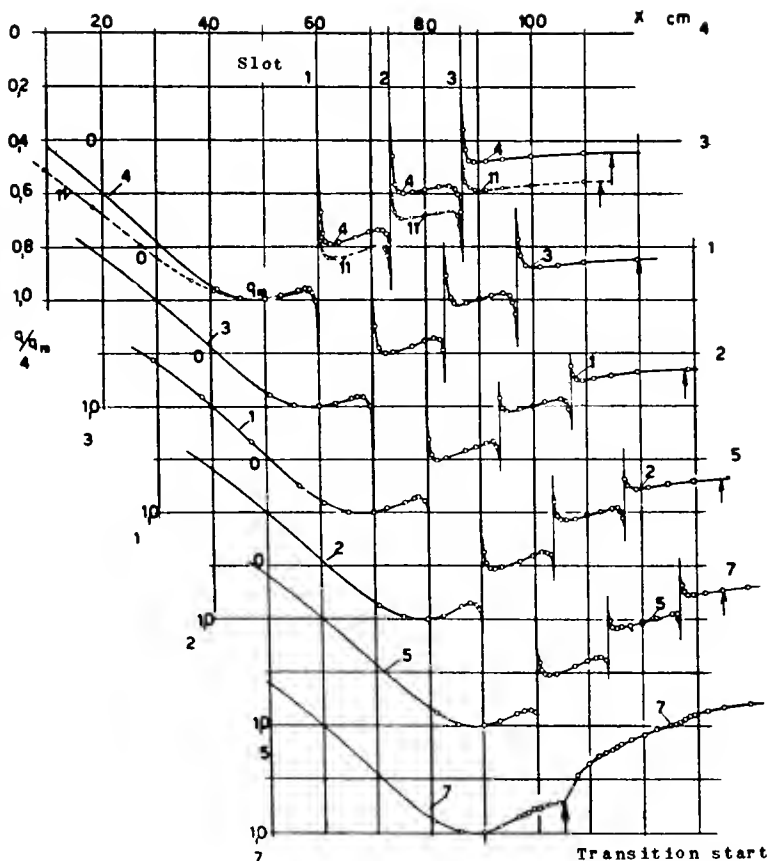


Figure 29.- Laminar suction tests with three suction slots. Static pressure at the test plate for various suction quantities and tunnel widths.

$$q/q_m = 1 - \frac{\Delta p}{q_m} \quad b = 0.40 \text{ m.}$$

Table to figure 29.

No	Tunnel width mm	q_m kg/m ²	Q_a 10 ⁻³ m ³ /s		
			Slot 1	2	3
1	60	8.07	2.09	2.66	2.55
2	60	7.50	1.66	2.14	2.13
3	60	8.15	2.55	3.65	3.39
4	60	8.15	3.79	4.75	4.34
5	60	8.20	1.36	1.79	1.57
7	60	5.17	Without suction		
9	40	14.6	3.76	4.66	4.24
5	40	12.9	Without suction		
11	30	8.2	1.92	2.29	2.17

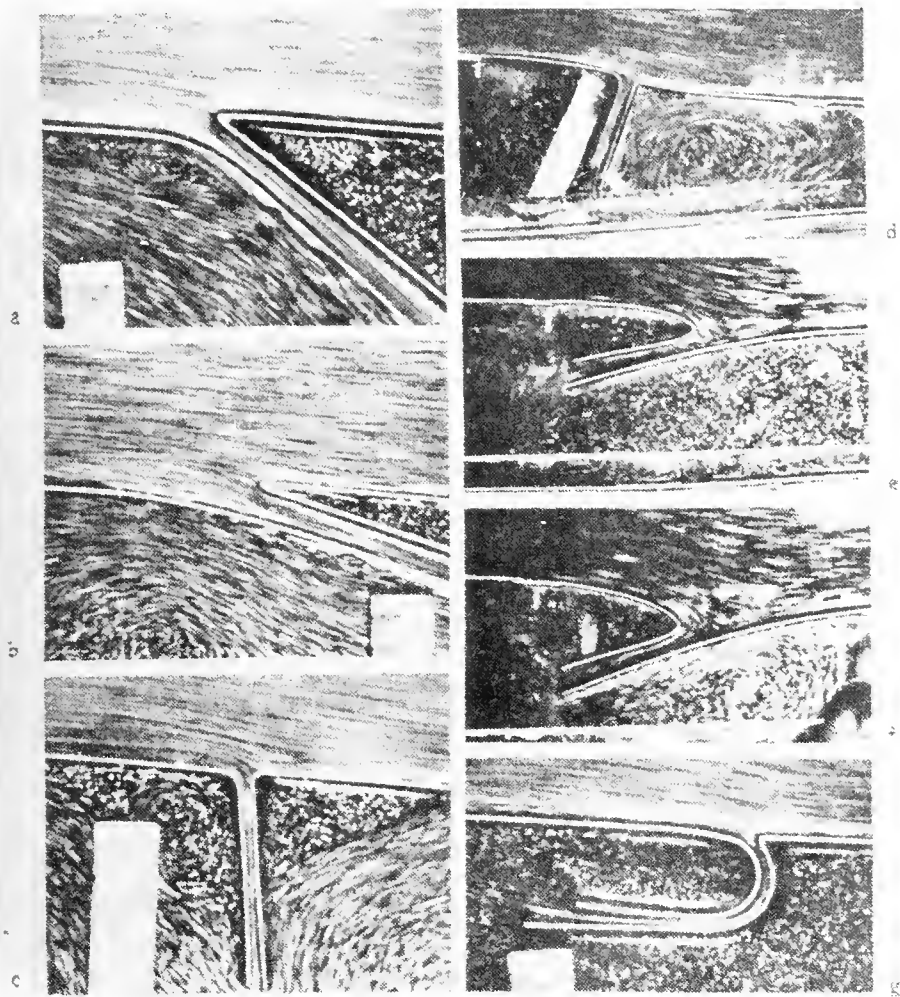


Figure 30.- Flow photographs in the water tank with laminar boundary-layer suction. Flow direction from the left.

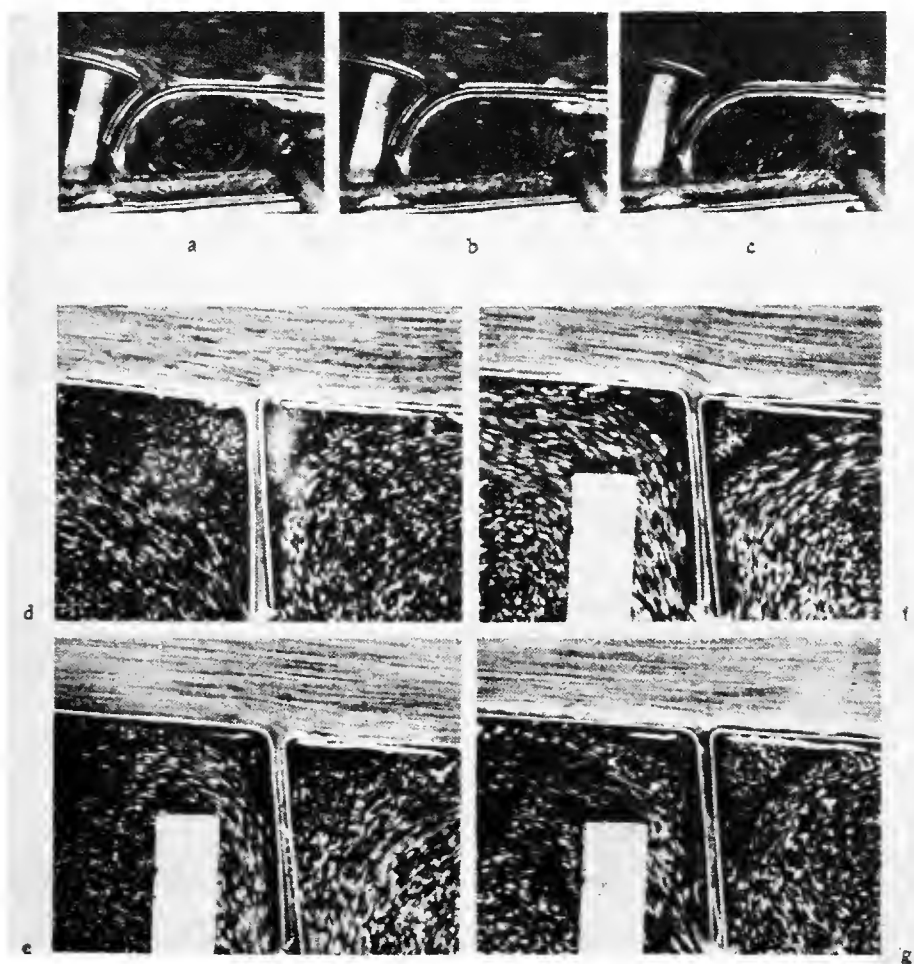
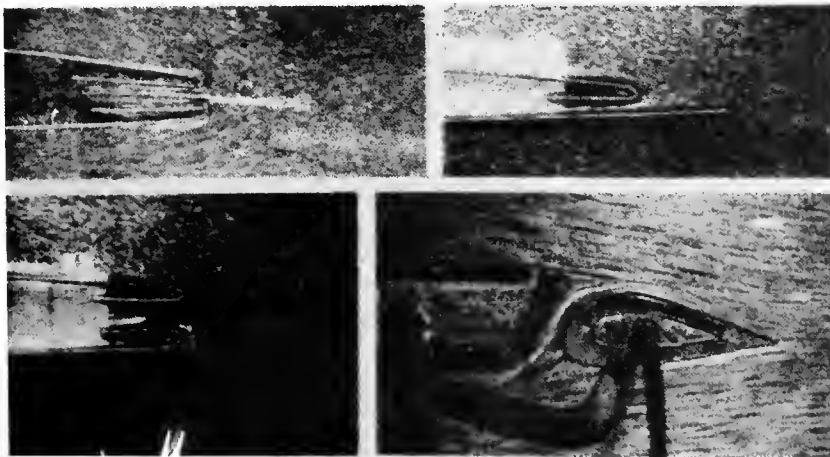


Figure 31.- Flow photographs in the water tank with laminar boundary-layer suction. Flow direction from the left.



Figure 32.- Flow photographs in the water tank with laminar boundary-layer suction. Flow direction from the left.



Figures 33,34.- Flow photographs in the water tank with laminar boundary-layer suction. Flow direction from the left.

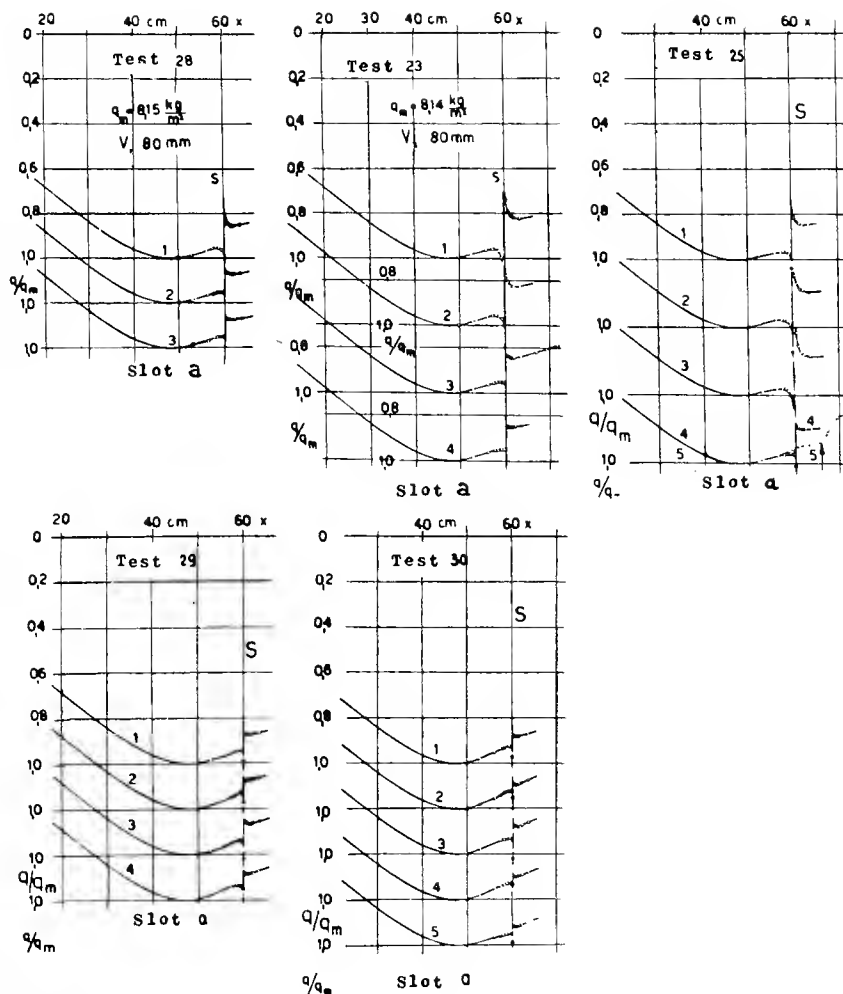


Table to figure 35.

Test	s mm	h mm	$Q_a \cdot 10^{-3}$ m^3/s	Q_a/Q_{δ^*}	q_m kg/m^2	Test	s mm	h mm	$Q_a \cdot 10^{-3}$ m^3/s	Q_a/Q_{δ^*}	q_m kg/m^2
23.1	0.85	0.35	1.97	0.268	8.14	29.1	0.85	0.35	0.77	0.106	8.14
23.2			1.24	0.170		29.2			0.62	0.085	8.14
23.3			0.77	0.106		29.3			0.55	0.063	4.07
23.4			0.60	0.082		29.4			1.14	0.187	16.28
25.1	0.80	0.60	0.80	0.109	8.16	30.1	0.85	0.7	0.82	0.113	8.14
25.2			1.25	0.171		30.2			0.64	0.087	8.14
25.3			1.95	0.270		30.3			0.56	0.092	4.07
25.4			0.62	0.085		30.4			1.17	0.134	16.28
25.5			0	0		30.5			0.81	0.111	8.14
28.1	0.85	0	1.25	0.171	8.15						
28.2			0.79	0.108							
28.3			0.61	0.084							

Figure 35.- Laminar suction tests with the single suction slot (a). Opposite wall V, tunnel width 80 millimeters. Tests 23, 25, 28, 29, 30: Influence of the suction quantity Q_a and the shifting of the slot trailing edge on the pressure distribution (sink effect).

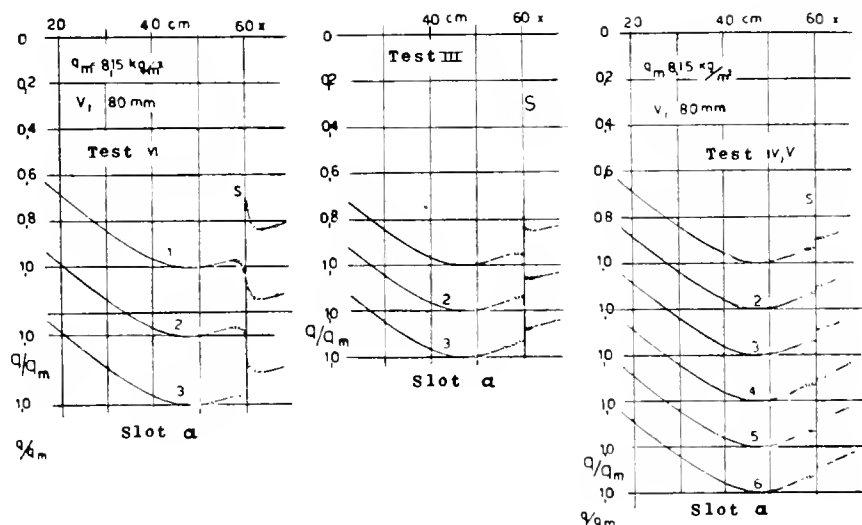


Figure 36.- Laminar suction tests with the slot (a). Tunnel width 80 millimeters. Tests III, IV, V, VI: Influence of the suction quantity and slot width on the pressure distribution (sink effect). $q_m = 8.15 \text{ kg/m}^2$.

Table to figure 36.

Test	s mm	h mm	$Q_a \cdot 10^{-3} \text{ m}^3/\text{s}$	$Q_a Q_{\delta^*}$	Test	s mm	h mm	$Q_a \cdot 10^{-3} \text{ m}^3/\text{s}$	$Q_a Q_{\delta^*}$
III, 1	0.52	0.3	0.80	0.109	V, 4	0.2	0.15	0.19	0.026
2			0.63	0.086	5			0.42	0.057
3			0.44	0.060	6			0.32	0.043
IV, 1	0.3	0.2	0.313	0.042	VI, 1	1.25	0.5	1.97	0.270
2			0.235	0.032	2			1.26	0.172
3			0.405	0.055	3			0.83	0.114

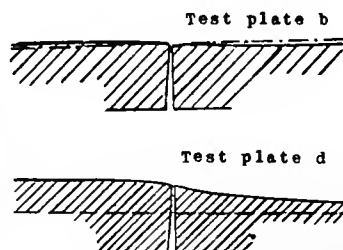
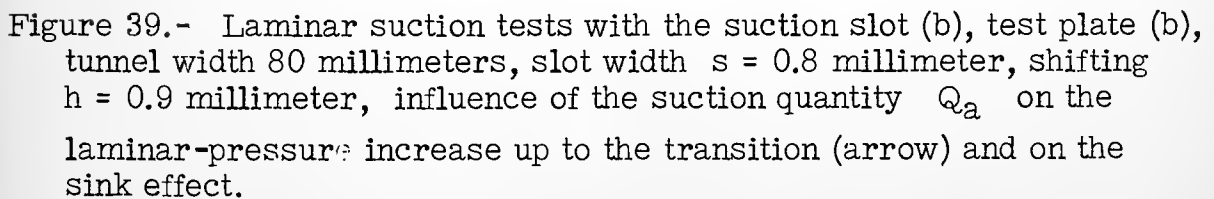
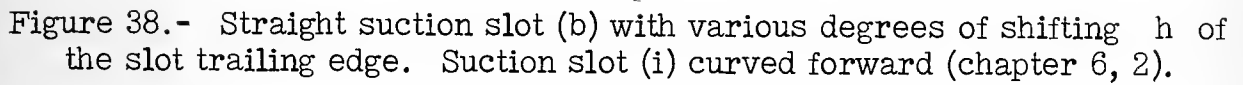


Figure 37.- Shape of the test plate (b) and (d) with the single suction slot (b) (fig. 38). It was located at the place of the first slot in the tests with three slots (chapter 5, 1).

[illegible]

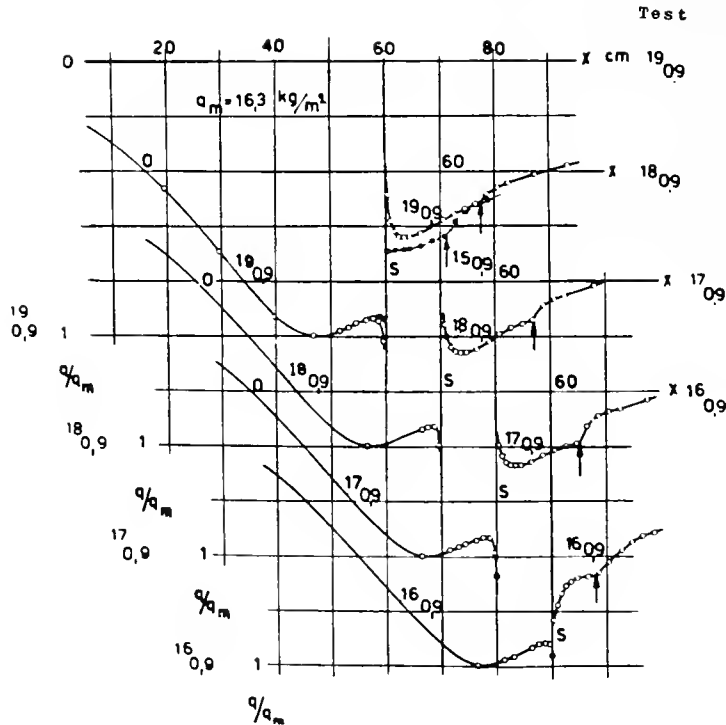


Figure 40.- Laminar suction tests with the suction slot (b), test plate (b), 40-millimeter tunnel width, $s = 0.8$ millimeter, $h = 0.9$ millimeter, $q_m = 16.3 \text{ kg/m}^2$. Influence of the suction quantity Q_a on the laminar-pressure increase up to the transition (arrow) and on the sink effect.

No.	190,9	180,9	170,9	160,9	150,9	140,9
$Q_a \cdot 10^{-3} \text{ m}^3/\text{s}$	5,67	4,07	2,76	1,19	1,59	2,01
Q_a/Q_{δ^*}	0,674	0,483	0,328	0,141	0,189	0,239

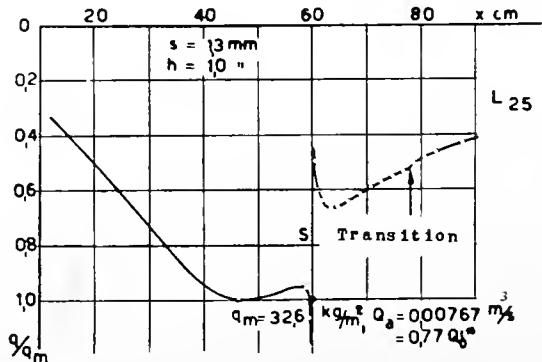


Figure 41.- Laminar suction test with slot (b) (L 25), test plate (b) 40-millimeter tunnel width, $s = 1.3$ millimeters, $h = 1.0$ millimeter, $q_m = 32.6 \text{ kg/m}^2$, $Q_a = 0.00767 \text{ m}^3/\text{s} = 0.77 \times Q_{\delta^*}$.

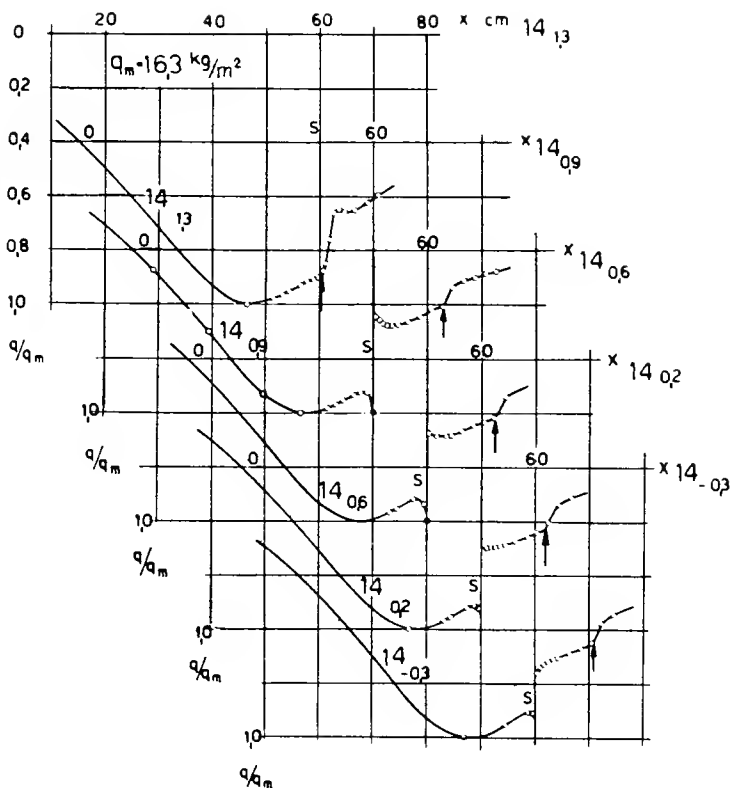
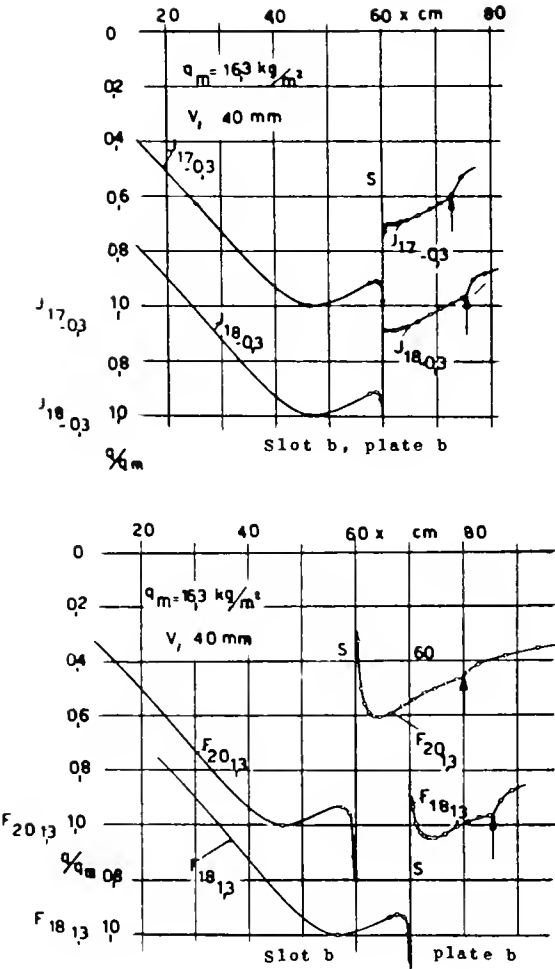


Figure 42.- Laminar suction tests with slot (b), test plate (b), 40-millimeter tunnel width, $s = 0.8$ millimeter, $q_m = 16.3 \text{ kg/m}^2$, $Q_a = 0.00201$
 $m^3/s = 0.239 \times Q_s^*$. Influence of the shifting h of the slot trailing edge (fig. 38) on the laminar-pressure increase up to the transition (arrow) and the sink effect.

Test	141,3	140,9	140,6	140,2	14-0,3
h mm	1,3	0,9	0,6	0,2	-0,3



Figures 43,44.- Laminar suction tests with slot (b), test plate (b), 40-millimeter tunnel width, $s = 0.8$ millimeter, $q_m = 16.3$ kg/m². Pressure distribution up to the transition (arrow) for considerable outward shifting ($h = -0.3$ mm) or inward shifting, respectively, ($h = 1.3$ mm) of the slot trailing edge.

Test	h mm	$Q_a \cdot 10^{-3}$ m ³ /s	Q_o, Q_{d*}
/ 17-0,3	0,3	2,75	0,325
/ 18-0,3	0,3	4,12	0,488
F 201,3	1,3	12,2	1,45
F 181,3	1,3	4,05	0,48

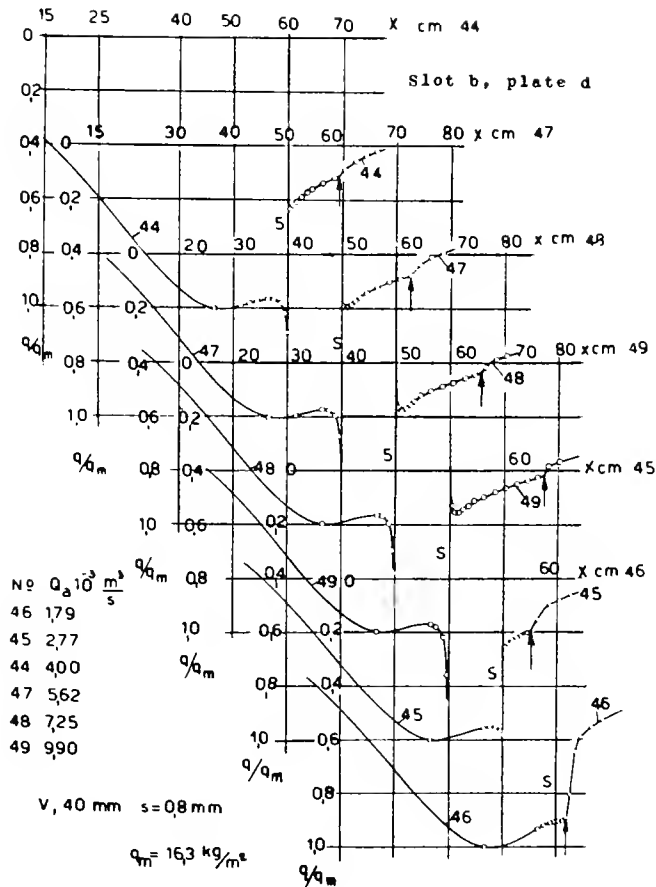


Figure 45.- Laminar suction tests with slot (b), test plate (d) (fig. 37), 40-millimeter tunnel width, $s = 0.8$ millimeter, $q_m = 16.3 \text{ kg/m}^2$. Influence of the suction quantity Q_a on the laminar-pressure increase up to the transition (arrow) and the sink effect.



Figure 46.- Suction slot (g).

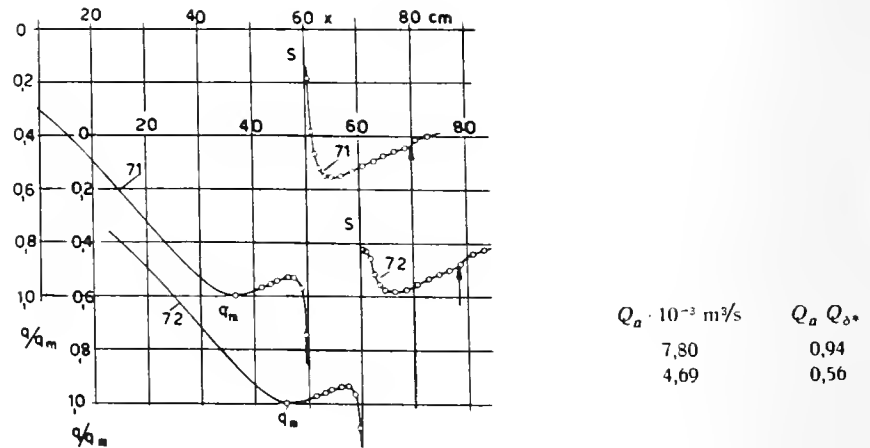


Figure 47.- Laminar suction tests with the slot (g), 40-millimeter tunnel width, $s = 0.8$ millimeter, $q_m = 16.3 \text{ kg/m}^2$. Pressure distribution at the test plate. Transition marked by arrow.

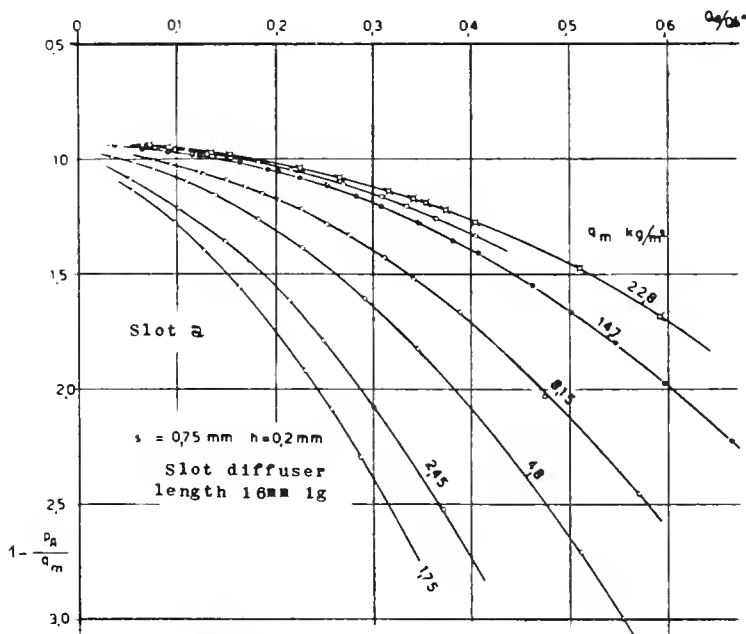


Figure 48.- Laminar suction tests with the suction slot (a) (fig. 27). 80-millimeter tunnel width, slot diffuser length 16 millimeters. Static pressure $1 - p_A/q_m$ in the suction chamber for various suction quantities Q_a/Q_{δ^*} , stagnation pressures q_m and slot widths s .

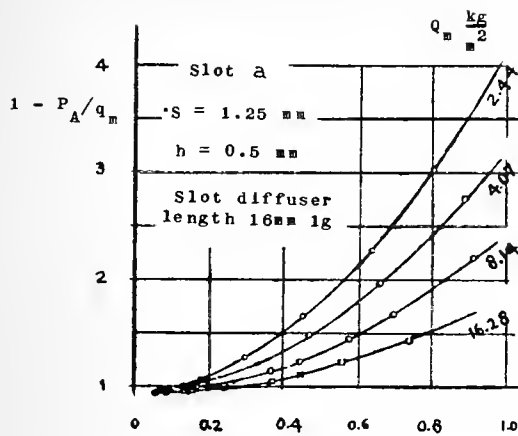


Figure 49.

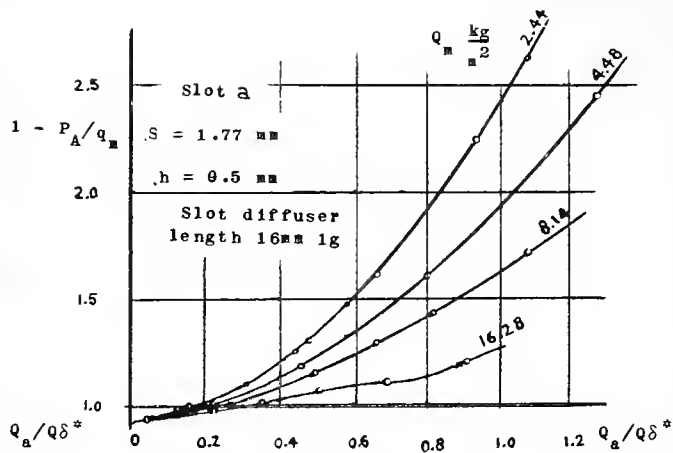


Figure 50.

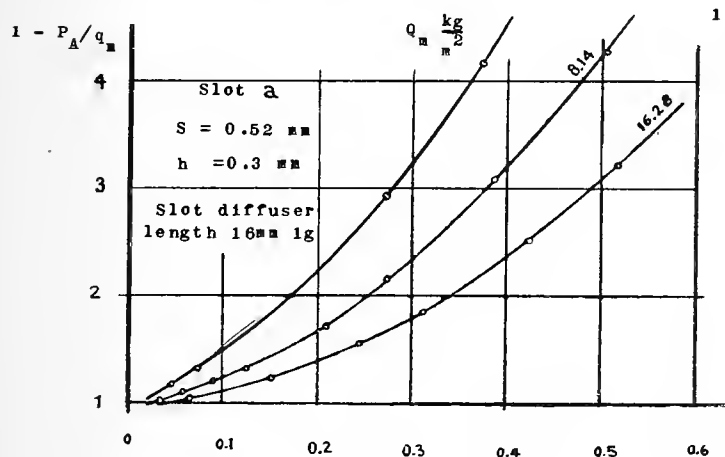


Figure 51.

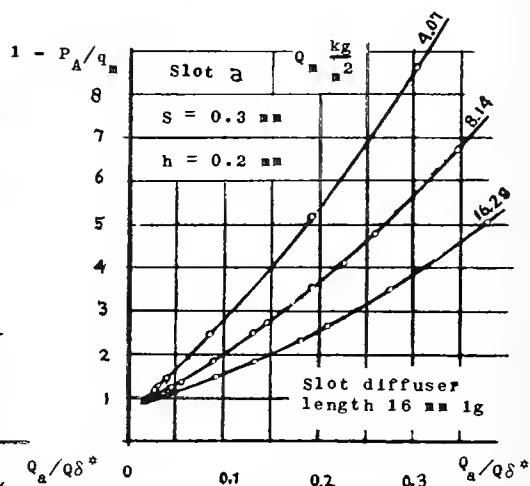


Figure 52.

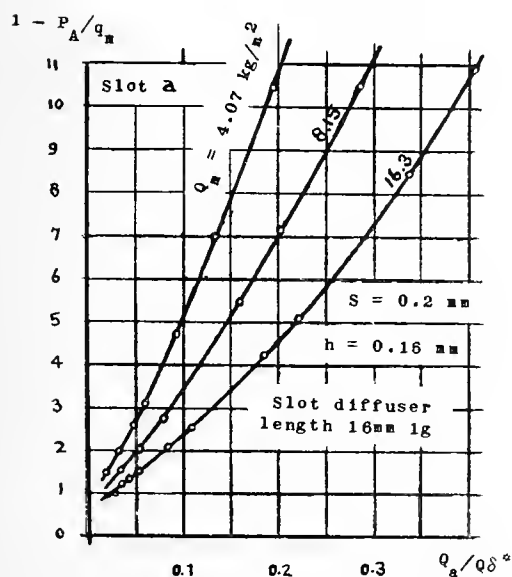


Figure 53.

Figures 49-53.- Laminar suction tests with the suction slot (a) (fig. 27). 80-millimeter tunnel width, slot diffuser length 16 millimeters. Static pressure $1 - P_A/q_m$ in the suction chamber for various suction quantities $Q_a/Q\delta^*$, stagnation pressures q_m and slot widths s .

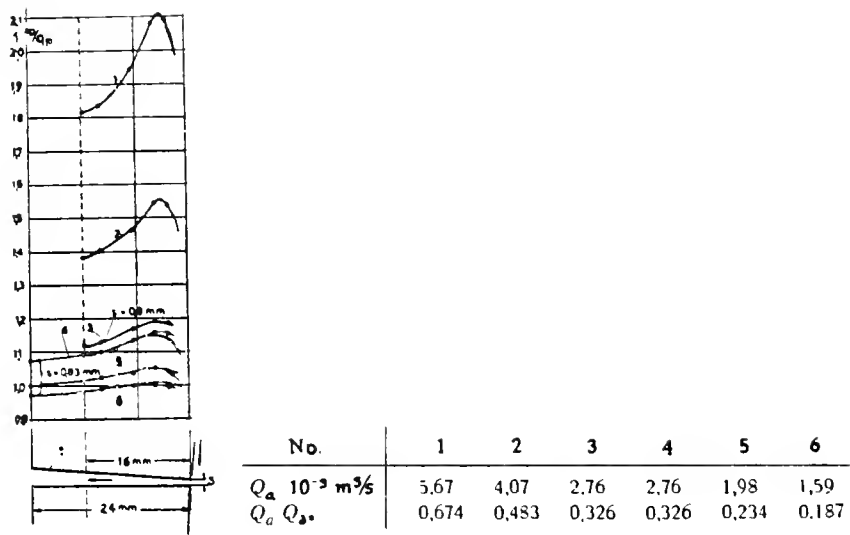


Figure 54.- Laminar suction tests with slot (b), test plate (b), (figs. 37 and 38), 40-millimeter tunnel width, $q_m = 16.3 \text{ kg/m}^2$. Static pressure $1 - \Delta p/q_m$ in the suction slot for various suction quantities Q_a/Q_{δ^*} .

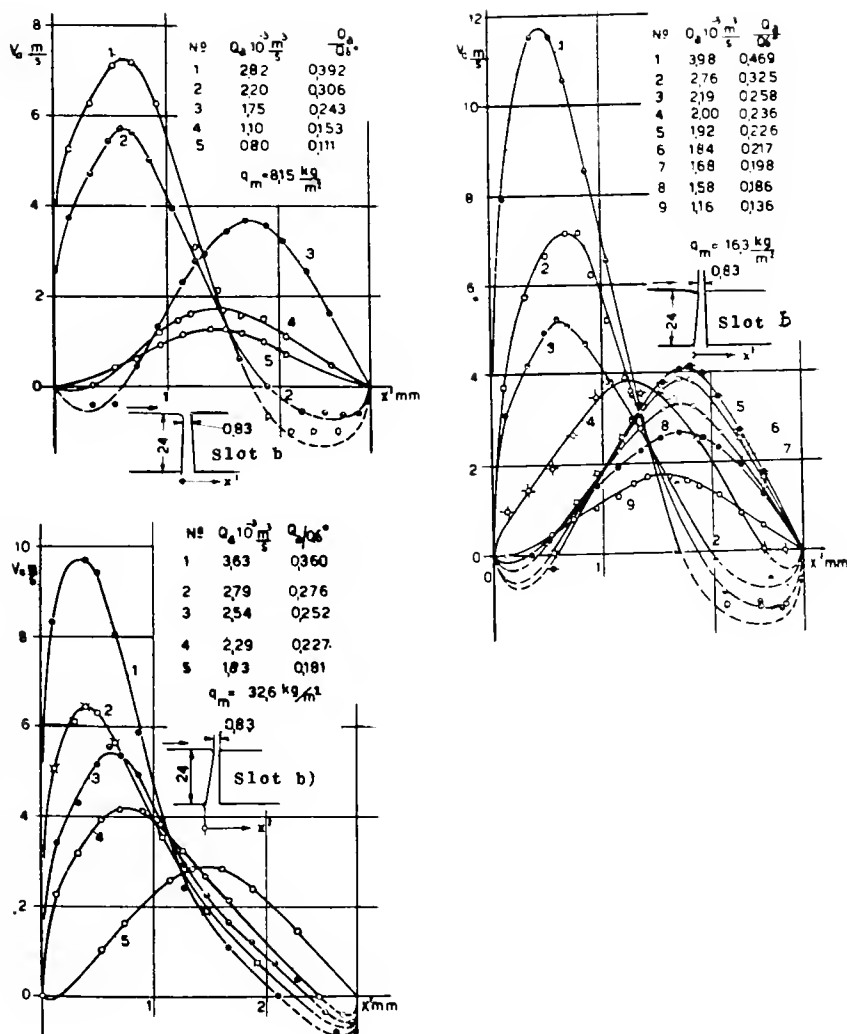


Figure 55-57.- Laminar suction tests with slot (b), test plate (b), 40-millimeter tunnel width, $s = 0.83$ millimeter, slot diffuser length 24 millimeters. Velocity distribution at the slot exit for various suction quantities Q_a and stagnation pressures q_m .

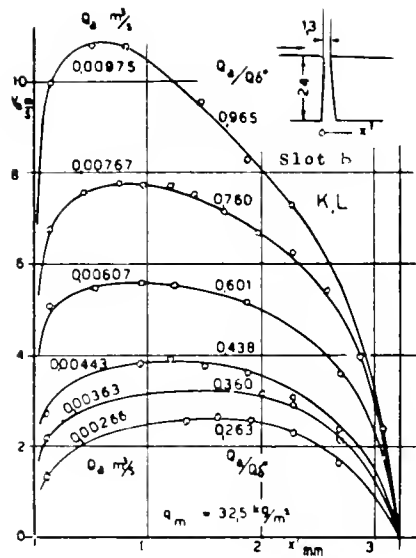


Figure 58.- Velocity distribution at the slot exit for various suction quantities, $q_m = 32.5 \text{ kg/m}^2$.

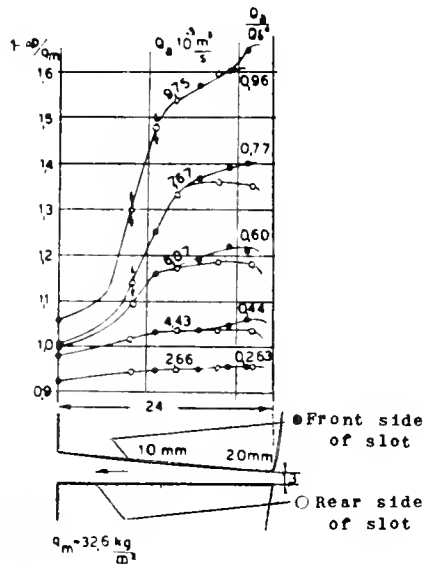


Figure 59.- Static pressure along the slot diffuser for various suction quantities, $q_m = 32.5 \text{ kg/m}^2$.

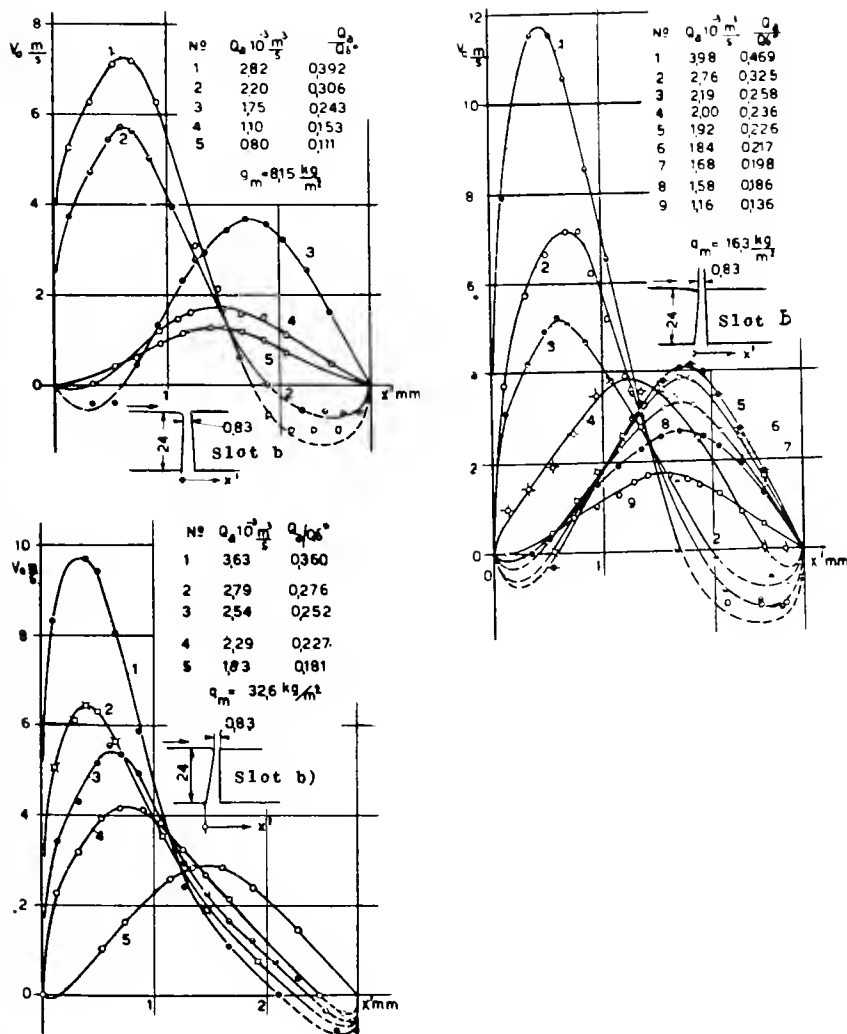


Figure 55-57.- Laminar suction tests with slot (b), test plate (b), 40-millimeter tunnel width, $s = 0.83$ millimeter, slot diffuser length 24 millimeters. Velocity distribution at the slot exit for various suction quantities Q_a and stagnation pressures q_m .

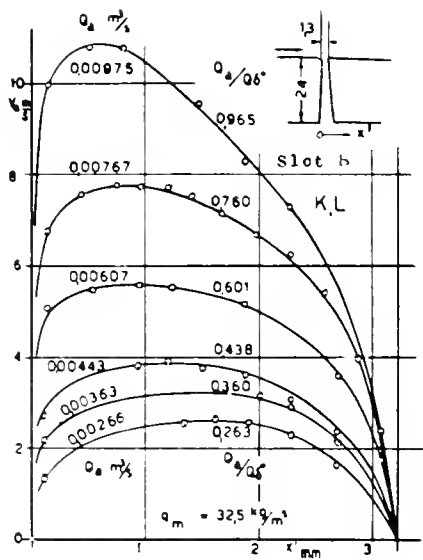


Figure 58.- Velocity distribution at the slot exit for various suction quantities, $q_m = 32.5 \text{ kg/m}^2$.

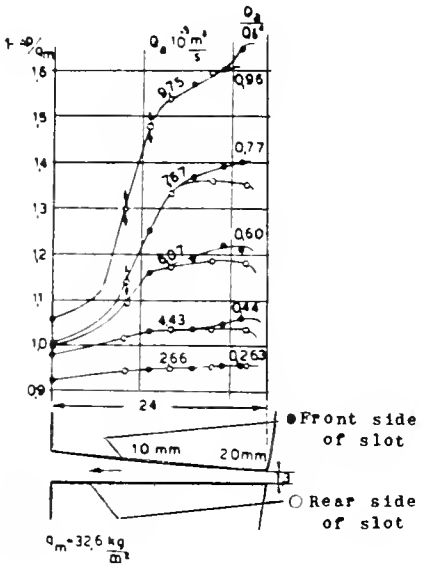


Figure 59.- Static pressure along the slot diffuser for various suction quantities, $q_m = 32.5 \text{ kg/m}^2$.

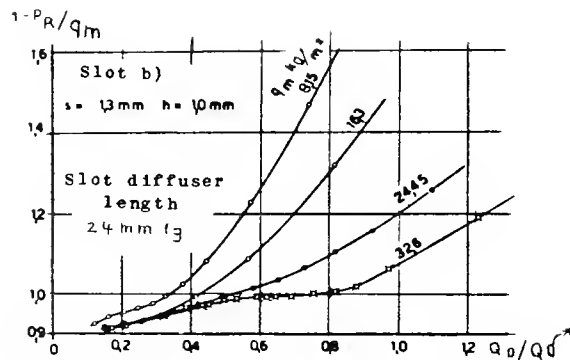


Figure 60.- Static pressure in the suction chamber for various suction quantities Q_a / Q_{δ^*} and stagnation pressures q_m .

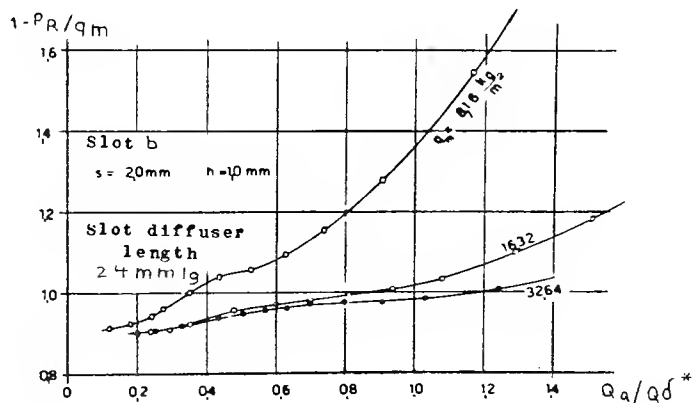


Figure 61.- Laminar suction tests with slot (b), test plate (b), 40-millimeter tunnel width, $s = 2.0$ millimeters, $h = 1.0$ millimeter. Slot diffuser length 24 millimeters. Static pressure in the suction chamber for various suction quantities Q_a / Q_{δ^*} and stagnation pressures q_m .

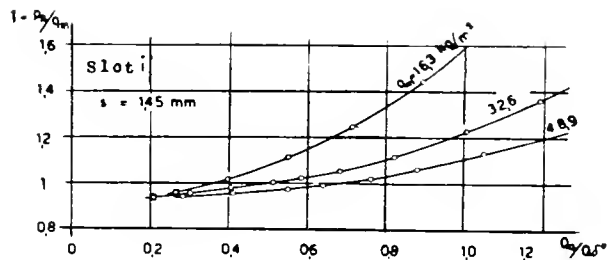


Figure 62.- Laminar suction tests with suction slot (i) curved forward (fig. 38), test plate (b), $s = 1.45$ millimeters, 40-millimeter tunnel width. Static pressure in the suction chamber for various suction quantities and stagnation pressures.

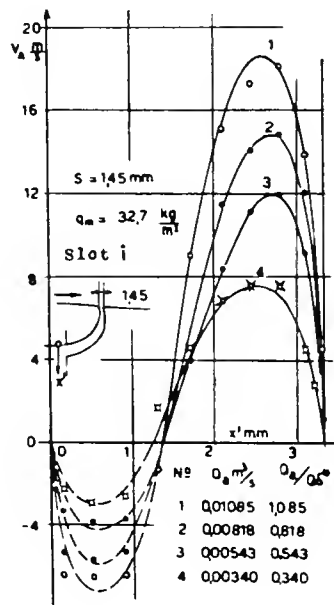


Figure 63.- Laminar suction tests with forward curved suction slot (i) (fig. 38), test plate (b), $S = 1.45$ millimeters, 40-millimeter tunnel width. Velocity distribution at the slot exit for various suction quantities, $q_m = 32.7 \text{ kg/m}^2$. The slot flow undergoes laminar separation on the front side of the slot.

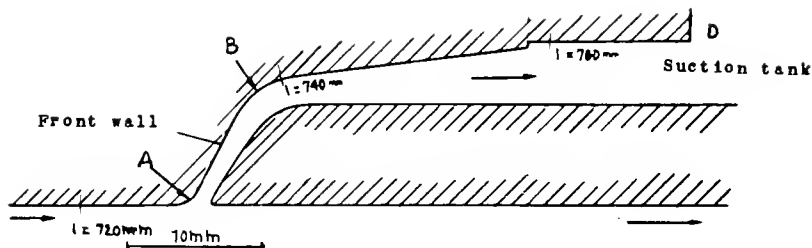
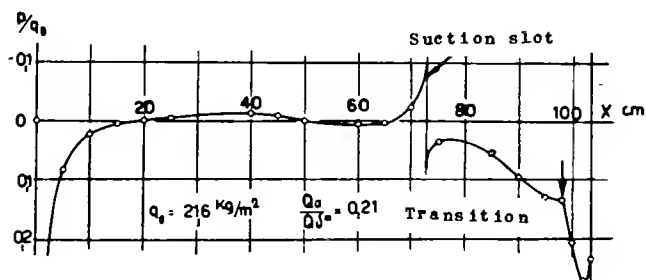
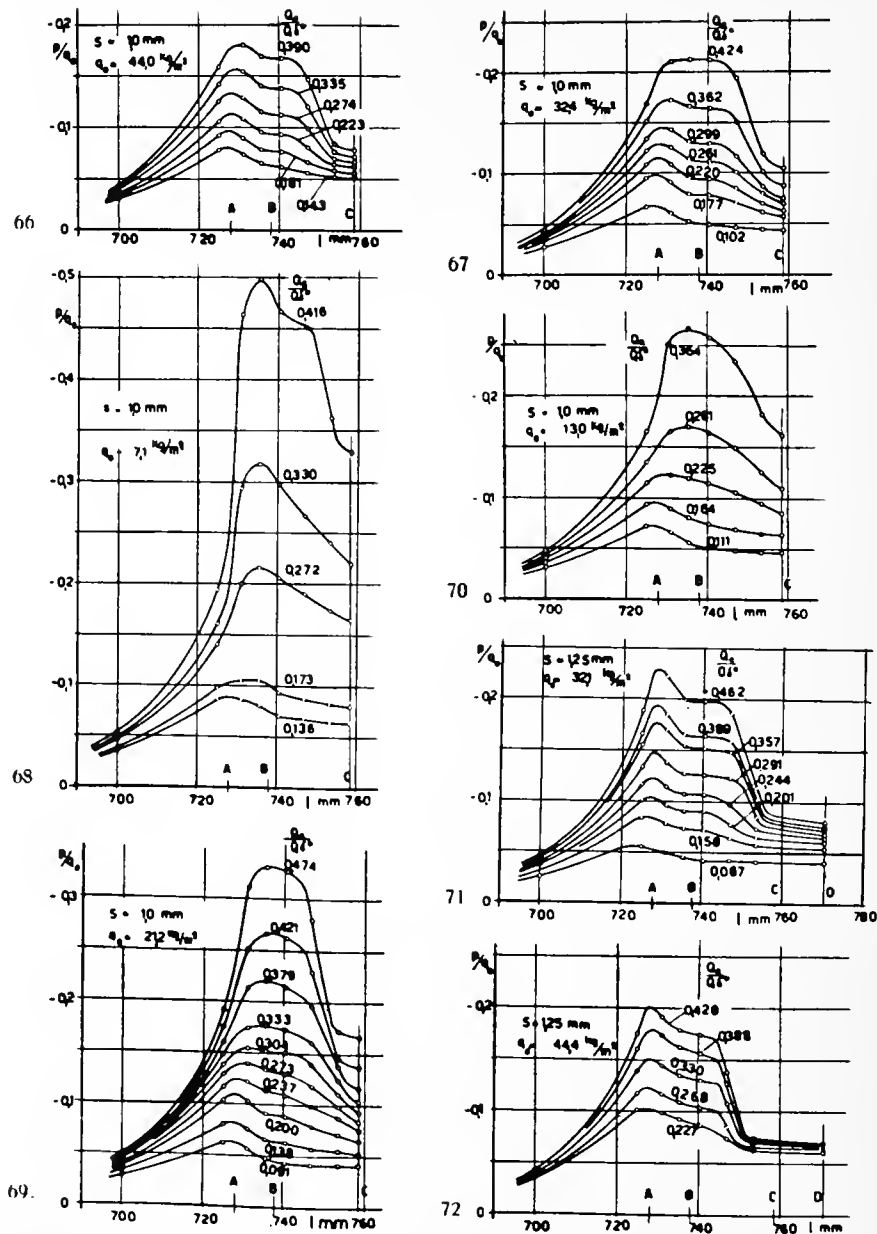


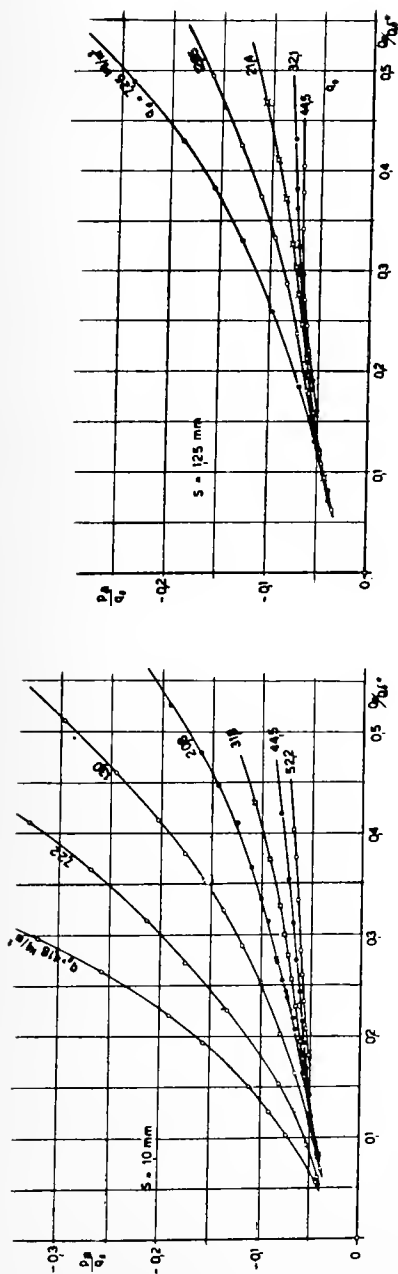
Figure 64.- Rearward curved suction slot h.

Figure 65.- Laminar suction tests with slot h. Static-pressure distribution p/q_0 along the chord.



Figures 66-72.- Laminar suction tests with slot h . Distribution of the static pressure p/q_0 ahead of the slot and along the slot diffuser for various suction quantities $Q_2/Q\delta^*$ and stagnation pressures q_0 . Minimum slot width $s = 1.0$ millimeter and 1.25 millimeters. $\delta^* =$ displacement thickness ahead of the slot.

Table for Figures 66-72.					
q_0 kg/m ²	32,1	44,0	7,1	21,2	13,0
$Q_{\delta^*} \cdot 10^{-3}$ m ³ /s ($b = 0,18$ m)	5,10	5,52	3,48	4,60	4,05



Figures 73, 74.- Laminar suction tests with slot h. Static pressure p_A/q_0 in the suction chamber for various suction quantities Q_a/Q_0^* and stagnation pressures q_0 , $s = 1.0$ millimeter and 1.25 millimeters.

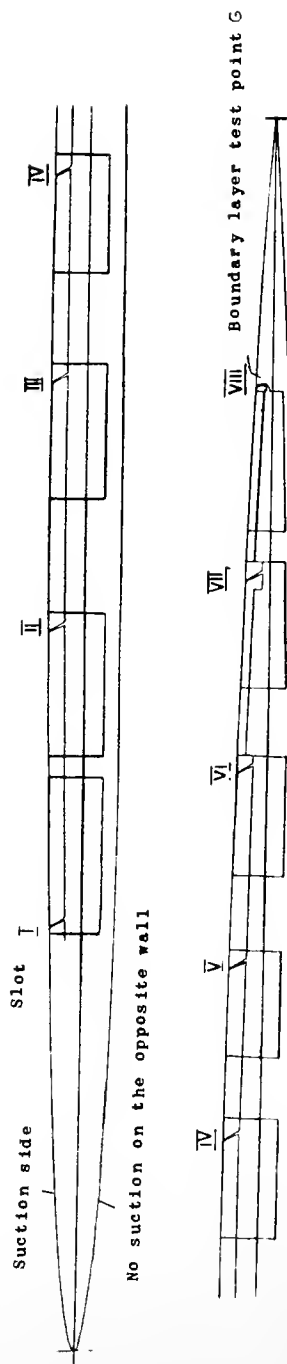


Figure 75(a).- Symmetrical laminar suction profile with eight suction slots, $d/t = 0.0335$, $t = 2.032 \text{ m}$.

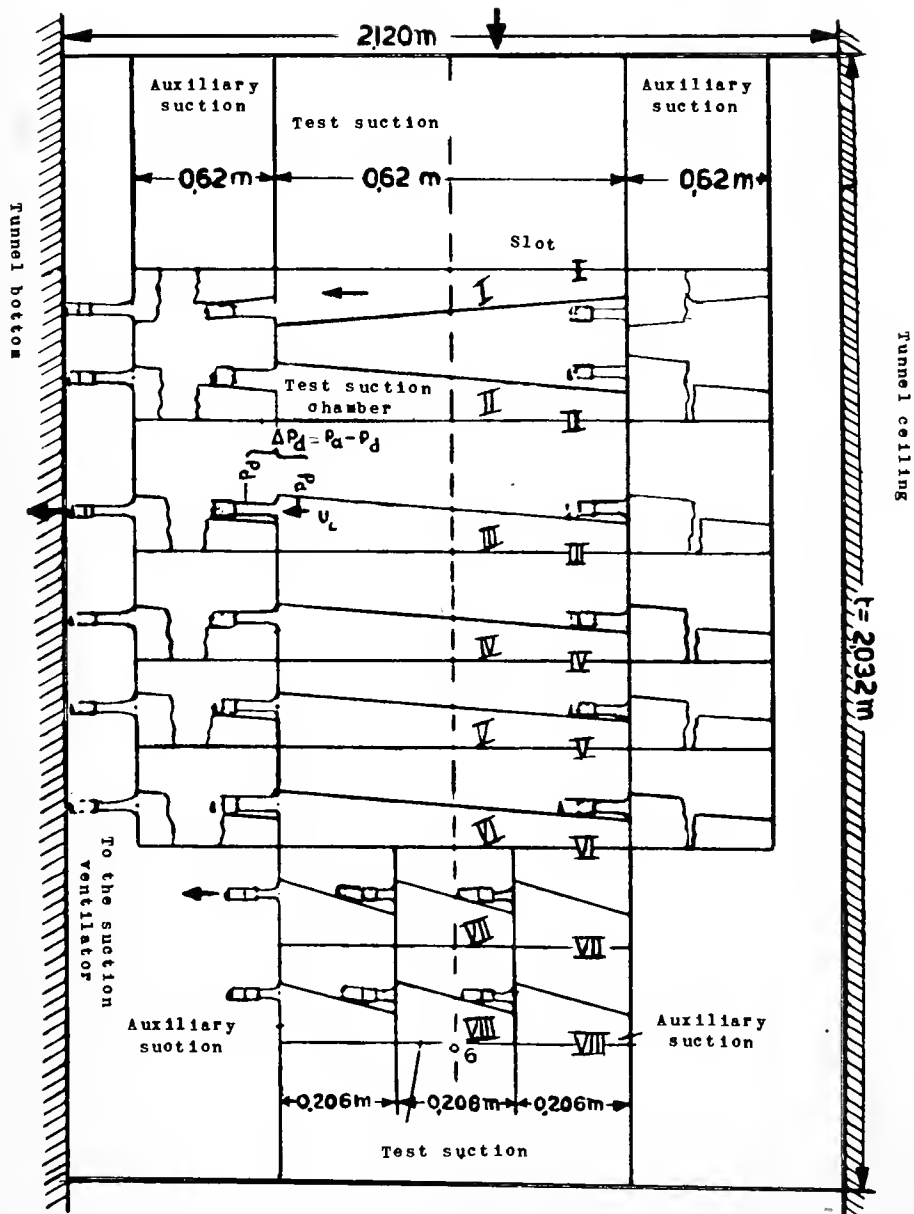


Figure 75(c).- Test nozzles for measurement of suction quantities.

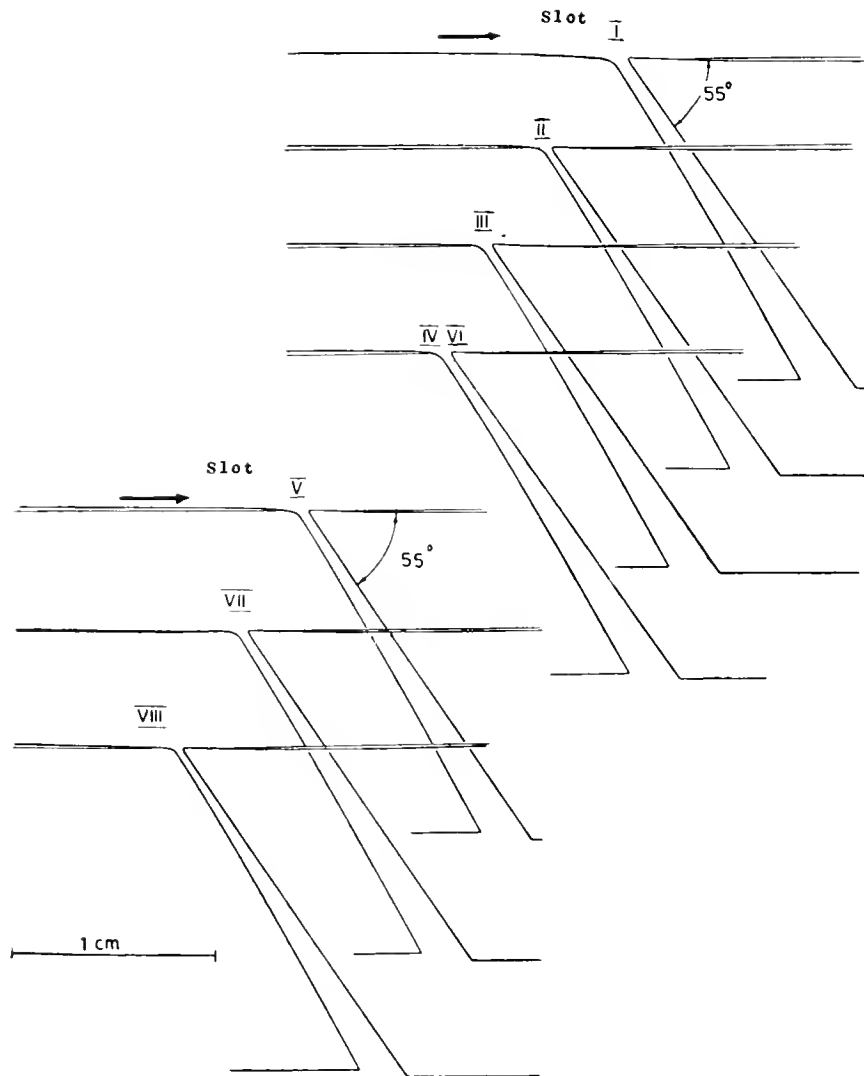
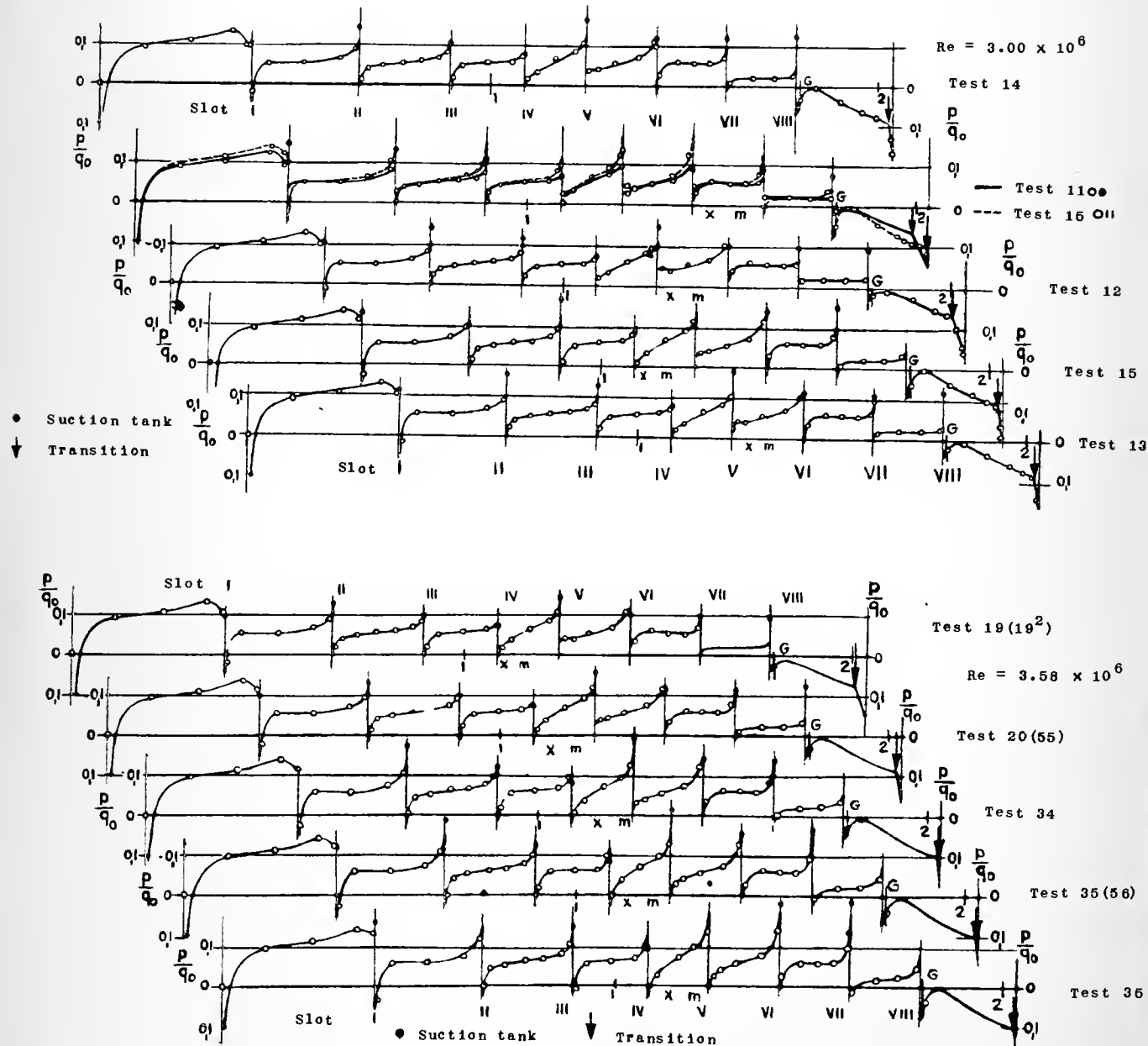
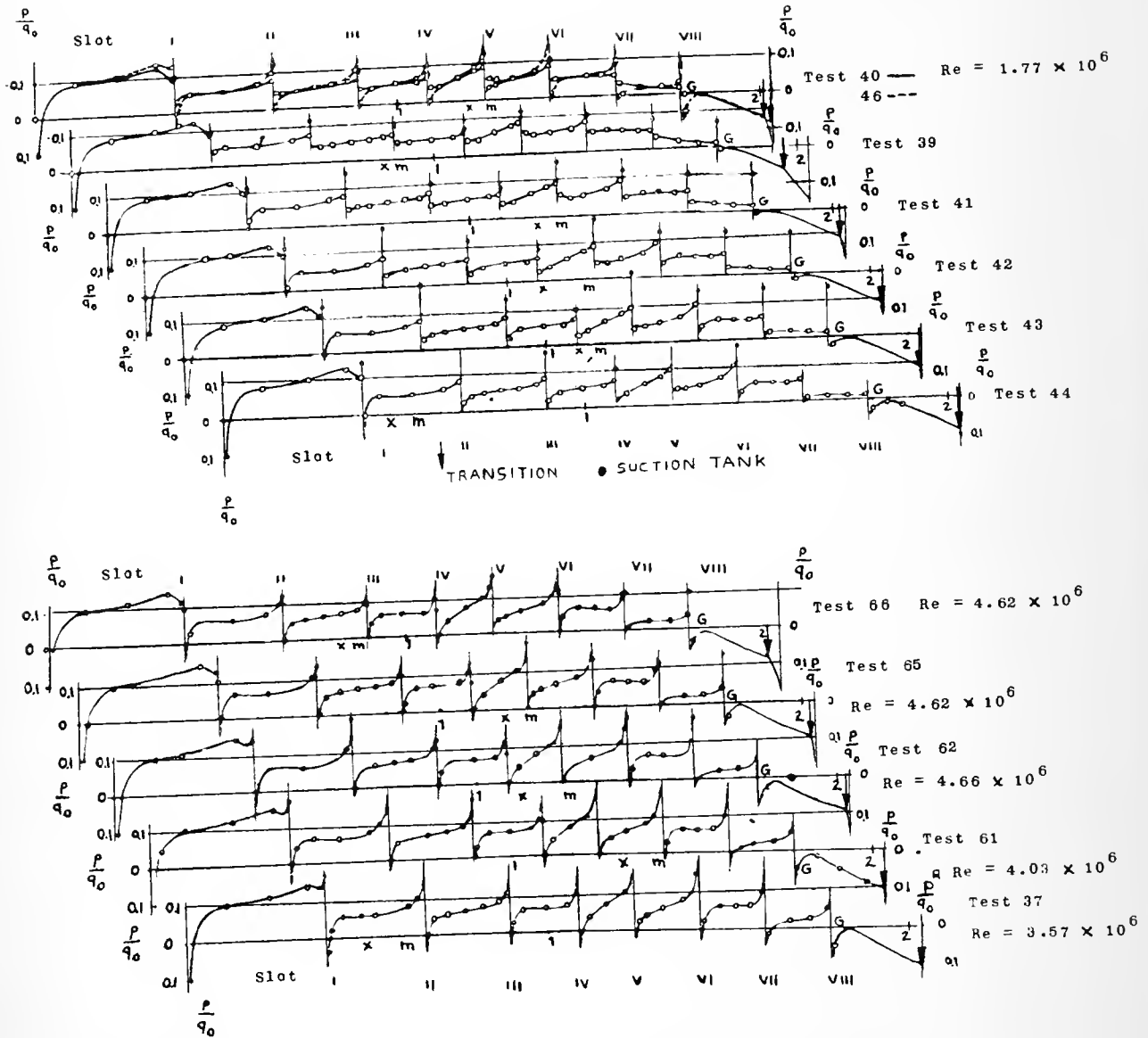


Figure 76.- Suction slots I - VIII.



Figures 77,78.- Pressure distribution along the chord, static pressure in the suction chambers (solid circles) and transition start (vertical arrows) for various Re and suction quantities. G = boundary-layer test point.



Figures 79,80.- Pressure distribution along the chord, static pressure in the suction chambers (solid circles) and transition start (vertical arrows) for various Re and suction quantities. G = boundary-layer test point.

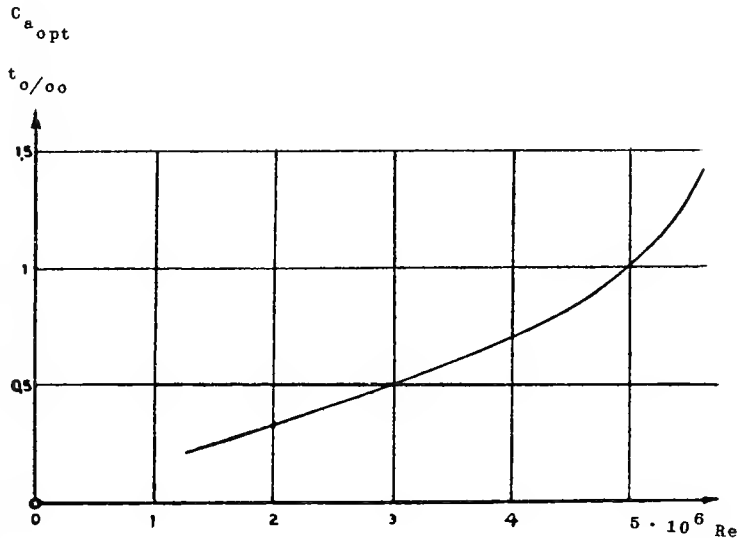
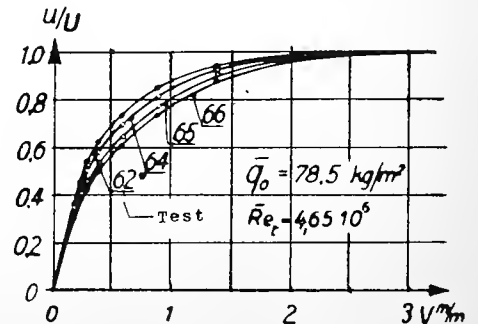
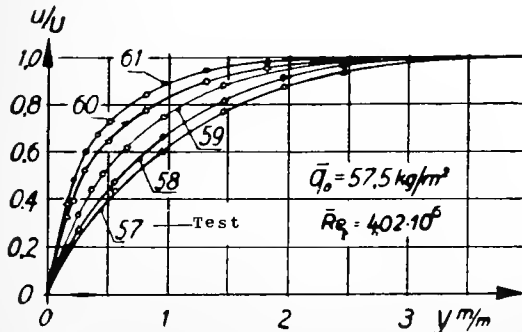
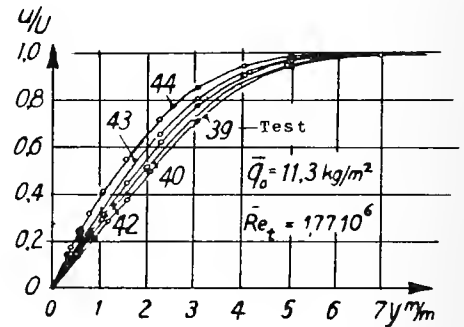
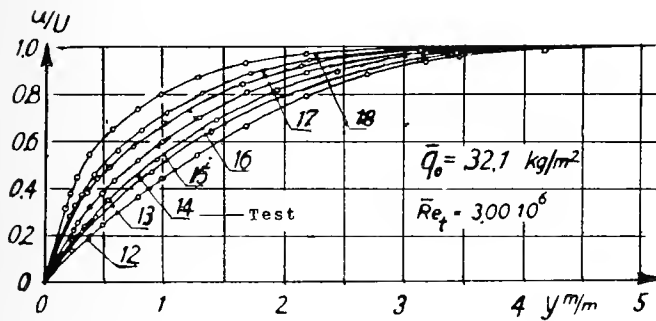
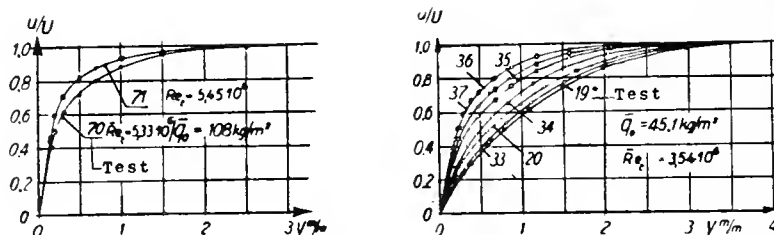


Figure 81.- Optimum total suction quantity $c_{Q_{t,opt}}$ (Re) for optimum total drag (calculated for both wing sides).



Figures 82-85.- Velocity distribution u/U (y) in the boundary layer at the point G 9 millimeters behind the slot VIII for various Re and suction quantities.



Figures 86,87.- Velocity distribution $u/U(y)$ in the boundary layer at the point G 9 millimeters behind the slot VIII for various Re and suction quantities.

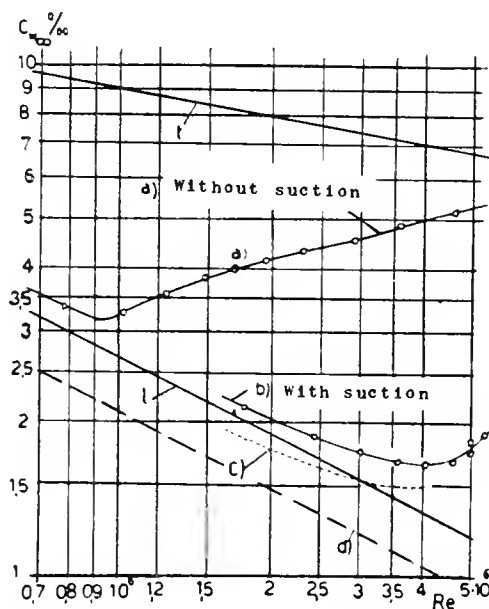


Figure 88.- Drag variation $c_{w\infty}(Re)$ without suction (curve a) and with laminar suction (curve b), suction blower power included. Presuppositions: $\eta_g = 1$ and acceleration of the sucked air to U_0 . The kinetic energy of the sucked air in the suction chambers was taken into consideration. $c_{w\infty}$ is calculated for both wing sides. The drag increase for higher Re is caused by the wind-tunnel turbulence. l = laminar friction of the flat plate (Blasius (47)), t = turbulent friction of the flat plate (Schlichting), (a) = $c_{w\infty}$ without suction, (b) = $c_{w\infty}$ with suction, (c) = $c_{w\infty}$ with suction, if there were two more suction slots arranged behind slot VIII (mathematically), (d) = $0.787c_{wR}l$.

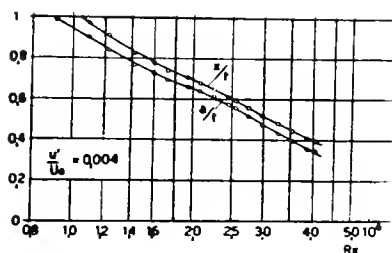


Figure 89.- Transition-point position for various Re on the not-sucked opposite wall (observations by stethoscope). a = transition start, x = start of the developed turbulent boundary layer (measured from the front).

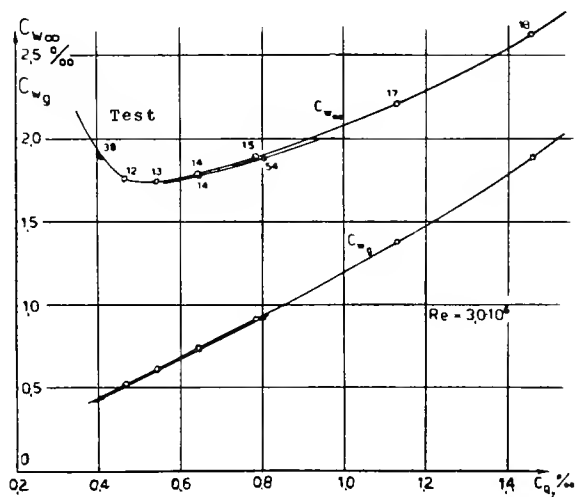


Figure 90.- Influence of the total suction quantity c_{Qt} on the total drag c_{W_∞}

and the drag contribution c_{Wg} of the suction blowers. c_{W_∞} , c_{Wg} , c_{Qt} are calculated for both wing sides. $Re = 3.00 \times 10^6$. In the tests 54, 14*, 38 (solid circles) one somewhat widened the suction slots, thus reducing the negative pressure in the suction chambers and therewith c_{Wg} and c_{W_∞} .

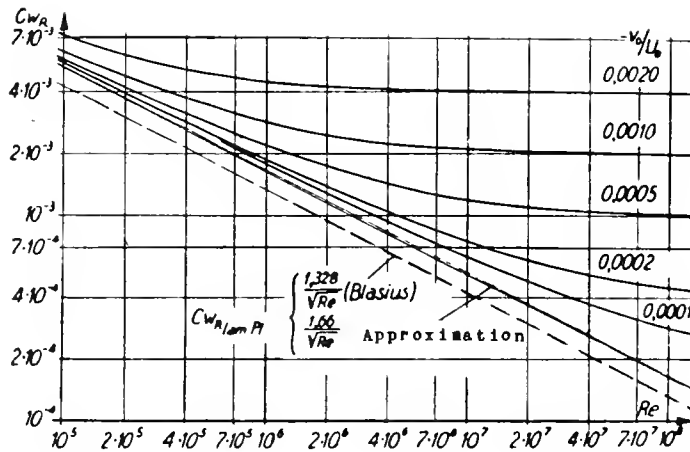


Figure 91.- Frictional drag c_{WR} of a laminar flat plate with area suction for various Re and suction velocities $-v_0/U_0$ according to Schlichting (70).

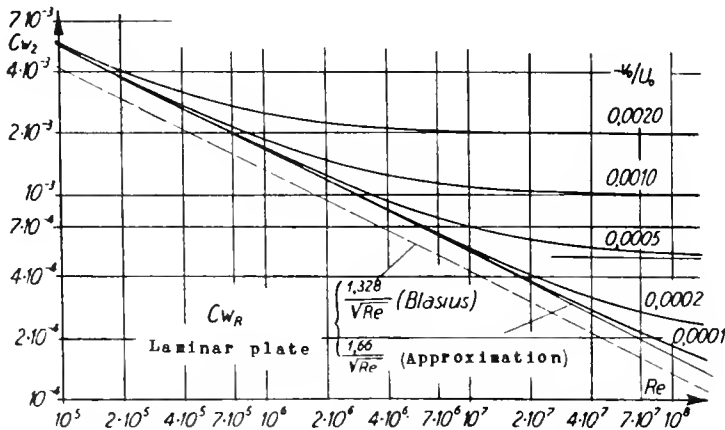


Figure 92.- Drag c_{W2} of a laminar flat plate with area suction for various Re and suction velocities $-v_0/U_0$ for lossless acceleration of the sucked air to U_0 (suction blower power included).

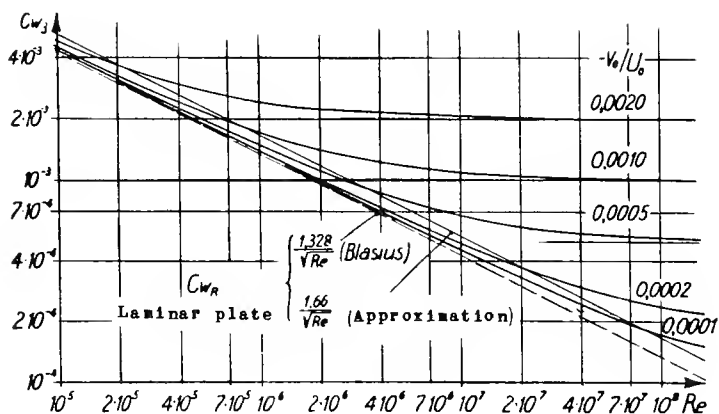


Figure 93.- Drag c_{w3} of a laminar flat plate with area suction for various Re and suction velocities $-v_0/U_0$ for lossless acceleration of the sucked air and the boundary layer at the plate end to U_0 (suction blower power included).

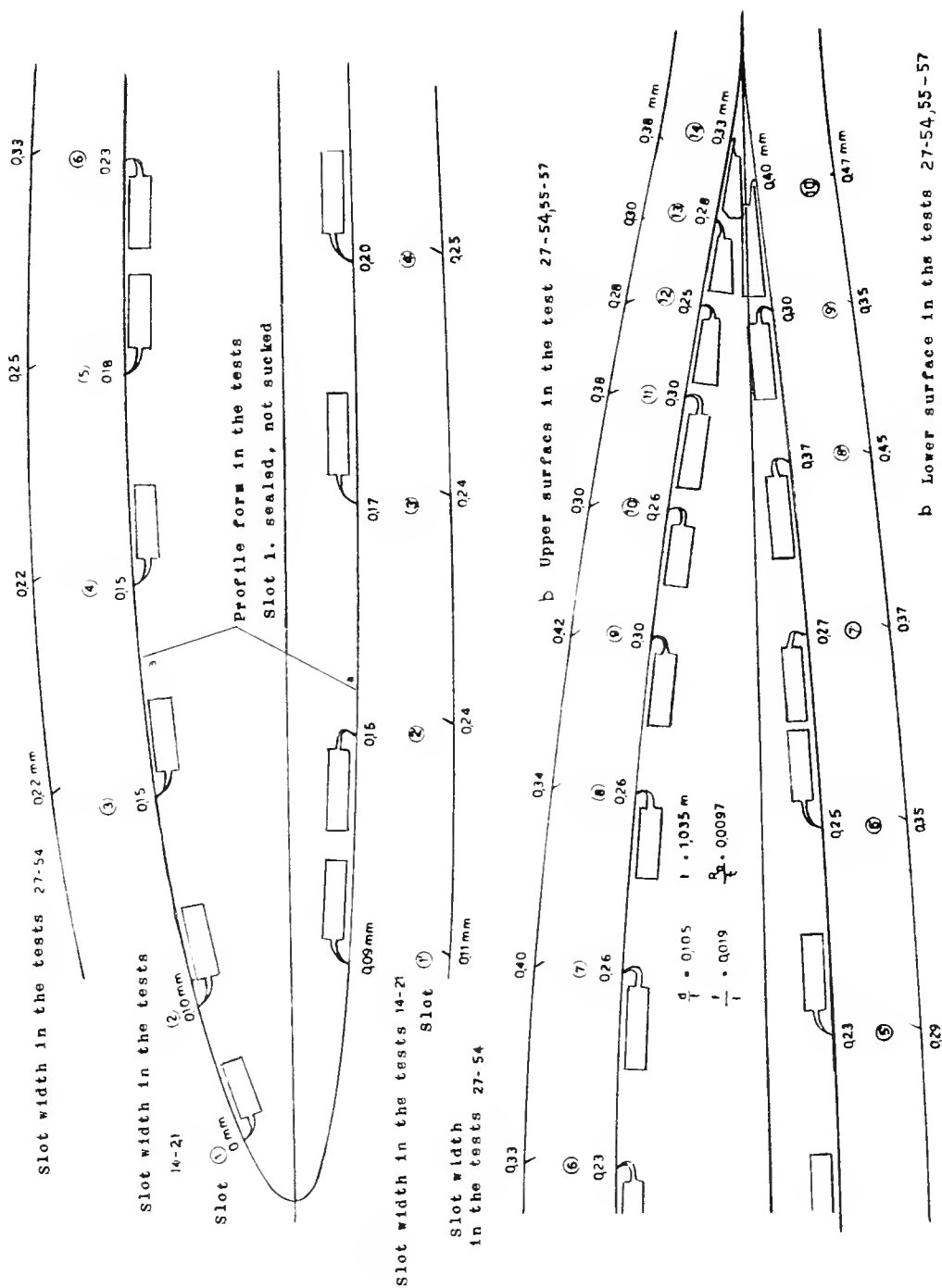


Figure 94.- Laminar suction profile, $d/t = 0.105$, $f/t = 0.019$. Profile shape, shape and position of the suction slots.

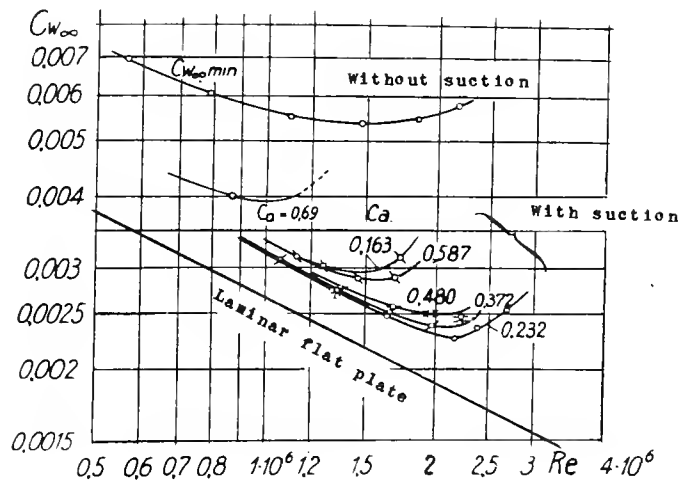


Figure 95.- Laminar-suction profile, $d/t = 0.105$. Optimum total drag $C_{W\infty}$ with suction (suction-blower power included) for various Re and C_a , furthermore, $C_{W\infty \min}$ without suction.

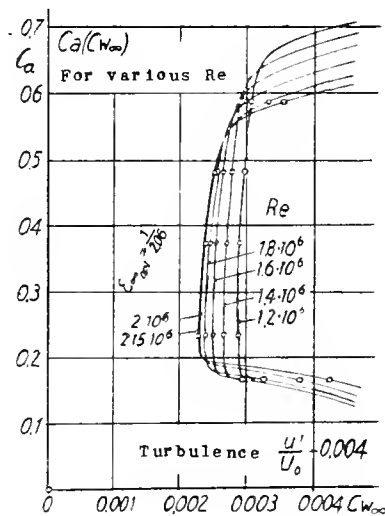


Figure 96.- Laminar suction profile, $d/t = 0.105$. $C_a(C_{W\infty})$ with suction for various Re (suction-blower power included).

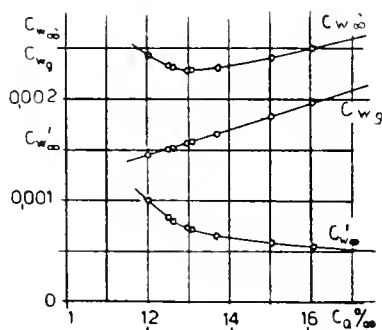


Figure 97.- Laminar-suction profile, $d/t = 0.105$. Influence of the suction quantity c_Q on $c_{w\infty}$, $c'_{w\infty}$, c_{wg} .

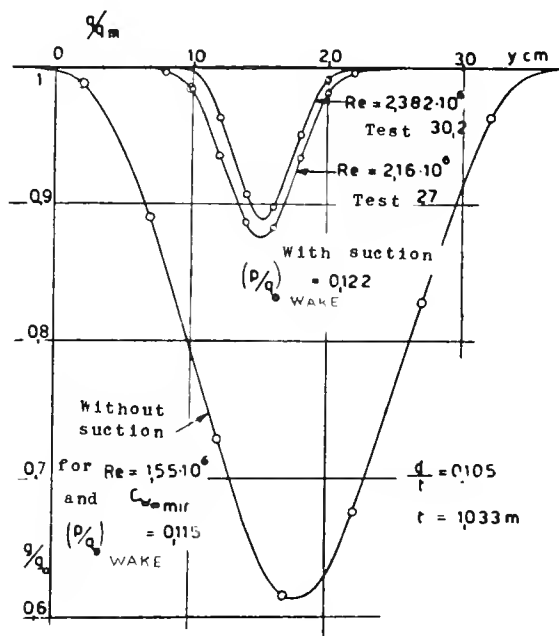
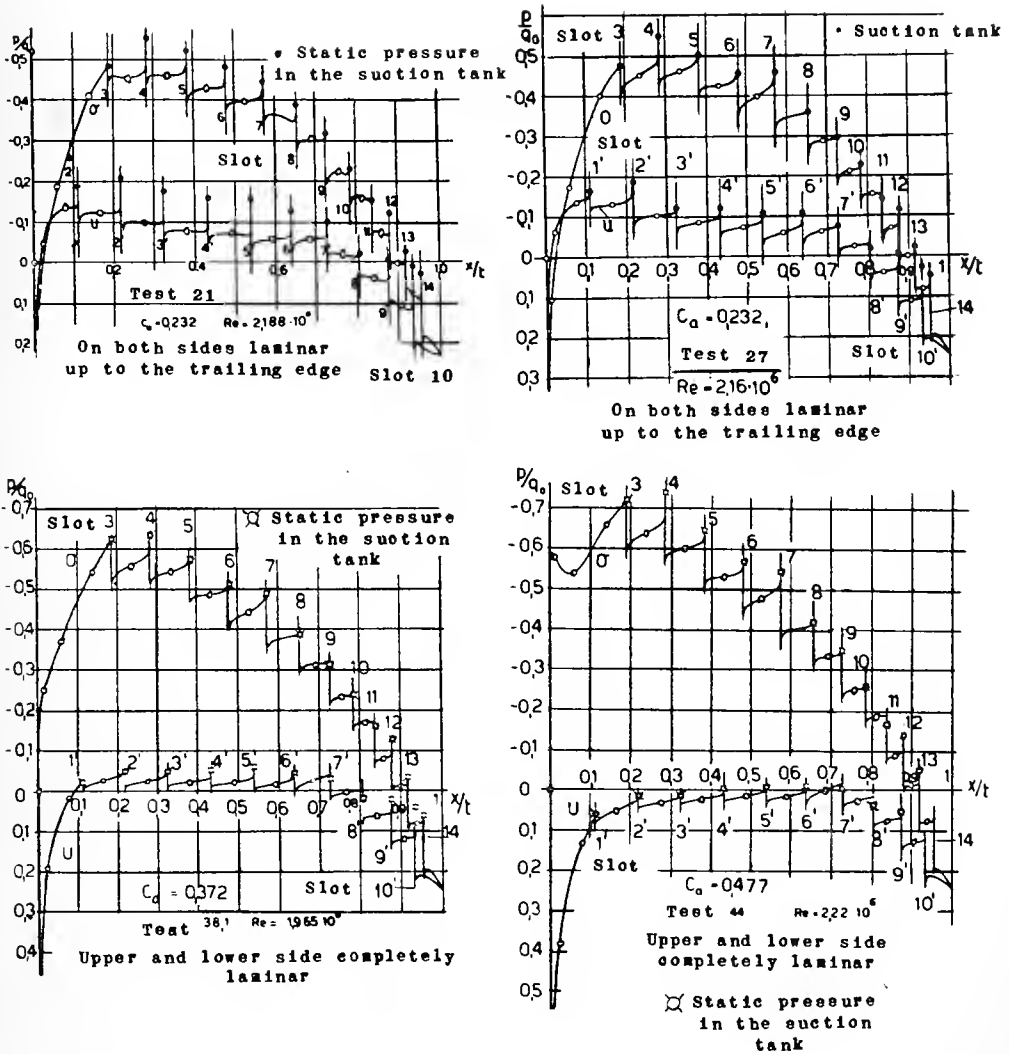


Figure 98.- Laminar-suction profile, $d/t = 0.105$. Total-pressure distribution in the wake with and without boundary-layer suction.



Figures 99-102.- Laminar-suction profile, $d/t = 0.105$. Pressure distributions along the chord for various C_d . In test 21 the sink effect is weaker than in the corresponding test 27.

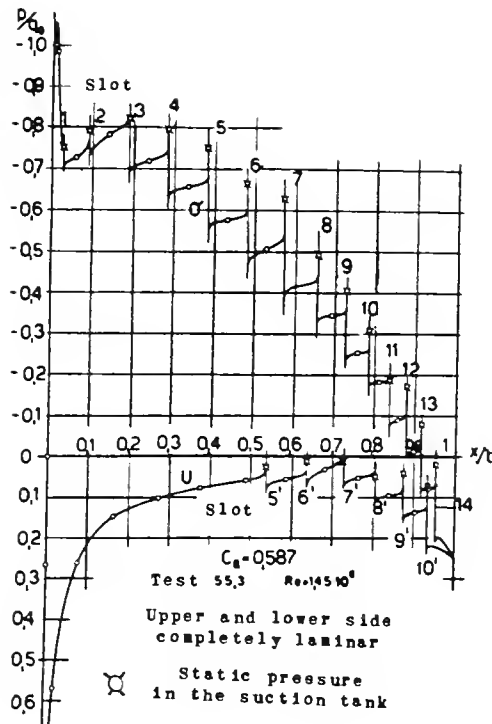


Figure 103.- Laminar-suction profile, $d/t = 0.105$. Pressure distributions along the chord for $c_a = 0.587$.

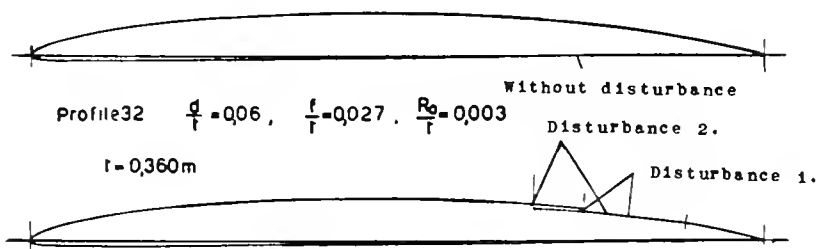


Figure 104.- Profile 32, $d/t = 0.060$, smooth wing, and with disturbances (1) and (2).

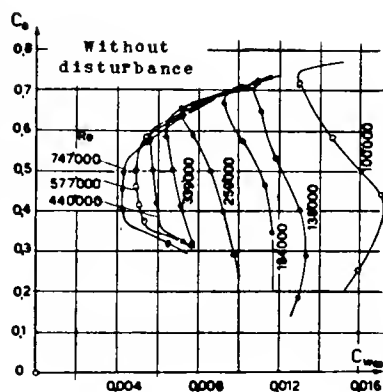


Figure 105.- Profile-drag polars of the profile 32 without disturbances (smooth wing).

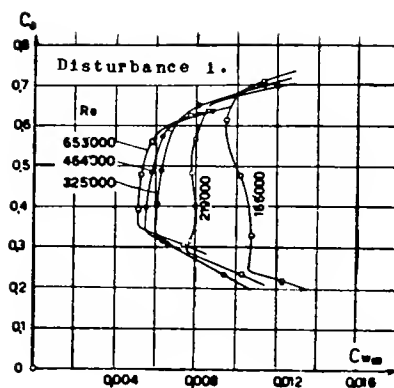


Figure 106.- Profile-drag polars of the profile 32 with disturbance 1.

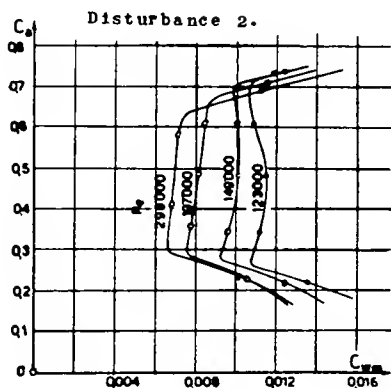


Figure 107.- Profile-drag polars of the profile 32 with disturbance 2.

UNIVERSITY OF FLORIDA



3 1262 08106 647 3

UNIVERSITY OF FLORIDA
DOCUMENTS DEPARTMENT
120 MARSTON SCIENCE LIBRARY
P.O. BOX 117011
GAINESVILLE, FL 32611-7011 USA